Karya#33 Plagiasi

by Marjoni Imamora

CrossMark

Advances in porous and high-energy (001)-faceted anatase TiO₂ nanostructures

Akrajas Ali Umar [a, *], Siti Khatijah Md Saad [a], Marjoni Imamora Ali Umar [b], Mohd Yusri Abd Rahman [a], Munetaka Oyama [c]

[a] Institute of Microengineering and Nanoelectronics, Universiti Kebangsaan Malaysia (UKM), 43600 Bangi, Selangor, Malaysia
[b] Department of Physics Education, Faculty of Tarbiyah and Education, Institut Agama Islam Negeri (IAIN), Batusangkar, 27213, West Sumatera, Indonesia
[c] Nanomaterials Chemistry Laboratory, Department of Materials Chemistry, Graduate School of Engineering, Kyoto University, Nishikyo-ku, Kyoto, 615-8520, Japan

ARTICLE INFO

ABSTRACT

In this review, we present a summary of research to date on the anatase polymorph of TiO₂ nanostructures containing high-energy facet, particularly (001) plane, with porous structure, covering their synthesis and their application in photocatalysis as well as a review of any attempts to modify their electrical, optical and photocatalytic properties via doping. After giving a brief introduction on the role of crystalline facet on the physico-chemical properties of the anatase TiO₂, we discuss the electrical and optical properties of pristine anatase TiO₂ and after being doped with both metal and non-metals dopants. We then continue to the discussion of the electrical properties of (001) faceted anatase TiO₂ and their modification upon being prepared in the form of porous morphology. Before coming to the review of the photocatalytic properties of the (001) faceted anatase and (001) with porous morphology in selected photocatalysis application, such as photodegradation of organic pollutant, hydrogenation reaction, water splitting, etc., we discuss the synthetic strategy for the preparation of them. We then end our discussion by giving an outlook on future strategy for development of research related to high-energy faceted and porous anatase TiO₂.

© 2017 Elsevier B.V. All rights reserved.

1. Introduction

TiO₂ is a wide band gap semiconducting materials that has been for decades attracting a wide interest for broad range of applications ranging from cosmetic to photocatalysis [1–3], solar cell [4], sensor [5,6], hydrogen energy harvesting from water dissociation [7–10], fuel cell [11–14], application related to environment benefits [15–17] and optoelectronics [18–21] due to its unique physico-chemical properties, such as band gap energy level that enables for a facile charge injection or extraction, high-chemical stability that resists to photo-bleaching and non-toxicity and etc [19,22–25]. TiO₂ can be mostly found in the form of three polymorph, i.e. rutile, anatase and brookite and its electrical, optical and other physicochemical properties depend on its crystalline phase state. Unique to anatase, it demonstrates superior properties in many aspect compared to others two phases, particularly its

photoactivity and surface physico-chemical properties [26]. These crucial feature has made anatase polymorph become the center of interest, particularly for an application in the field of photocatalytic and energy conversion. Up to this stage, there is still a continuous interest in the synthesis of anatase polymorph of TiO₂ with peculiar morphology that may facilitate enhanced photophysical processes in this material, such as wide surface area high-energy facets dominant structure. In anatase phase, the order of the surface energies follows the sequences of (110) > (001) > (100) > (101) with surface energy (γ) of 1.09, 0.90, 0.53 and 0.44 J m^{-2}, respectively [27]. The high-energy facet are thermodynamically un-stable and rapidly annealed into a highly-stable (101) plane. For that reason, preserving the high energy facet during the nanocrystal growth in order to obtaining a reactive TiO₂ nanocrystals is a challenging task. Considering the role of TiO₂ surface in many photophysical processes, to develop methods to realize anatase TiO₂ with a wide area of high-energy facet is highly demanded for further augmenting their performance in applications. We have recently witnessed a number of attempts in realizing the nanostructured anatase TiO₂

with exposed high-energy facets and porous morphologies for wide surface area availability. These efforts have produced anatase TiO$_2$ with variety of high-energy facet morphology, such as nano-plates, nanosheet and other two-dimensional morphology [28,29]. In addition to peculiar high-energy facet properties, porous structures not only provide a wide surface area but also produces additional cavity effect [30], the result of photon energy entrapment in small hole structure, may further expand the photophysical effect in applications, gaining photocatalytic performance or other photophysical processes.

Besides increasing the surface area by engineering the anatase TiO$_2$ in order to have porous structure to expand their intrinsic properties, introduction of metal or non-metals doping has been seen to offer a sophisticated approach to further enrich the electronic and optical properties of anatase TiO$_2$ [31–33]. Amongst a potential effect in metal doping is the shifting of the energy bad gap of the anatase TiO$_2$ to visible region (narrowing the band gap), induces carrier trap density and oxygen vacancy or increasing the free-carrier density. This effect enhances the photosensitivity of the anatase TiO$_2$, improving the performance in photocatalysis, sensing, dye sensitized solar cell and etc.

In this review, we will present an analysis of the photocatalytic properties of anatase TiO$_2$ nanostructures containing high-energy facet as well as the available synthetic strategy for their realization. In discussing the synthetic approach, the method to prepare large-surface area of high-energy facet, such as porous structure, will also be overviewed. It is also described in this review the effort to introduce metal or non-metal doping in such porous morphology of anatase TiO$_2$ in order to further enhance their photoactivity. The discussion is continued on the review of the photocatalytic properties high-energy faceted anatase TiO$_2$ in selected applications, such as pollutant degradation, water splitting or oxygen reduction reaction. There have been available a wide range of reported literature on the synthesis of anatase TiO$_2$ with variable morphology that span from porous, nanowires and nanorods, high-energy facet structure [34], nanotubes synthesis as well as the reviews on their applications in photocatalysis, water splitting, energy storage, photoelectrochemistry, self-cleaning, etc. Review on the bulk and surface properties of the TiO$_2$ [35] and the surface chemistry for photocatalyst [36] as well as doped with non-metal [37] and metal have also been well documented. Here, we highlight the method that leads to the formation of anatase TiO$_2$ nanostructure containing large-scale high-energy facet of (001) with porous properties and doped with metal or non-metal dopants, for high-performance in photocatalysis applications.

2. Electronic and optical properties

2.1. Pristine system

2.1.1. Electrical property

Anatase is one of the polymorph of TiO$_2$ that has received a great deal of attention for application in photocatalysis, water splitting and dye-sensitized solar cell. The anatase TiO$_2$ has energy band gap of approximately 3.2 eV. Its valence band is constructed by energetic O p$_\pi$ at the top level of the valence band. Meanwhile its conduction band is from Ti 3d and 4s as well as small portion from the O p$_\pi$ (the lowest conduction band region). This condition is little bit different if compared to the rutile and brookite polymorphs where the ratio between O p$_\pi$ state and Ti 3d at the conduction band in both polymorphs are higher. With high O p$_\pi$ state in conduction band make the carrier mobility in rutile and brookite

polymorphs are lower than the anatase as the result of high-resistivity due to high surface trap density contributed by the O electronic species [22]. Such unique electronic structure in anatase TiO$_2$, has led to the high mobility of n-type charge carriers [38]. In addition, the resistivity and Hall effect analysis also indicated the existence of an insulator–metal transition in a donor band in anatase TiO$_2$ due to the fact of a large Bohr radius of donor electron in anatase TiO$_2$, expanding the applicability of this materials in a broader fields, particularly nanoelectronics. Such phenomena was not observed in rutile phase [39]. Its electrical resistivity is approximately 10^{15} Ohm cm^{-1} and it is influenced by several factor including oxygen vacancy, interstitial of titanium and defect of surface lattice, creating carrier traps. In many process, the carrier trap resulted from the interstitial Ti can go up to as high as 0.5 eV below the conduction band, enabling facile electron inter-band excitation and transfer. It has also been observed that there is the existence of bulk transport of exciton, from the excitation of deep level of electronics, to the surface of the nanocrystal [26]. These unique properties are amongst the key factor for a highly physicochemical activities on the anatase crystal surface, such as unique adsorption, coordination, trapping or charge-transfer between the anatase and adsorbate molecules, accelerating the reaction for photocatalysis or producing unusual surface physics phenomena for photocatalysis, sensor and optoelectronics applications. As the results, the anatase TiO$_2$ exhibits superior performance compared to its closes competitor of rutile polymorph.

2.1.2. Optical property

Amongst the attractive features of the anatase TiO$_2$ is its optical properties. For example, it has an optical absorption edge exhibits a large dichroism as the existence of a significant optical anisotropy in the components parallel and perpendicular to the crystal c axis. This is attributed to the existence of the energetic lowest energy nonbonding d$_{xy}$ orbitals of TiO$_2$, permitting dominant perpendicular component in direct dipole transitions [22]. Such unique behavior is known as adjustable via dopant introduction either with transitions metal [40,41], lanthanide [42], nitrogen and co-doping [22] or defect introduction in the lattice [43], which may significantly shift the absorption edge and the energy level of the lowest nonbonding orbitals [33]. Plasma treatment on the anatase TiO$_2$ may also produce another interesting effect to the optical properties. It is known that the plasma irradiation induces the formation of Ti^{3+} and the oxygen vacancy inside the materials that then improves the optical absorbance and optical absorption region [44]. This feature envisages the applicability of anatase TiO$_2$ as potential photoactive materials for photovoltaic and photocatalysis applications.

In different analysis, Ohta et al. indicate that the optical properties of anatase polymorph of TiO$_2$ is pressure dependent. For example, the absorption edge and the luminescence center of the anatase shifts at a rate of 10 and 33 meV/Gpa, respectively. It is understood that they are due to the high Stokes energy shift of the exciton energy level compared to the band gap. Despite this special phenomenon, the luminescence spectrum exhibits a wide band. It is understood due to the intense recombination of self-trapped exciton [45]. It has been well-known that the emission in anatase TiO$_2$ is mainly originated from the recombination of trapped electron with the hole in the valence band and is normally occurred at the Ti^{4+} site in the anatase TiO$_2$ [46,47]. Meanwhile, the higher energy emission, typically green emission, is originated from the recombination of the trapped holes with the mobile electron at the oxygen vacancy site [48]. Such imminent exciton trapped in anatase

TiO$_2$ has a wide range of effect to the transport properties in the materials. Deep trap level, which is resulted from highly defect lattice, will impede the carrier transport and moderate trap may facilitate better carrier diffusion inside the materials. It has been demonstrated that such trap level can be manipulated via a solvent- and a morphology control and application of external bias [46].

The optical properties of anatase polymorph also indicates a larger absorption edge, approximately 0.2 eV, compared to the rutile, revealing the anatase optical properties, reflected by the exciton self-trapping, strongly dependent on the imperfection in the lattice [49]. It has been demonstrated that the absorption edge is an exponential energy dependence and is less steep than the absorption edge of the rutile, indicating the exciton self-trapping and stronger influence of imperfections in the anatase [49]. Such unique optical properties of the anatase TiO$_2$ has also been earlier observed by Chiad et al. [50] as the obtaining of a significant light amplification scattering effect on TiO$_2$ nanoparticles, enabling them as a promising light scatterer in random lasers applications [21].

Interesting optical properties of the anatase TiO$_2$ is also exhibited in its unique photoluminescence properties with the existence of visible broad band emission that is related to the emission from the self-trapped excitons localized on TiO$_6$ octahedra. And these properties is temperature dependent and shift toward higher energy when temperature was increased from liquid helium to room temperature [51]. Time-resolved photoluminescence study near the band gap of anatase TiO$_2$ has shown that it exhibits highly stable Wannier exciton, generated from $2p_{x,y}$ exciton that is followed by 1s exciton state [52].

Such understanding on the optical process in anatase TiO$_2$ nanostructure led improved the performance of TiO$_2$ in catalysis, solar cell and sensing applications. For example, Pallotti et al. discovered that large modulation of PL intensity can be obtained by manipulating the PL active center due to specific morphology of hierarchical structure, facilitating prime interplay between PL active center, trapped charge and adsorbed gaseous molecules. It is found that the modification of the nature of charge trap in the anatase TiO$_2$ has led to the generation of enhanced optical responsivity up to 1100% under the exposure of oxygen gas [53], which are promising for high-performance in currently existing applications.

2.2. Doped system

The possibility to modify the optical and electronic properties of anatase TiO$_2$ is a fundamental factor that makes anatase polymorph to be extensively studied over the years. In order to modify the

electrical and optical properties of anatase TiO$_2$, doping process — whether from metal or non-metal impurities — has always been carried out. In typical process, the insertion of doping can shift the band edge to visible region, induces carrier traps density, induce oxygen vacancy or increase the free carrier, etc., enhancing the visible photosensitivity or conductivity correspondingly [54].

Similar to Si, the possibility to manipulate the carrier type, whether electron or hole, via doping are also there, allowing for the preparation of n-type or p-type material system. In typical doping process, the dopant can replace either Ti or O sites in the TiO$_2$ lattice. The effectiveness of the doping process and the resulting properties after being doped determined by several factors, such as the atomic radius on the dopant and the electronegativity of the dopant (oxidation number). Successful doping process is likely to occur if using dopant with comparable radius with the atom to be replaced in the lattice. Large difference may cause structural deterioration and electronic properties instability via the creation of additional defect or carrier trap in the lattice. To use several dopants, or in other word co-doping process, to modify the properties of anatase TiO$_2$ has been adopted to further improve the performance of anatase TiO$_2$ because the co-doping may either further synergistically enhance the effect produced by other dopant or neutralizes negative effect created by other dopant. Fig. 1 shows general mechanism of doping process in the pristine TiO$_2$. In pristine TiO$_2$, the electron transport is governed by the hopping process amongst the resonance state adiabatically of shallow traps until reaching the electrode (Fig. 1a). The transport properties is strongly influenced by the density of such shallow trap. In the meantime, the deep trap may exist and may behave as recombination site in the materials. When doping introduced, the deep trap density may be decreasing or increasing. In the case of deep trap density decreasing, both conduction band and the Fermi level are shifted upward (Fig. 1b). These process may overall reduce the electron injection potential, but it vulnerably lowers the short-circuit current density. However, it improves the open circuit voltage. For the case of doping enhances the density of the deep trap states, the conduction band and the Fermi level shifted downward. A most prominent effect caused by this process is the recombination process is enhanced. Thus, the open circuit voltage decreases. Depending on the offset between the lowest unoccupied molecular orbital of sensitizer molecules and the conduction band of TiO$_2$, the electron injection may improve, augmenting the short circuit current density in the materials.

2.2.1. Non-metal doped anatase TiO$_2$
Various scale of band gap shift have been reported so far when the anatase TiO$_2$ doped with metal or non-metal. Rumaiz et al., by
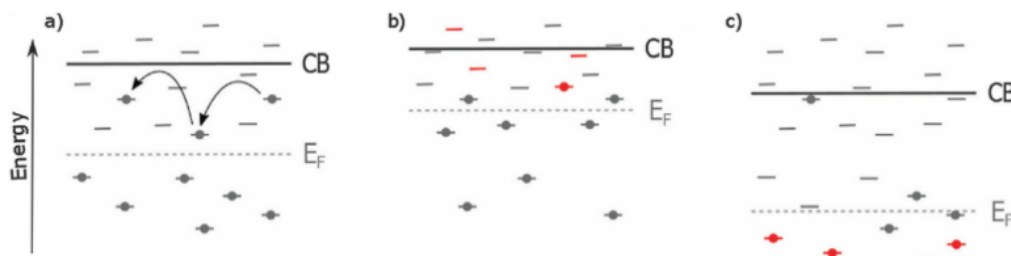

Fig. 1. Schematic visualization of the effect of TiO$_2$ doping on the CB and EF, showing the doping decrease (b) or increases (c) the deep trap density. (a) Pristine TiO$_2$. (Reprinted from Ref. [54], Copyright 2015 The Royal Society of Chemistry).

using first-principle study and hard X-ray photoelectron spectroscopy (HAXPES), discovered that the introduction N anion into the anatase lattice has created large scale oxygen vacancy in the lattice [55]. Altogether with the N impurity in the lattice and the oxygen vacancy has enabled a visible light photocatalyst in the N doped anatase TiO_2. While initially this process has been associated with the narrowing of the band gap or the effect of dopant N 2p state localization above the O 2p state valence band maximum, the HAXPES analysis showed that the N doping has created a tail like state of N 2p slightly below the O 2p state, decreasing the valence-band maximum to a lower binding energy. In their effort to obtain a clear description of the extent of N doping to the electronic properties of anatase, they have carried out a first-principle analysis. However, they discovered that the introduction of N anion has apparently created a tail like state at the conduction band edge (conduction band minimum). Although in contrast to the HAXPES analysis result that shows the tail like state at the valence band maximum, it could be related to an overestimation of the first-principle study method. Nevertheless, this result reveals the unique of tail-like state formation in the N anion doping. Moreover, the calculation also indicated that in the presence of N doping and oxygen vacancies, there is an impurity level at the Fermi energy. Thus, all these phenomena are the reason for the shifting of photosensitivity of N doped anatase TiO_2 to the visible region.

In an earlier study by Finazzi and Di Valentine utilizing a scanning tunnelling microscopy, it was shown that the incorporation of nitrogen in the (101) anatase lattice also generated the formation of localized state in the band gap. Moreover, the presence of N impurity in (101) anatase has also created more electron traps at the Ti^{3+} for the electron generated from the oxygen vacancy state [56]. Nevertheless, although N anion doping into the anatase TiO_2 has profound effect on the electronic and optical properties, the N anion dopant are vulnerable to degradation or loss from the lattice site upon continuous ultraviolet irradiation. Chadwick et al. in their recent study found that the N anion dopant has totally loss upon continuously irradiated with UV A light for 28 days, which is correspond to the solar light irradiation (Fig. 2). Certainly, this enlightens that the excellent performance of N doped anatase TiO_2 may permanently disappear with times of use under UV irradiation [24].

Interesting phenomena generated from non-metal doping in the anatase TiO_2 was further confirmed by Muhich et al. In their first-principle study on the effect of non-metal doping, i.e. B, C and N,

on (101) anatase TiO_2, it was demonstrated that the non-metal dopants anions create filled band gap state with energies higher than O $2p_\pi$, enhancing the adsorption and reduction of oxygen molecules [57]. In a separate study, Sambandan et al. also found that the C doping into the anatase TiO_2 significantly shifts the energy band edge into the visible region. This has enhanced the photocatalytic properties of C- TiO_2 in the degradation of carmabazepine for several order higher compared to pristine anatase TiO_2 [29]. However, despite the dopant effectively improve the visible light photoactivity, doping may at the same time creates BO_2, CO_2 and NO_2, due to the high exothermicity of O_2, on the surface of (101) anatase TiO_2, deactivating the O_2 reduction [57].

New interesting facts has also been recently discovered in phosphor (P) doped TiO_2, where the type of dopant species might determine the overall properties of P-doped TiO_2. For example, it was found that the P^{5+} species dopant could enhance the photo-generated carrier for several order higher compared to the pristine TiO_2, improving the photocatalytic properties. In contrary, in the region with P^{3-} dopant rich site, the photoactivity that is reflected by the generation of photogenerated electron was severely reduced, disrupting the photocatalytic performance of the TiO_2 [58]. Similar process was also observed in the case of anatase TiO_2 doping with S anion, where at a particularly low S concentration, a significant alteration in the energy band gap with the existence of impurity level due to a mixing of S 3s and O 2p states at the energy band gap was revealed. However, it produces impurity levels so that its photocatalytic activity lower than the P anion doping [59].

Abu Bakar and Caue Ribeiro indicated that the photocatalytic performance of anatase TiO_2 with rich (001) facets dramatically enhanced by introducing the N and S anions into the TiO_2 lattice. They found that the introduction of dopant has significantly shift the absorption edge to the visible region, enhancing the photo-responsivity of the anatase TiO_2. It was also observed that the (001) facet behaves as the reservoir for the photogenerated electron-hole pair, boosting the photocatalytic process at this crystallographic plane [60]. In separate study, Chung et al. indicated that the S anion doping into the anatase TiO_2 facilitate effective adsorption of organic dye onto the surface of anatase TiO_2 and accelerated the surface reaction. Meanwhile, the N anion doping enhanced the visible light absorption, improving the formation of delocalised state at the band gap [61]. Similar phenomena were also observed in the hydrogenated anatase TiO_2 [62,63] and doped with F anions [64] due to the formation of unique defect centers for enhanced charge transfer process to the adsorbed species for enhanced photocatalytic process, where in many cases, e.g. rutile case, the introduction of anion doping create Ti-interstitial. Meanwhile, in anatase, oxygen vacancy is favoured to be formed. For example Liu et al. [62] observed a remarkable enhancement in the photocatalytic of range of commercially available TiO_2 in the H_2 evolution reaction upon being hydrogenated at high pressure. In typical process, they found that the hydrogenated anatase TiO_2 demonstrated multiple order enhancement compared to the pristine anatase TiO_2 (See Fig. 3). HRTEM analysis indicated the development of large-density of defect centers in the materials for the promotion of charge transfer process, enhancing the photo-activated surface reaction process.

While the non-metal doping of N anions induces variety of impact on the optical and electronic properties of anatase TiO_2 [65], the obtained performance still can be further improved by many ways particularly via co-doping with boron [66], phosphor [67], fluorine [68], cobalt [14], tungsten [69], ammonia vapor treatment [70], carbon [71], niobium [10], vanadium [72], lanthanium [73] etc. The co-doping process was found to increase the N uptakes so that the oxygen deficiency as the origin for the improvement of photocatalytic process is enhanced. Meanwhile, the ammonia vapor
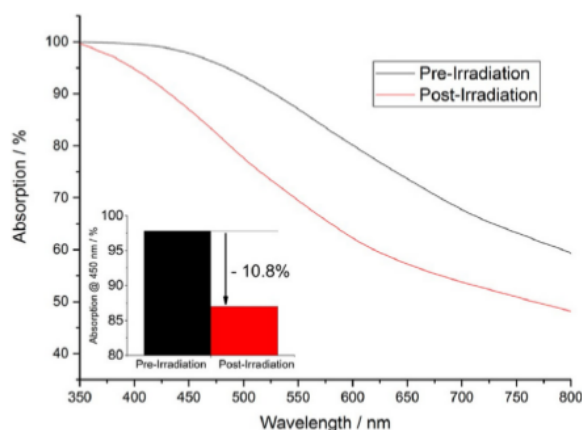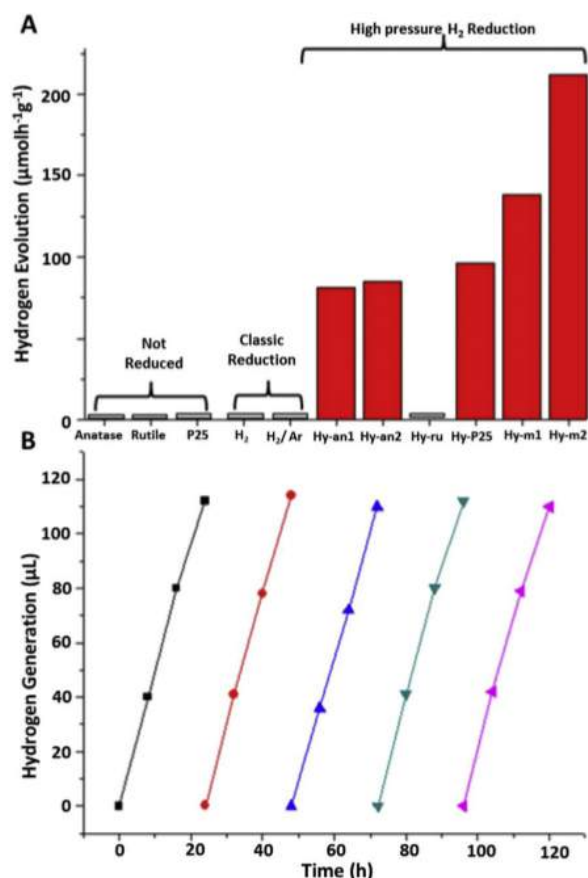

Fig. 2. Effect of photo irradiation on the optical density in TiO_2 nanocrystals (normalized to N content) after 28 days irradiation by UV A light. (Reprinted from Ref. [24], Copyright 2017 The American Chemical Society).

Fig. 3. Comparison of photocatalytic hydrogen evolution rate on TiO$_2$ particle of different anatase, rutile and mixed phase before and after hydrogenation (Hy-) under AM 1.5 (100 mW/cm^2) illumination at 500 °C, 20 bar treatment. b) Hydrogenated anatase samples (Hy-an1) performance in hydrogen production over 5 days of continuous AM 1.5 illumination. (Reprinted from Ref. [62], Copyright 2014 Wiley-VCH Verlag GmbH & Co.).

treatment may decrease surface electron-hole recombination by reducing surface trap via hydroxyl formation on the surface. Fig. 4 show typical photocatalytic performance of anatase TiO$_2$ when N anions dopant co-doped with other metal and non-metal dopants.

2.2.2. Metal-doped anatase TiO$_2$

More or less similar phenomena are also observed in the case of metal doped anatase TiO$_2$. Modification of valence and conduction band density of state are the most common effect observed for the enhancement of optical and electrical properties of metal doped anatase TiO$_2$. Transition metal is the most often used metal in the purpose of modification of intrinsic properties of anatase TiO$_2$. The most common metal used for doping from this group are Au, Ag, Pt, Pd and Cu. In typical study, they expand the catalytic properties of anatase TiO$_2$ and have a profound effect in the narrowing of the energy band gap of anatase TiO$_2$, enabling visible light photo-activation in catalysis application.

Zhang et al. demonstrated that by introducing W cation into the anatase TiO$_2$ found that the position of the doped TiO$_2$ conduction band decrease (positive shift) with the increasing of W doping content. Such positive shift has several profound effect such as suppression of electron-hole recombination and expanding the carrier life time [74], an important parameters for excellent photocatalytic properties.

Electron paramagnetic resonance (EPR) spectroscopy indicated that the metal doping may decrease the photogenerated electron-hole recombination and increase charge carrier for photoactivity. It is envisaged that the metal doping functioned as a center for adsorbed species evolution [75]. Jovic et al. [75] examined such effect in the study of interfacial charge transfer phenomena and any process that takes a role in the enhanced photoactivity of TiO$_2$ nanostructure in the presence of Au metal impurity in the H$_2$ production from ethanol under UV irradiation. They evaluated electronic excitation under magnetic field via EPR in pure anatase and rutile phases and mixed anatase-rutile phase. They also discovered that in the pure anatase TiO$_2$, hole and electron trap sites, from the surface and lattice sites, especially at the Ti^{4+}, are both exist and play a critical role in charge transfer process. This is indicated by the presence of intense peaks at a proportionality factor g normal of 1.990 and weak and broad peak at g parallel of 1.958 under high magnetic field (See Fig. 5A–B). Another strong signal at high magnetic field, namely at g normal of 1.975, is observed in both pure anatase and P25 TiO$_2$ sample. This signal is actually generated from rutile phase electron trap. The existence of rutile phase can be simply understood due to phase purity issues, which in many case its presence plays a critical role in facilitating facile electron transfer at the anatase-rutile interface.

Surprisingly, the signal related to the electron trap at the surface and lattice site is reduced in the presence of Au nanoparticle in the TiO$_2$ system (see Fig. 5C at the g normal 1.990 and 1.975). This is a strong indication of an active charge injection from both anatase and rutile phase has been occurring. This reveals that under UV excitation large portion of photoexcited in rutile will transport to the anatase via a distorted Ti^{4+} sites, which then separated and is available for a photoreaction. The charge separation become more active in the presence of Au metal nanostructure that is existent at the anatase-rutile interface. Thus, highly efficient H$_2$ gas production can be realized from ethanol oxidation (See Table 1).

The catalytic performance of anatase TiO$_2$ enhanced due to the effect of the presence of a surface species. This effect has helped the generation of active hydroxyl radical species for rapid photo-degradation of contaminant molecules. In this case, it is elucidated that the presence of doping on the surface of anatase TiO$_2$ has promoted the reaction and behaved as co-catalyst along with the anatase TiO$_2$ [76]. For example, the photocatalytic performance of the anatase TiO$_2$ dramatically enhanced when it is being co-doped with Mn and Ce, which is much higher compared to individual photocatalytic performance of Mn and Ce doped TiO$_2$ (see Fig. 6). Spectrokinetic analysis of the reaction reveals that the co-doped system has enhanced the formation of hole related species, accelerating the photo-oxidation of toluene. It is well-known that toluene photo-oxidation on TiO$_2$ is a hole triggered reaction. The introduction of Mn into the TiO$_2$ further increase the density of hole related species formation in the TiO$_2$ system. Addition of such high-performance into intrinsically high photocatalytic activity of Ce doping on TiO$_2$, co-doped TiO$_2$ system with exceptionally high photocatalytic performance is achieved.

C. Christoforidis and Fernández-García discovered that the introduction of Cu^{2+} and V^{4+} into the anatase TiO$_2$ has modified the photocatalytic properties in oxidation of toluene. They found that the photocatalytic properties is metal doping dependent where
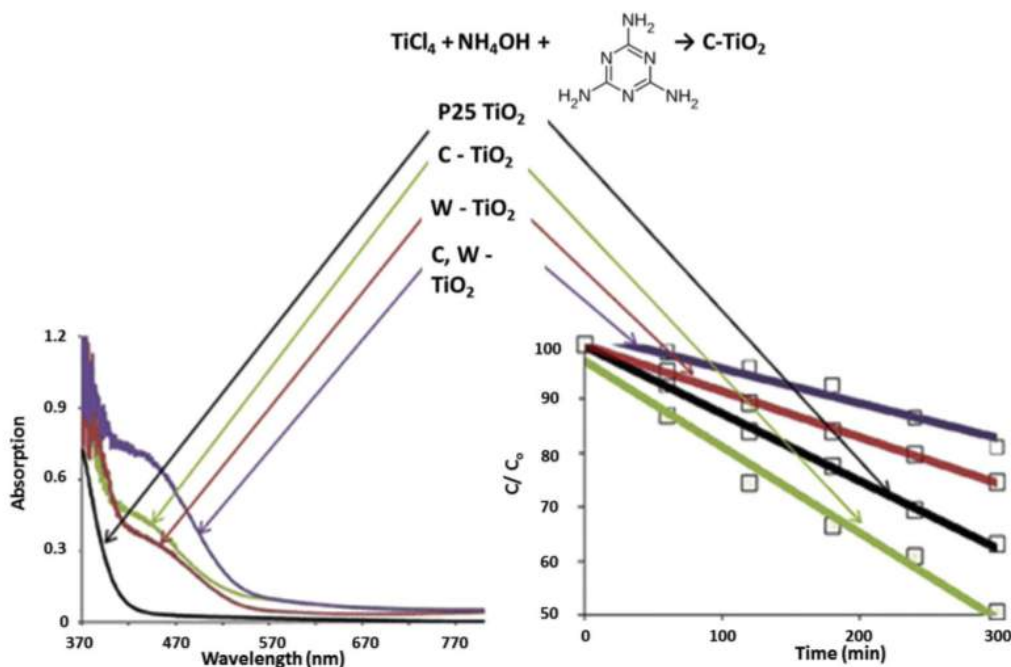
Fig. 4. Photocatalytic performance of TiO₂ upon being doped with several elements. (Reprinted from Ref. [71], Copyright 2012 American Chemical Society).

low-level doping was suitable for enhanced photodegradation of toluene via facile separation of photogenerated electron-hole pair. Meanwhile, high doping level may retard the photoactivity because of the metal dopant may act as the recombination center. They also realized that the metal doping functioned as the center for the photoinitiated charge formation. From this work, the mechanism for the improvement of the photocatalytic properties of anatase TiO₂ via metal doping and provides avenue for further enhancement in the performance is envisaged [25]. It has also been shown that the photoactivity of the anatase TiO₂ effectively enhanced by Sm^{3+} anion doping. It was obtained that the resonant excitation energy transfer between the anatase TiO₂ surface and the gaseous species was improved upon being doped as the result of active function of metal dopant anion as the center for energy transfer, enabling facile energy transfer to the trapped state (defect), which in turn transferred to the adsorbed gaseous analytes for enhanced gas sensing performance [77].

Recent study by Lian et al. on the Pt doped anatase TiO₂ showed that the existence of Pt, besides modifying the band edge absorption and the Fermi level, creates a Pt–O bridge on the surface of the anatase lattice and facilitates a facile transfer of high-density photogenerated electron from bulk to the surface of the doped anatase TiO₂. They found that the density of photogenerated electron transfer increases as high as 2.5 times compared to the pristine anatase TiO₂. This properties will enhance the reduction of H^+ to produce H₂ [31]. Similar phenomena were also observed in Mo doped anatase TiO₂. By incorporating a Mo layer via reactive electron beam etching forming an array of trenches on the surface of anatase TiO₂, the photogenerated electron improved up to 56 times compared to the pristine anatase TiO₂ and linearly depend on the thickness of the Mo layer (See Fig. 7A). The system was operated at the visible light region [32]. It is assumed as the result of the existence of large density of carrier located at the bottom of the trenches, which is hardly saturated and exhibits a linearly

increasing with the depth of the trench (Fig. 7B–D). It is indicated that the sharp current increase is due to an extremely large parallel diffusivity of the carrier in the films compared to the perpendicular diffusivity. This is related to the effect of the difference in the Fermi level of the base that is higher than the surface layer, generating a self-built electric field directed toward the surface layer at the interface. Thus, electron will be swept into the bottom layer, while holes to the surface layer, during the light illumination. Because of the carrier transport within the depletion layer is fast, the recombination between electron and hole is neglected.

In different metal doping of anatase TiO₂, i.e. tantalum (Ta), unique effect was induced by the dopant on the electronic and optical properties of doped anatase TiO₂. In typical procedure, the presence of Ta in the TiO₂ lattice has also improved the charge separation for potential solar driving water splitting. This unique facile charge separation was enabled by the existence of facile phase segregation of Ta both in bulk and the surface of anatase TiO₂ during the growth process relative to the applied redox potential, where the segregation of Ta on the surface is higher under oxidizing condition and lower under reducing condition, manifesting the accumulation or depletion of Ta on the surface during the photoprocessing. Thus, this allows a better control over the photoactivity of Ta-doped TiO₂ in photocatalytic water splitting applications [78].

Wang et al. via first –principle study demonstrated a generalized understanding on the effect of the introduction of metal dopant into the lattice of the anatase TiO₂. In their study, they used a local density approximation (LDA) exchange-correlation functional with Perdew-Burke-Ernzerh generalized gradient approximation (GGA) that is implemented in Castep module and carried out the calculation on the anatase lattice model with $2 \times 1 \times 1$ supercell model. The doping were carried out by substituting the Ti atom with 3d transition metal atom (V, Cr, Mn, Fe, Co, Ni, Cu and Zn) and 4d transition metal atoms (Y, Zr, Nb, Mo and Ag). The energy
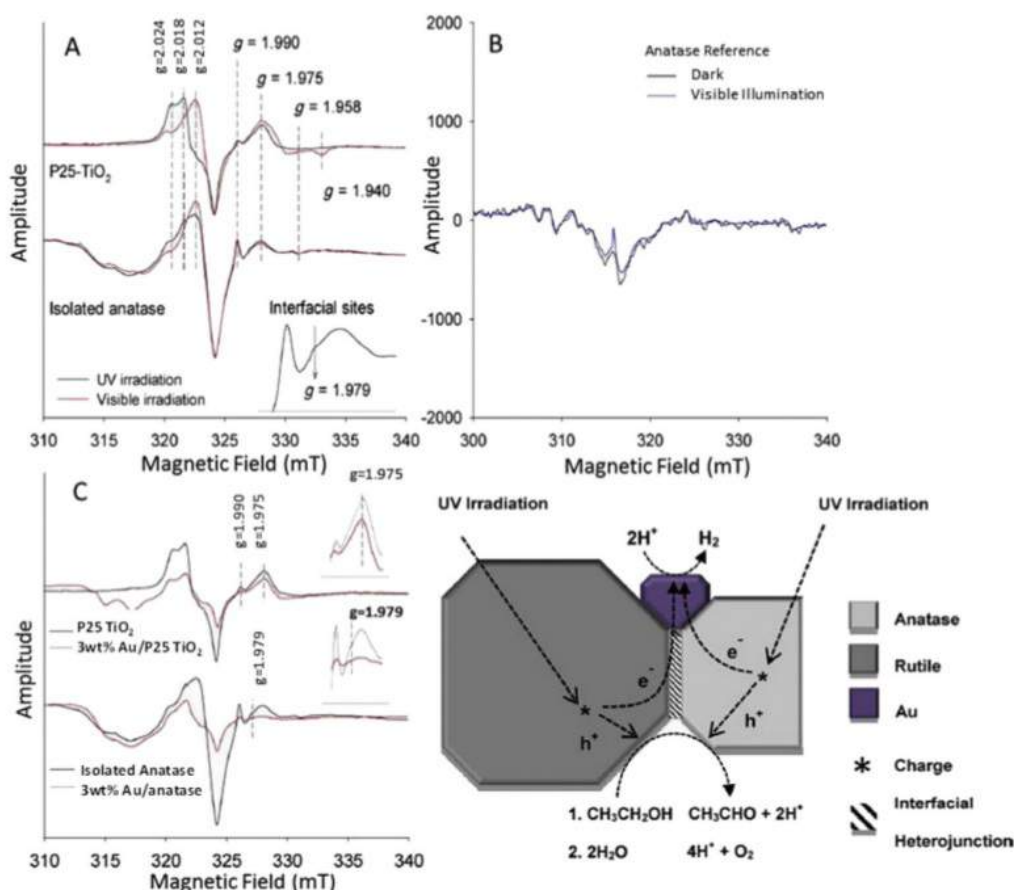
Fig. 5. A. Comparison of EPR spectra of P25 TiO₂ and isolated anatase under irradiation of UV (black lines) and visible (red lines) light. Inset: High-resolution scan of the isolated anatase spectrum showing the electrons trapped at residual anatase-rutile interfacial sites. B. EPR spectra of anatase reference powder. C. Corresponding EPR spectra of P25 TiO₂ and isolated anatase after being doped with 3 wt% Au/TiO₂ under UV irradiation and its expanded scan (insets). The cartoon is the proposed mechanism for photocatalytic H₂ production from ethanol/water mixtures over Au/P25 TiO₂. (Reprinted with permission from Ref. [75], Copyright 2015 Wiley-VCH Verlag GmbH & Co.). (For interpretation of the references to colour in this figure legend, the reader is referred to the web version of this article.)

Table 1
The physical and photocatalytic data for the various TiO₂ and Au/TiO₂ photocatalyst. (Reprinted from Ref. [75], Copyright 2015 Wiley-VCH Verlag GmbH & Co.).

Sample	Mean Au particle size (nm)	S_{bet}^a (m^2g^{-1})	($mmol\ g^{-1}\ h^{-1}$)	H₂ production rate ($mmol\ m^{-2}\ h^{-1}$)	($mol_{H2}\ molAu^{-1}\ h^{-1}$)
P25 TiO₂	–	49.6	1.3	0.025	–
Anatase (from P25 TiO₂)	–	51.2	1.4	0.027	–
Rutile (from P25 TiO₂)	–	30.4	0.4	0.014	–
3 wt% Au/P25 TiO₂	5.50	46.5	31.5	0.676	221
3 wt% Au/P25 TiO₂	5.49	48.5	21.7	0.447	147
3 wt% Au/P25 TiO₂	5.45	27.9	10.3	0.369	72
Physical mixture[b]	5.50	45.4	17.0	0.374	120

[a] Brunauer-Emmett-Teller surface area.
[b] Physical mixture: 3 wt% Au/anatase +3 wt% Au/rutile (85:15 wt%).

gap of anatase TiO₂ has significantly changed up to 0.27 and 0.54 eV when being doped with 3d and 4d transition metal atoms, respectively, dependent on the type of the metal dopant used (Fig. 8). They also found that the impurity levels formation in the doped anatase TiO₂ were mainly due to the hybridization of 3d or 4d state of dopant with O 2p and Ti 3d states. Such effect has significantly shifted the photoactivity of the doped anatase TiO₂ into the visible region [79].

3. Porous and doped (001) faceted system

Lattice structure of anatase TiO₂ with (101) and (001) facet are shown in Fig. 9. In typical synthetic process, anatase is thermodynamically grown into a nanostructure that ends with a highly stable face, namely (101) plane. This plane is characterized with rich 6 coordination (6c) of Ti ion, which is the most stable state of Ti in the lattice and 5c Ti ion that are topologically buried under the background of 2 and 3 coordination of O ions. Such geometry makes the

(101) face relatively stable and inert compared to the high-energy facet of anatase polymorph, such as (001) face. As can be seen from Fig. 11b, i.e. the geometry of high-energy facet of (001) face, its geometry is much different compared to the (101) face, where in (001) plane the surface is characterized by the highly energetic 5c Ti ions with a highly active 2c O ions at the topmost of the surface. With Ti−O bond on the (001) surface is much higher compared to the Ti−O bond in (101) up to 1.2% higher, the electron density distribution along the bond become weakly bound to the atoms, generating highly energetic electrons that are vulnerable for an active charge transfer and surface reaction as well as optical interactions.

The surface atoms of (001) faceted anatase TiO₂ reconstructs to (1 × 4) and the entire properties produced from the (001) faceted structure are originated from such this surface atoms construction [80,81]. The atomic site with reduced Ti pairs or oxidized Ti pairs plays a key role in the chemical activity of the surface. For example, it has been witnessed in the dehydrogenation methanol via the formation of water molecules at the defect site. The methoxy are then form the site and further generates CH₃ radical, forming formaldehyde and again methanol via disproportionation reaction. Large-range of distinguish properties of (001) faceted anatase TiO₂ in current existing application have then been discovered. In a recent study, it was found that the (101) facets could only absorb water molecules on its surface while the (001) facets could dissociate the water molecules, thanks to its high- unsaturated Ti atoms on the surface, producing hydroxyl radicals [82]. Similar chemical activity has also been observed in wide range of organic species adsorption on these surface, such as bacterial inactivation [82,83], verifying the unique surface chemistry of (001) high-energy facet of anatase TiO₂, promising high-performance in current applications.

3.1. Synthetic methods

3.1.1. Non-porous systems

There have been a couple of method to realize a thermodynamically stable (001) faceted- TiO₂ nanostructure. They can be grouped into two-general method, i.e. hydrothermal and solvothermal. The key parameter in the preparation of (001) faceted anatase TiO₂ prepared using these two procedures lay on the
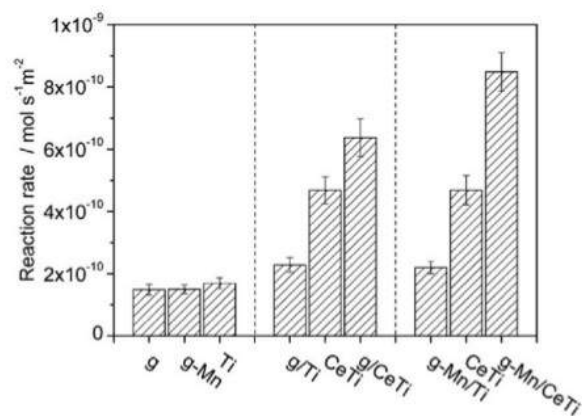

Fig. 6. Toluene photooxidation (C0 = 700 ppm, relative humidity = 70%, T = 30 °C) on Mn and Ce doped TiO₂. (Reprinted from Ref. [76], Copyright 2014 The American Chemical Society).
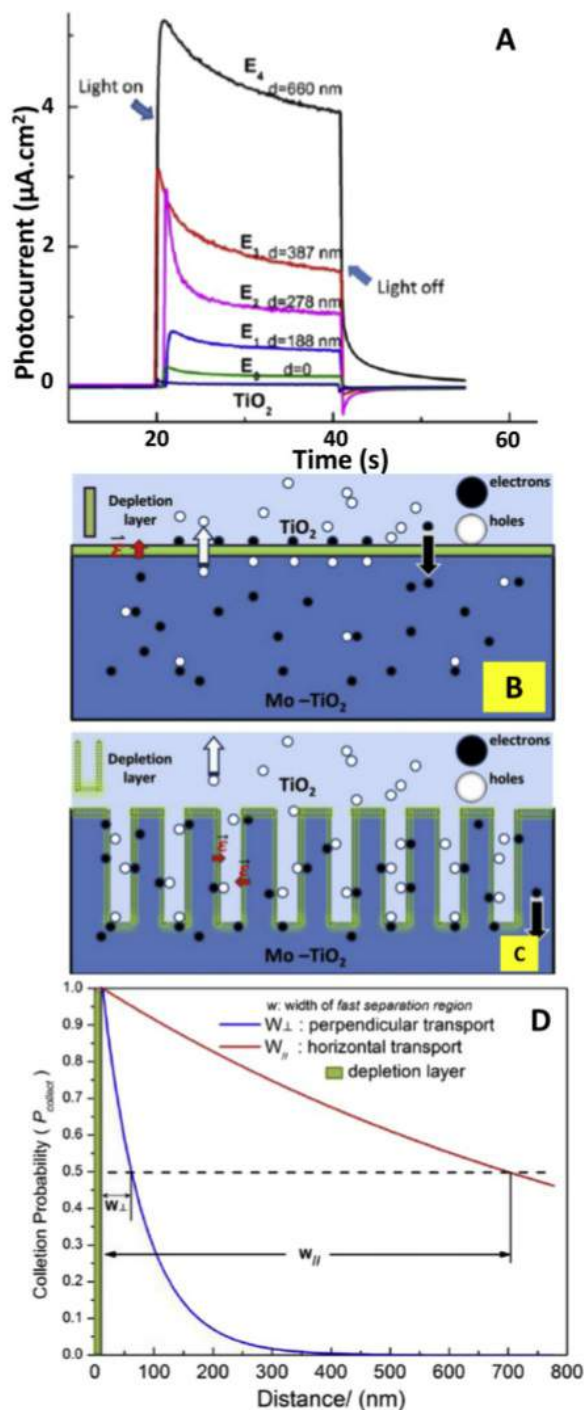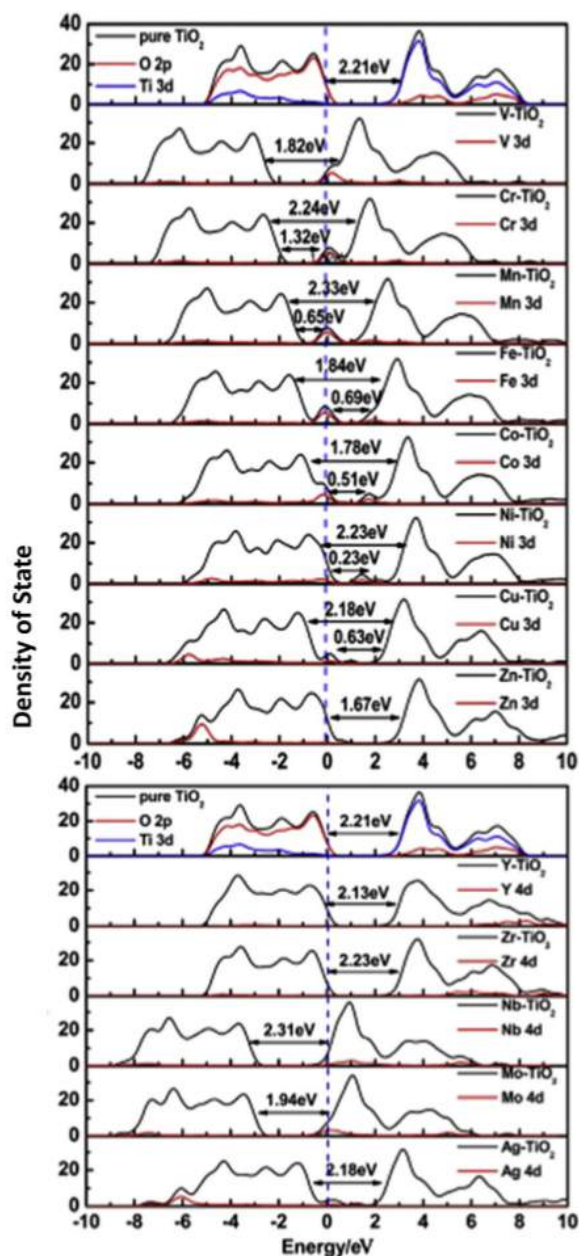

Fig. 7. (A) Photocurrent density in samples with different etching depths (B and C) Schematic of the carriers transfer near a planar and array depletion layers. (D) Relation between the collection probability and distance away from the edge of a depletion layer. (Reprinted from Ref. [32], Copyright 2014 The American Chemical Society).

Fig. 8. (Top panel) Comparison of the TDOS and PDOS of 3d transition metal-doped TiO$_2$. Black, red and blue-dashed lines are TDOS, impurity's 3d states and Fermi level, respectively. (Lower panel) Comparison for the TDOS and PDOS of the 4d transition metal-doped TiO$_2$ with pure TiO$_2$. (Reprinted from Ref. [79], Copyright 2014 Springer International Publishing AG). (For interpretation of the references to colour in this figure legend, the reader is referred to the web version of this article.)

directing agent or the surfactant used during the reaction. The key materials can be fluor, amine, malic acid and etc [85]. For example, Liu et al. realized the formation of (001) facet rich anatase TiO$_2$ via a malic acid assisted-hydrothermal synthesis [86]. The approach is very simple involving the dripping of TiCl$_4$ into 50 mL of deionized water containing D,L-malic acid (about 1.82 mmol) and 0.3205 g of polyvinylpyrrolidone (PVP, MW~ 40 000). The solution mixture was transferred into a 30 mL Teflon-lined autoclave for a hydro-thermal reaction at 120 °C for 10 h. In the typical procedure, (001) faceted nanocrystal of anatase TiO$_2$ were formed and the structure can change to boxed by modifying the ratio between the malic acid and TiCl$_4$ precursors (see Fig. 10). The evolution of (001) faceted TiO$_2$ nanocrystal is assumed due to the accelerated Oswald annealing process of the structure in the presence of maleic acid and the existence of high-yield structural crack in the body of the nanocrystal. It should find potential application for reactor applications.

Hydrolysis of titanium complex in the presence of tetra-fluoroborate ionic liquid [87] has also been demonstrated. For example, Zhao et al. effectively realized the formation of (001) faceted anatase TiO$_2$ nanocrystal by applying a solvothermal approach on a mixture of titanium tetraisopropoxide (TTIP) in acetic acid (HAc) in the presence of an ionic liquid 1-butyl-3-methylimidazolium tetrafluoroborate ([bmim] [BF$_4$]) capping agent. The dimension of the nanocrystal were found to be strongly dependent on the reaction condition particularly the composition of [bmim] [BF$_4$], water, and HAc in the quaternary solution system. The formation of nanocrystal of anatase TiO$_2$ with (001) facet is assumed to be due to the effective capping of ionic liquid molecules on the (001) facet of anatase TiO$_2$.

Surface fluorination [88–90] was also recognized as a powerful method to promote the formation of (001) facet rich anatase TiO$_2$ nanocrystals. For example, Yang et al. have succeeded to control the portion of (001) facet in the anatase TiO$_2$ nanocrystal by simply adjusting the hidrofluoro acid concentration in a hydrothermal synthesis of TiO$_2$ [88]. Hydrothermal of titanium complex in hy-drofluoric acid [91] and benzyl alcohol in the presence of oleyl amine [92] media, and liquid-phase deposition method in the absence of fluoride scavenger [93–96], etc., were also discovered to be capable for the preparation of (001) faceted anatase TiO$_2$. However, amongst the available techniques, surface fluorination is considered as versatile approach for controlling the faceting in the nanocrystal of anatase TiO$_2$ [88] as its capability to change the surface energy of the facet. So far, via the fluorination method, the percentage of facets on the anatase TiO$_2$ crystal can be controlled, for example the (001) facet portion can be upgraded from 18% up to 90% by simply controlling the reaction condition and approach (Fig. 11). A clean, free-fluorine surface can then be obtained via calcination without deteriorating the surface structure and morphology.

So far, fluorinated method was thought to be the most versatile method to obtain (001) faceting in the TiO$_2$ nanostructure. How-ever, non-fluorinated process has also been reported by several researcher that included the solvothermal alcoholysis of TiF$_4$, gas-phase thermal oxidation of TiCl$_4$ or borate-based ionic liquid surfactant and surface chlorination using hydrochloric acid. Similar to fluorinated method, the anatase TiO$_2$ nanostructure produced using these method also indicated a variety of morphology including nanocube, nanosheet and other platonic morphologies. Cheng et al. [97], for example, used hydrochloric acid (HCl, 36.5–38 wt %) that was diluted with 1 mL of water and added into toluenic solution of titanium n-butoxide [Ti(OC$_4$H$_9$)$_4$, TBT] and was transferred into an electric oven for a hydrothermal reaction at 180 °C for 24 h. It was found that thin nanosheet of anatase TiO$_2$ with (001) facet has been successfully obtained. In their approach, the typical nanosheet dimension was ranging from several ten to hundreds of nanometers (Fig. 12). The nano-sheet was single crystalline in nature.
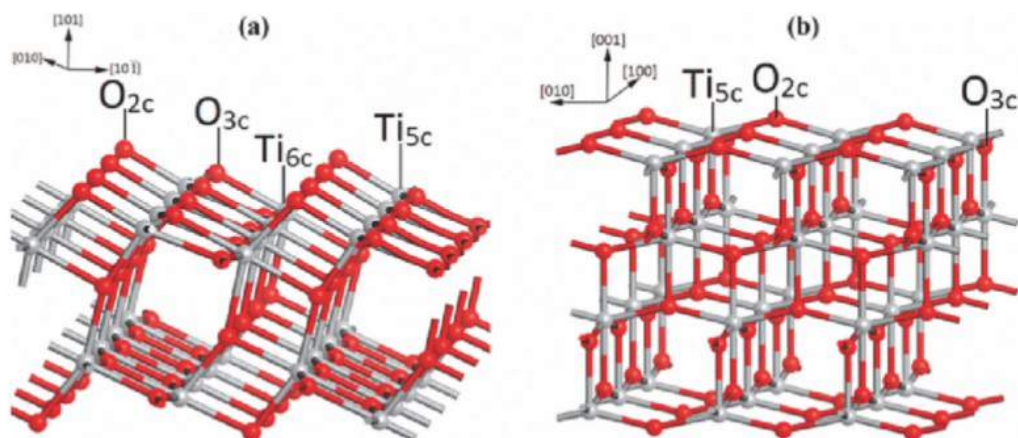
Fig. 9. Lattice structure of (101) (a) and (001) (b) planes of anatase TiO_2. (Reprinted from Ref. [84], Copyright 2014 The American Institute of Physics).

Chen et al. [98] reported a different versatile method to grow anatase TiO_2 nanocrystal with variety of morphology and high-energy facet percentage via microwave-assisted topochemical conversion reaction. Layered titanate structure of $K_{0.8}Ti_{1.73}Li_{0.27}O_4$ (KTLO) that was synthesized by hydrothermal treatment of 5.1 g of KOH, 0.6 g of $LiOH \cdot H_2O$, and 6.9 g of TiO_2 (anatase form) in 25 mL of distilled water at 250 °C for 24 h was firstly prepared in this study. The sample was then treated in a 0.2 M HNO_3 solution for 24 h to facilitate ion exchange between lithium and potassium ions with hydrogen. Layered titanate of $H_{1.07}Ti_{1.73}O_4$ (HTO) was obtained from this process and it was dried under freeze condition. The HTO colloidal was prepared by mixing the sample with 0.1 M of n-propylamine and was stirred for 24 h. The pH of the colloidal solution was adjusted using HCl and KOH. The anatase TiO_2 nanocrystal were then prepared by following a microwave-assisted hydrothermal process under a temperature of about 175 °C. Typical results are (001) faceted nanocrystal with several portion of different facet, depending on the reaction condition, particularly the temperature of the reaction (microwave power), pH of the reaction and reaction time. Fig. 13 described a general picture of morphology transformation of anatase TiO_2 under different reaction condition. For example, under different microwave power, the morphology of the anatase TiO_2 nanocrystal changed from amorphous-like morphology to well-defined platonic structure
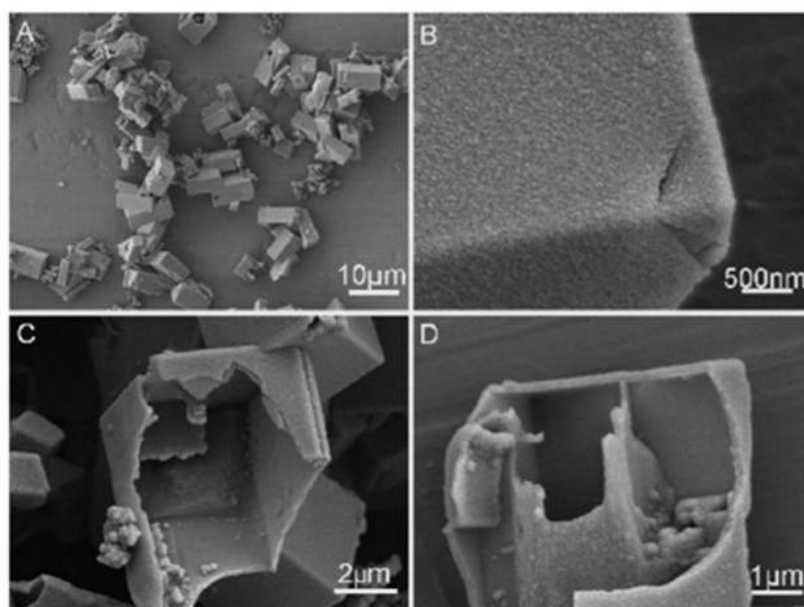
Fig. 10. (A–D) Typical FESEM images of (001) faceted anatase TiO_2 prepared using malic acid assisted hydrothermal process prepared at 120 °C for 10 h. (Reprinted from Ref. [86], Copyright 2009 The American Chemical Society).

when the hydrothermal temperature increased from 95 to 175 °C. Meanwhile, under the temperature of 175 °C, the nanocrystal morphology changed from square shape nanosheet to platonic nanorods when the reaction time elongated from 1.5 h to 11.5 h (Fig. 13). This method provides a versatile strategy to obtain nanocrystal with different percentage of active crystalline facet for specific in applications, such as photocatalytic and DSSCs.

The use of amines functional group surfactant has also been capable for controlling the facet growth in the TiO₂ nanocrystals. Roy et al. [28], for example, added a diethyl amine (DEA) into a reaction that contains TiO₂ precursor of titanium tetraisopropoxide and tetrabutyl ammonium hydroxide (TBAH). The growth process was carried out using a hydrothermal method. It was found that by changing the concentration ratio between TBAH and the DEA, the amine surfactant, the morphology of the TiO₂ nanocrystal could be control from nanorod, nanocubes and nanosheet with different dominant facet exposure (See Fig. 14). As can be seen from the figure, the control of morphology indicated the possibility to obtain TiO₂ nanostructure with particular facet

dominant structure. For example, the nanorods, the dominant facet is (101) that contains up to 70% of the total area of the nanorods. Meanwhile, the nanocubes, the dominant facet is (001) with almost 100% of total surface area. Such nanostructure with particular unique morphology has enabled the study of facet-related physicochemical and photo activity properties in the anatase TiO₂ nanostructures (see Table 2).

3.1.2. Porous system

There are various method to prepare porous anatase TiO₂. In Table 3 we summarize several available methods to date that are available for the preparation of anatase TiO₂. They can be grouped into several general categories, i.e. template, etching, alcoholysis and surfactant directed methods. Although the methods are very versatile to grow anatase TiO₂ nanostructure with exceptionally high porosity properties, nevertheless, most of the methods realized the formation of porous TiO₂ nanostructure with morphology containing less-reaction facet, such as (101) plane. However, the method that leads to the formation of porous TiO₂ nanostructure
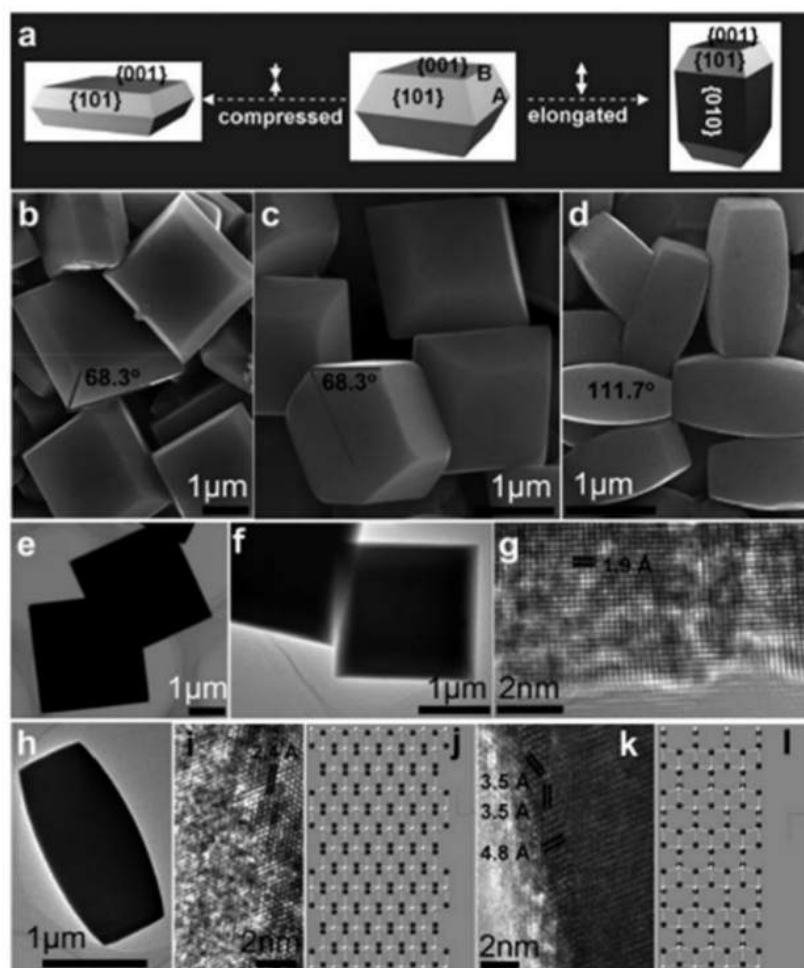
Fig. 11. Typical structure of (001) faceted anatase TiO₂ crystals prepared via fluorination method. (a) Schematic illustration of facet portion in anatase TiO₂. (b–d) Typical morphology of TiO₂ nanocrystal prepared using different concentration of HF (120, 80, and 40 mL) (e-h,j,k) Typical low and high-resolution TEM images of the samples with different morphology. (j, l) Schematic atomic models along 1½ 10 and [010] directions; white Ti4+, black O₂. (Reprinted from Ref. [88], Copyright 2008 Nature Publishing Group).
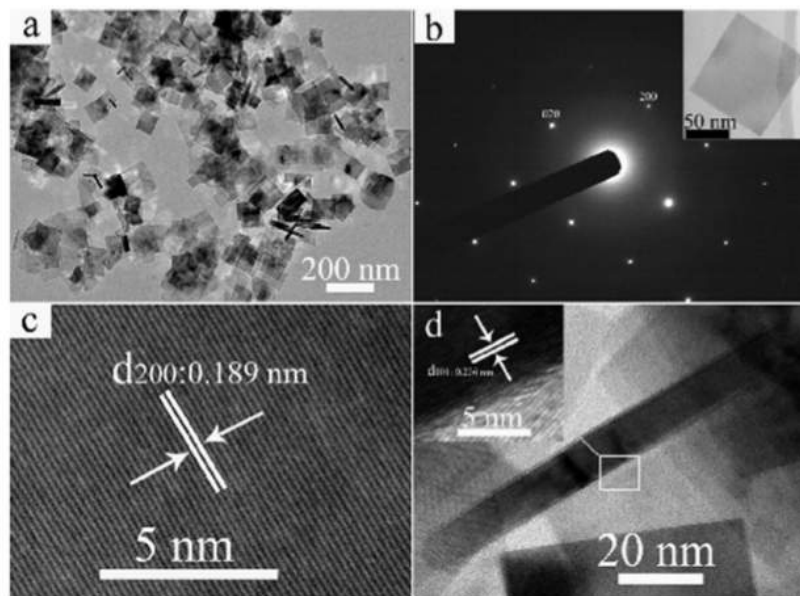
Fig. 12. Typical FESEM image of anatase TiO$_2$ prepared using alcoholysis method. (a and b) Low-magnification TEM image and SAED pattern of TiO$_2$ nanosheet sample., and (c and d) corresponding HRTEM image of flat and vertical orientation anatase TiO$_2$ nanosheet. (Reprinted from Ref. [97], Copyright 2014 The American Chemical Society).

with high-energy facet have been limitedly demonstrated up to this stage. In the following, we will discuss a few typical synthetic strategy of the available method in each group that are capable for the formation of porous morphology containing high-energy facet of (001).

3.1.2.1. Template method. In many approach, templated porous synthesis provide facile strategy to obtain TiO$_2$ nanostructure with controlled porosity properties. Depending on the type of template used, the method can be further grouped into the hard and soft template approaches. The hard template approach is normally used hard inorganic template as the scaffold of mesoporous TiO$_2$ nano-crystal growth. Meanwhile, the soft template approach always uses organic materials as the scaffold for TiO$_2$ nanostructure growth, such as metal organic framework or MOF, polymer template, lipids or protein template, surfactant template, etc. Quite recently, gra-phene has also been used as the template for producing porous TiO$_2$ nanosheet. By combining the template and suitable deposition methods of TiO$_2$ layers, such as sputtering, atomic layer deposition, liquid phase deposition, electrochemical deposition, hydrothermal methods, etc., as well as using an appropriate method for removing the initial templates, TiO$_2$ nanostructure with large-range of porosity and morphology properties can be realized.

Regarding the hard template method, common template used is highly-ordered porous silica. For example, Zheng et al. [117] re-ported that by using silica templates coupled with a hydrothermal growth method could produce anatase TiO$_2$ with controlled porosity properties with nanostructure basal plane of (001). The porous anatase TiO$_2$ were formed via a negative replication of silica template and the porosity properties depended on the growth parameter, including hydrohalic acid condition, seed density, and temperature. In typical process, they prepared a silica template using powder of as synthesized silica spheres (approximately 5 g) by mixing them into a dilute aqueous solution of titanium tetra-chloride (TiCl$_4$). The mixture was heated at 70 C for 1 h. After that the silica template were rinsed and then re-sintered at 500 °C for

30 min with ramping time of 150 min. From this process, they were successfully prepared TiO$_2$ nanoseed on the surface of silica spheres template. The porous anatase TiO$_2$ were then prepared by following a hydrothermal method at 150–220 °C for 12 h. The reaction contained a titanium butoxide in a solvent of mixture of water and hydrofluoro acid (50%) and 360 mg seeded-silica templates. The samples were then collected via a centrifugation and the silica template was removed by etching in 2 M NaOH at 80 °C for 1 h. (see Fig. 15).

In Fig. 15, it is also shown typical mesoporous anatase TiO$_2$ product obtained from this process. As can be seen from the figure, the typical product is mesoporous nanoseed with pore diameter as high as approximately 50 nm. Sheet morphology was assumed to form due to the presence of F anion that actively attach onto the growing crystalline facet of the TiO$_2$ and modify its surface energy. Thus two-dimensional crystal growth was achieved. The dimension of the nanosheet is quite large with edge-length varied from 700 to 800 nm with thickness as low as 150 nm. One interesting point highlighted in this study was no nanosheet morphology were ob-tained when the F anion absence in the reaction.

The porous TiO$_2$ gave excellent performance in hydrogen evo-lution reaction due to synergetic effect of wide surface area and exposed high energy facet of anatase TiO$_2$. They also found that the enhanced photocatalytic performance is due to the combinative activity of high-energy facet rutile TiO$_2$ (110) and anatase (001) in the porous TiO$_2$ which provides reductive site for photoreduction process and oxidative process, respectively. These feature promise excellent strategy for energy conversion purpose utilizing porous TiO$_2$ nanostructure.

In separate study, Crossland et al. [19] used similar method with a modification to prepare mesoporous anatase TiO$_2$ (see Fig. 16). By controlling the concentration of TiCl$_4$ during the seeding process on the silica template, the morphology and porosity can be controlled. The mesoporous anatase TiO$_2$ may then accommodate high loading of organic perovskite, realizing a high-performance perovskite so-lar cell system. In the typical procedure, the power conversion
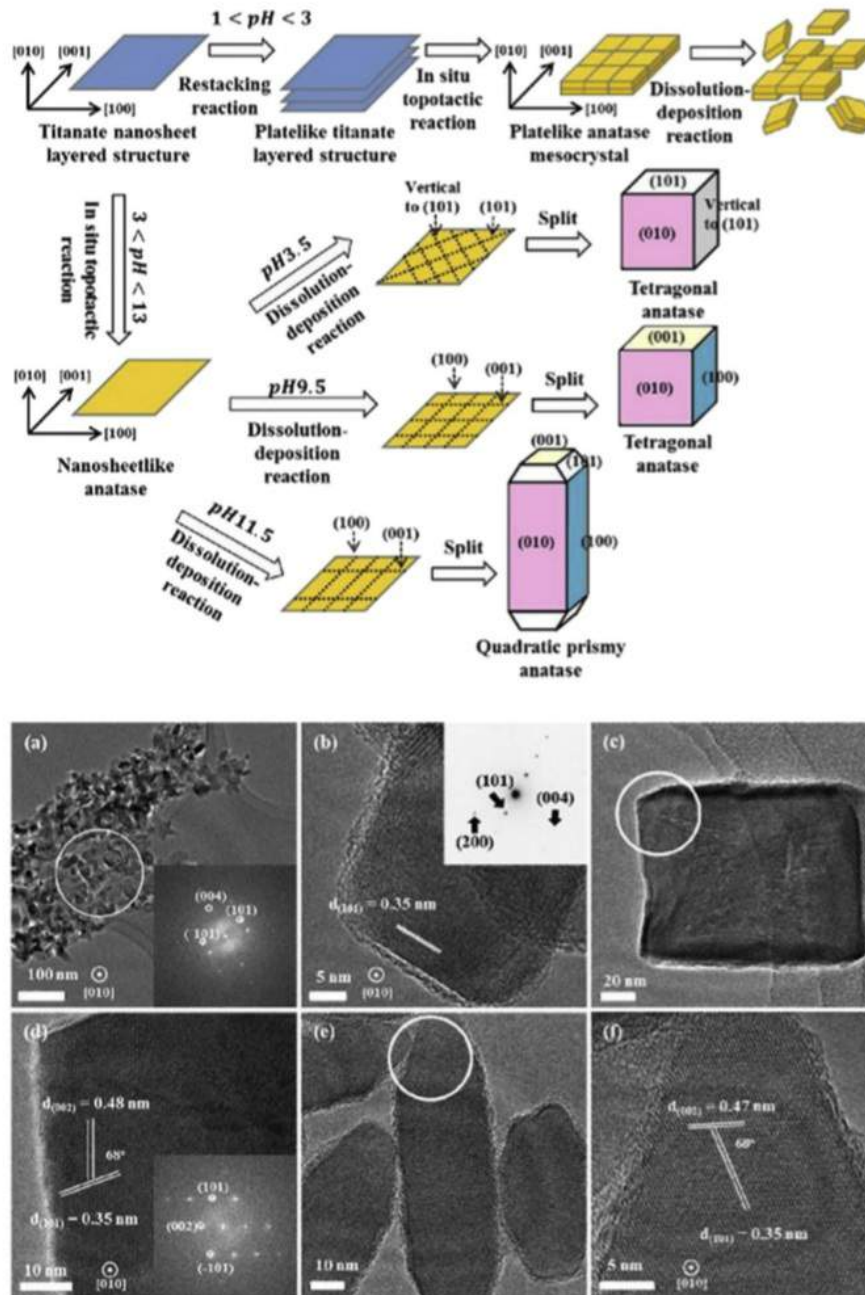
Fig. 13. (Top panel) Mechanism of the formation of (001) faceted anatase TiO_2 via microwave-assisted topochemical reaction. (Lower panel) Typical HRTEM image of (001) faceted anatase TiO_2 nanocrystals prepared using different reaction time, i.e. (a) 1.5, (b) 3.5, (c) 9.5 and (d) 11.5 h, respectively. Microwave power was 175 mW. (Reprinted n from Ref. [98], Copyright 2014 The American Chemical Society).

efficiency as high as 7.3% was achieved, thanks to high-surface area and an efficient carrier transportation in such highly-porous anatase TiO_2 system.

Different hard template has also been used in the synthesis of hollow and porous two-dimensional anatase TiO_2 nanostructure, such as demonstrated by Song et al., namely using α-Fe_2O_3 nanoplates [118]. In typical process, the two-dimensional hollow

nanoplates of TiO_2 were obtained by depositing the TiO_2 precursors onto a removable α-Fe_2O_3 nanoplates via a hydrothermal method. In normal process, the template were removed by using phosphate ion etchant. Two-dimensional nanostructure of anatase TiO_2 with average diameter and shell's thickness of approximately 600 nm and 30 nm, respectively, were the typical of the product.

There are still many hard templates [85] that have been used in
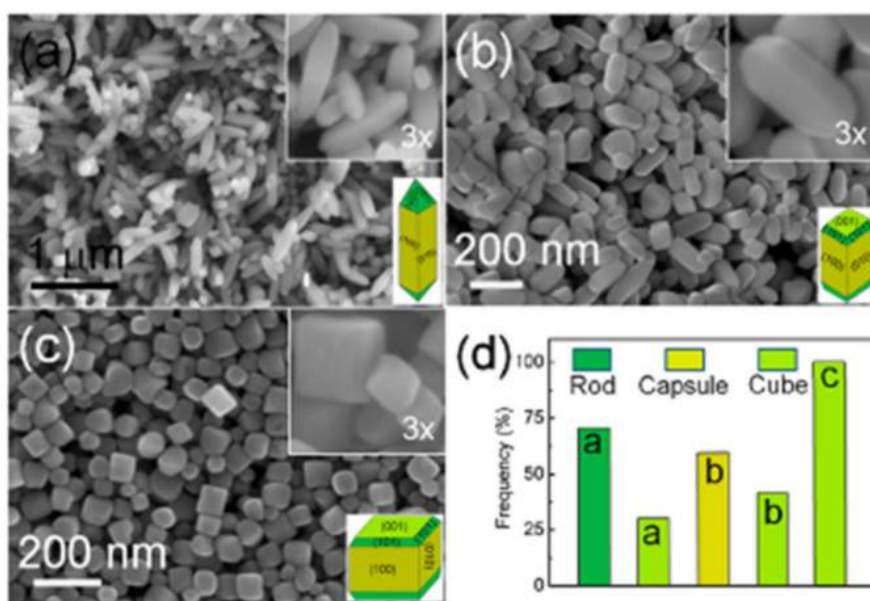
Fig. 14. Typical FESEM image of anatase TiO_2 nanocrystals prepared using different TBAH:DEA molar ratio, i.e. (a) 1:1, (b) 1:2 and (c) 2:5. The other reaction parameters, such as temperature, growth time and TTIP precursors concentration, are 225 °C, 24 h and 3 mmol, respectively. (Reprinted from Ref. [28], Copyright 2014 The American Chemical Society).

Table 2
Morphology-photoredox activity relationship of the anatase TiO_2 nanocrystals. (Reprinted from Ref. [28], Copyright 2014 The American Chemical Society).

Morphology	S_{bet} ($m^2 g^{-1}$)	Band gap (eV)	% of (101) facets	% of (001) facets	% of (100) facets	k_{MO} ($h^{-1} s^{-1}$)	k_{MB} ($h^{-1} s^{-1}$)
Nanoellipsoids	11.25	3.16	~100	0	0	0.048	0.070
Nanorods	6.22	3.17	25	0	75	0.220	0.150
Nanocapsules	18.92	3.07	13	14	73	0.073	0.060
Nanocuboids	22.05	3.21	25	28	47	0.078	0.099
Nanosheets	60.23	3.05	0	72	28	0.015	0.019
Degussa P 25	51.58	–	–	–	–	0.059	0.048

producing porous TiO_2 nanostructure, such as anodic aluminium oxide (AAO) template [119], porous carbon template [120,121], alumina membrane, disordered glass, polymer inverse opal [122], colloidal template [123,124], etc. Depending on the method used for the deposition of TiO_2 layer and a suitable method for the template removal, a porous TiO_2 nanostructure with variety pore size and density have been successfully obtained.

More or less similar with hard template approach for the realization of porous TiO_2 nanostructure, the soft template, namely the template that is mainly from the organic substances, offers interesting outcome with a straightforward process. Metal organic framework template has presented as a different potential alternative strategy for the preparation of porous TiO_2 nanostructures [125–127]. Xiu et al., for example, demonstrated that by using titanium metal organic framework (MIL-125 Ti), the highly porous titanium-based MOF MIL-125 (MIL = Materials of Institut Lavoisier) [128] (see Fig. 17), in a spray pyrolysis may produce porous microdisc of TiO_2 [129]. Recently Zhao et al. [130] reported that by utilizing titanium metal organic framework (MIL-125), it was realized the formation of highly porous 3D nanostructure of anatase TiO_2. That was achieved by simply hydrolyzing the precursor of titanium metal organic framework that was followed with a calcination process at 400 °C for 4 h in air. The typical result of the approach is characterized with a bimodal hierarchical porosity with mesopore diameters of up to 28 nm

along with a macropores diameters of up to 185 nm. Meanwhile, the BET surface area and the total pore volume are 147 $m^2 g^{-1}$ and 0.6238 $cm^3 g^{-1}$, respectively [125,130]. Mesoporous TiO_2 with different morphologies, such as porous nanosheet or plate [126,131], cake-like structure [132], hierarchical structure [133], etc., have also been realized using the MIL-125-Ti metal organic frameworks and they have found to have a high-performance in storage, photocatalysis and solar cell [131].

Different MOF template, namely hierarchical structure of Zeolitic Imidazolate Framework [134] (ZIF-8 and ZIF-67) (see Fig. 18), has also been widely used for the formation of micro-sized porous TiO_2 microcube. Yang et al. [135] reported that microscale hierarchical porous TiO_2 nanostructure with BET surface area as high as 800 m^2/g can be realized by coating the shell structure of TiO_2 via any available coating method on this template that was followed with a thermal decomposition of the MOF template. Liu et al. [136] in different study also demonstrated the facile formation of porous and high-energy facet TiO_2 nanostructure using ZIF-8 MOF template. In typical process, they used 0.4 g mesoporous TiO_2 beads and mixed with ZIF-8 with theoretical mass ratio of 1:2 between ZIF-8 to TiO_2 in methanol solution. The TiO_2-ZIF-8 composites were precipitated and washed using centrifugation and finally dried at 60 °C for 12 h. During the growth process, a layer of ZIF_8 polyhedron will cover the TiO_2 bead, producing faceted mesoporous TiO_2 nanocrystals (see Fig. 19).

Table 3
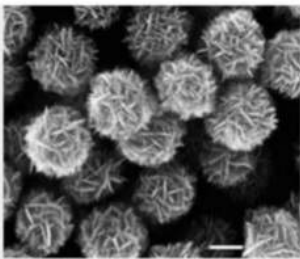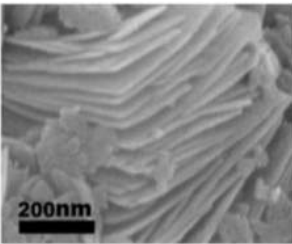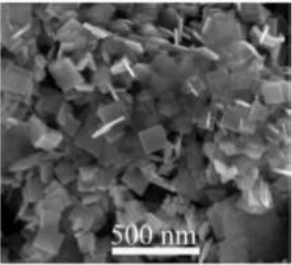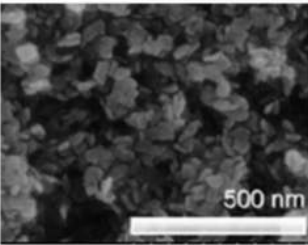Methods for the preparation of porous anatase TiO_2 nanostructures.
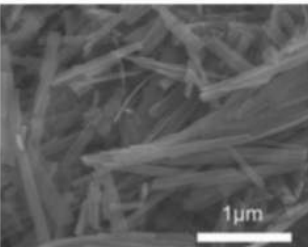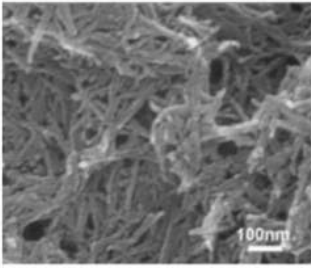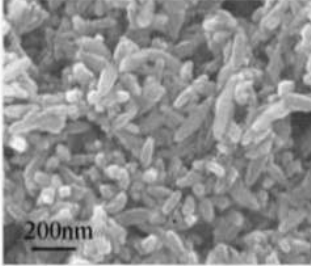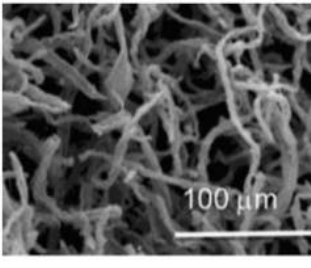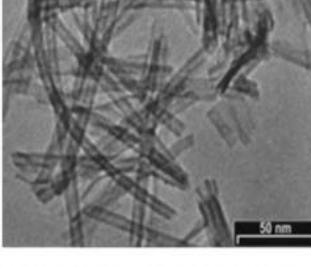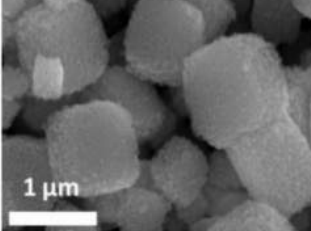
No	Sample	Picture	Method	Reference
1.	Anatase TiO_2 nanosheets-based hierarchical spheres		5 mL of acetic acid was added in a 0.01:0.03 M (TiF_4:DEG), magnetic-stirred for 3 h at room temp., then autoclave for 8 h at 180 °C. Scale bar is 100 nm.	[99]
2.	Hierarchical layer-by-layer self-assembled TiO_2 nanosheets		Titanium tetrafluoride (0.20 g) mixed in 80 mL of benzyl alcohol and stirred continuously for 4 h until a homogeneous solution obtained and transferred to a Teflon-lined stainless steel autoclave. It was then heated at 160 °C for 24 h. Through centrifugation, white, crystalline titania powder was collected, washed with ethanol, and dried in vacuum at 80 °C.	[100]
3.	HF-free synthesis of anatase TiO_2 nanosheets		9 mL of HCl, 36.5—38 wt % was diluted with 1 mL of water, and then transferred to a 45 mL Teflon-lined steel autoclave. 20 mL of toluene solution containing 0.6 mL of titanium n-butoxide [$Ti(OC_4H_9)_4$, TBT] added on top of mix solution without stirring and heated at 180 °C for 24 h. White powder precipitates was collected by centrifugation, followed by washing with ethanol and water for several times. The powder was then air- dried at 40 °C for 10 h.	[97]
4.	Anatase TiO_2 nanosheets		Anatase TiO_2 sheets were synthesized through the hydrothermal method. $(OC_4H_9)_4$ (50 mL) and HF solution (6 mL, concentration of ca. 40 wt %) were added to a 200-mL Teflon-lined autoclave, which was then heated to 180 °C for 24 h. After it was cooled down, the precipitates were obtained by centrifugation. It was then washed with ethanol and distilled water before being dried in an oven at 60 °C. Different HF content used (2, 4, 8, and 12 mL) for anatase TNSs sheets prepared under the same conditions.	[101]
5.	TiO_2 anatase nanowires		2 g of TiO_2 powder and 25 mL of 10 M NaOH aqueous solution were put into a Teflon lined stainless autoclave and heated at 150 °C for 72 h. After it was cooled down to room temperature, the precipitate was washed by H_2O and filtered in the vacuum before being put into 500 mL of HCl aqueous solution at pH 2 and stirred for 24 h. It was then centrifuged and repeated 3 times for HCl aqueous solution treatment.	[102]

Table 3 (continued)

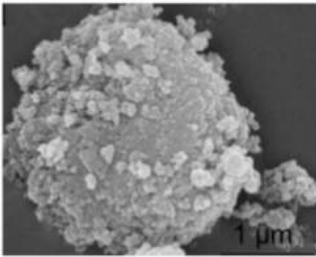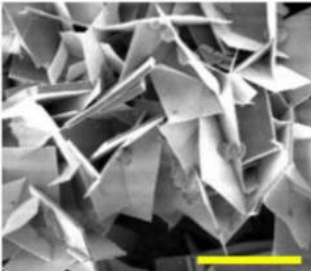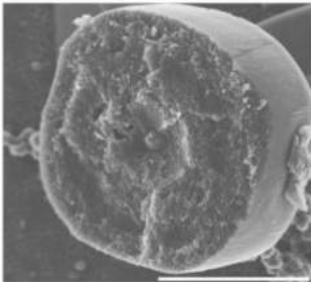| No	Sample	Picture	Method	Reference
6.	TiO$_2$ nanocrystal/nanotube double-layered films		Hydrolysis of titanium isopropoxide followed by a peptization process under hydrothermal condition. TiO$_2$ nanotubes were synthesized except that the obtained products did not undergo further drying process in order to keep the morphology of nanotube intact.	[103]
7.	TiO$_2$ nanorod		Titaniumisopropoxide (TIPT) mixed with triethanolamine (TEOA) at molar ratio of 1:2 then mixed with DDA and put into 100 ml Teflon autoclave 100 °C for 24 h	[104]
8.	Nanostructured TiO$_2$ hollow fibers		Mixed solution of (NH$_4$)$_2$TiF$_6$ and H$_3$BO$_3$, with concentration of the Ti(IV) precursor and the pH of the solution were adjusted to 0.03 M and 2.0 heated at 50 °C, as TiO$_2$ deposit on cotton fibers (Flawa, oxygen-bleached, hydrophilic, 100% pure cotton wool) for 5 h. Hydrolysis and dehydration of (NH$_4$)$_2$TiF$_6$ produces TiO$_2$ nanoparticulate films on hydrophilic cellulose fibers. The fibers were then washed with deionized water and dried. The cellulose template was then removed through annealing process at 500 °C for 3 h.	[105]
9.	TiO$_2$ porous tubes		TiO$_2$ powder was dispersed in an aqueous solution of NaOH (10 N) under vigorous magnetic stirring for about 1 h to form a white suspension, followed by placing it into a Teflon container (80 mL) in an oil bath with constant agitation at 160 °C. centrifuged and rinsed with distilled water and then with HCl solution until pH = 6–7	[106]
10.	(0 0 1) faceted mesoporous anatase TiO$_2$ microcubes		For mesoporous single crystal formation, 0.24 g of TiF$_4$ in 50 mL of pure water was acidified using HCl (pH 2) to prepare 40 mM solution with 1.67 ml of BMIM-BF$_4$ was added under constant stirring. Later, 1 g of the TiCl$_4$ treated silica template was added and stirred and then finally hydrothermally treated at 190 °C for 12 h. The product obtained was washed with DI water and then etched for 1 h in 170 mL of 2 M NaOH solution at 80 °C under constant stirring. It was then vacuum filtered and washed with DI water and ethanol using PTFE filter paper of 0.2 μm pore size.	[107]

Table 3 (*continued*)
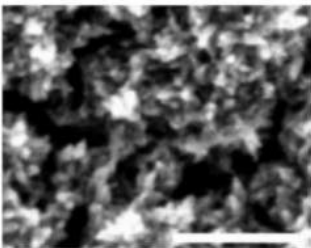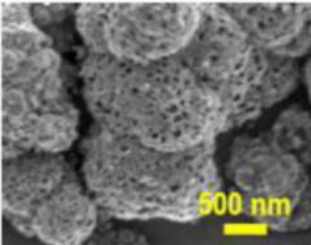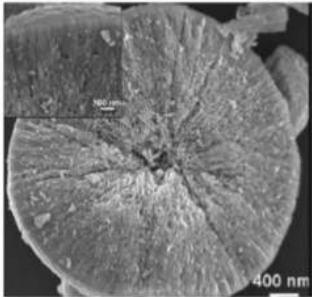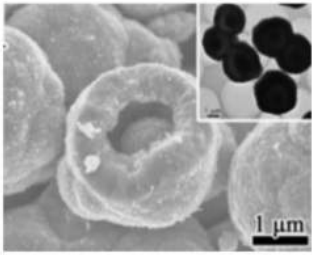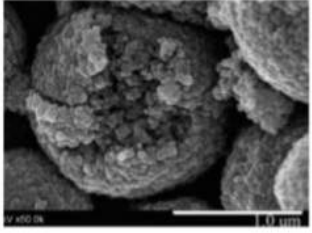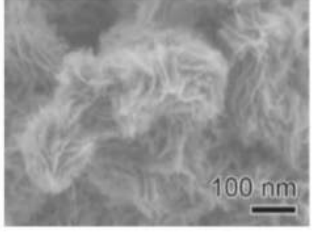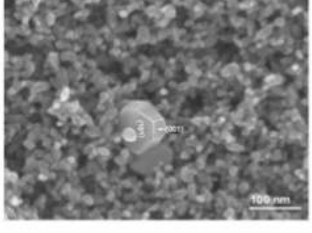
| No	Sample	Picture	Method	Reference
11.	Porous anatase TiO_2 derived from a titanium metal–organic framework		MIL-125 (Ti) was synthesized by a solvothermal method. Then the as-synthesized MIL-125 (Ti) was refluxed in water. Finally, the as-refluxed TiO_2 was calcined at 400 °C in air to remove the residual organic linkers.	[108]
12.	Nanowall of Cu-doped TiO_2		5 mL of 0.5 M $(NH_4)_2TiF_6$, 1 mL of 6.25 mM $Cu(NO_3)_2 \cdot H_2O$ and 1 mL of 0.5 M hexamethylenetetramine (HMT). The solution was ultrasonicated for 2 min, and then placed in a water bath for the reaction at a temperature of 90 °C. The growth time was for 10 h. Scale bar is 10 μm.	[109]
13.	Poriferous microtablet of anatase TiO_2		Growth solution containing 5 mL of 0.5 M $(NH_4)_2TiF_6$ and 5 mL of 1.0 M H_3BO_3 at room temperature for 15 h. The sample was taken out and rinsed with a copious amount of pure water and then dried under the flow of nitrogen gas. Finally, the sample was annealed in air at 400 °C for 1 h. Scale bar is 5 μm.	[94]
14.	TiO_2 nanograss		5 mL of 0.1 M $(NH_4)_2TiF_6$ and 5 mL of 0.2 M H_3BO_3 for a growth process of 25 h at room-temperature. The as prepared TiO_2 nanostructure was further annealed at temperature of 400 °C for 30 min. Scale bar is 100 nm.	[110]
15.	Mesoporous assembly of cuboid anatase nanocrystals into hollow spheres		13.6 mmol of $TiCl_4$ was added drop-wise to a 50 mL of water containing NH_4F. The reaction mix was immediately transferred into a 75 mL Teflon lined stainless steel hydrothermal vessel and autoclaved at 180 °C for 24 h. The autoclave then cooled to room temperature, the products washed several times with de-ionized water, followed by ethanol and then dried at 60 °C in an oven.	[111]

Table 3 (continued)

No	Sample	Picture	Method	Reference
16.	Hierarchically structured mesoporous anatase TiO$_2$ microspheres		0.5 mL TBT was mixed in 30 mL of 2 M H$_2$SO$_4$ aqueous solution for 30 min and transferred into a 60 mL Teflon autoclave. The autoclave was heated up to 180 °C for 5 h before being cooled down to room temperature. Precipitates was then collected by filtration, washed with distilled water and dried at 60 °C.	[112]
17.	Porous TiO$_2$ hollow microspheres		3 mL of titanium tetrachloride (TiCl$_4$) was added into 84 mL of isopropanol, magnetically stirred for 30 min. The solution was transferred into Teflon-lined autoclave and heated at 200 °C for 24 h before being cooled down to room temperature. The white precipitates obtained was filtrated and washed with ethanol, before being dried.	[113]
18.	Mesoporous TiO$_2$ core-shell spheres		PVP K30 (Mw = 25 000, 0.1–0.7 g) was dissolved in a mixture of ethanol (2.5 mL) and acetic acid (3.8 mL) with stirring. After 10 min, titanium butoxide (TBT, 7.0 mL) was added. The mixture was stirred continuously for 1 h to obtain a uniform pale yellow PVP-Ti sol and then was loaded in a syringe pump and then pumped through a small metal nozzle onto a large aluminum target placed about 35 cm away at a rate of 1.0 mL h^{-1}. A voltage of 35 kV was applied between the metal needle and aluminum target.	[114]
19.	Nanosheet-constructed porous TiO$_2$ −B		Mixed solution of TiCl$_4$ and ethylene glycol at room temperature, heated and condensed TiO$_2$ −B in the presence of ammonia solution.	[115]
20.	Trifunctional TiO$_2$ nanoparticles with exposed {001} facets		The 50 nm TiO$_2$ NPs with exposed (001) facets were synthesized using a fast microwave-assisted hydrothermal (FMAH) method and a commercial instrument.	[116]

Very recently, Ren et al. [137] prepared mesoporous three-dimensional hierarchical interconnected TiO$_2$ nanostructure via a biomolecular self-assembly method utilizing lipids and protein template [138]. The mesoporous TiO$_2$ nanostructure product is composed of interconnected nanoparticles. The resulting nanostructure exhibits excellent electrochemical properties with high initial Coulombic efficiency of up to 94% at 1C and capacity retention up to 90%. Thanks to the high-chemical stability of mesoporous TiO$_2$ 3D network, the porous system demonstrate high-degree charge-discharge recyclability and is predicted as potential candidate for high-performance photocatalytic system.

Surfactant template method has also been used to prepare
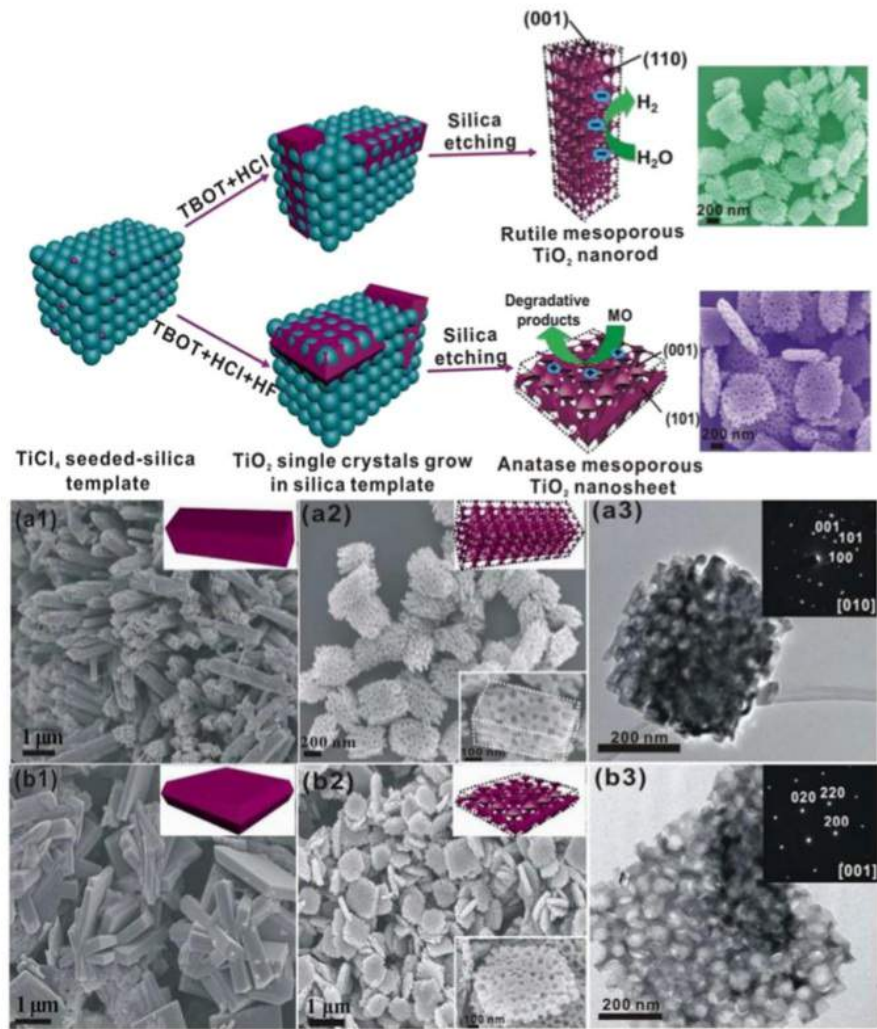
Fig. 15. (Top panel) Schematic method of porous anatase TiO₂ growth prepared using silica template by a hydrothermal method. (Lower panel) SEM images of solid (a1) TiO₂ nanorods and (b1) TiO₂ nanosheets prepared without SiO₂ template. (a2, b2) SEM images and (a3, b3) TEM images of mesoporous TiO₂ short nanorods (a2, a3) and mesoporous TiO₂ nanosheets (b2, b3). Seeding concentration: 0.3 mM, 180 °C, 12 h. The corresponding selected-area electron diffraction (SAED) patterns were shown in the insets. Left panels (a): no HF. Right panels (b): [HF] = 0.05 M. (Reprinted from Ref. [117], Copyright 2013 The American Chemical Society).

porous structure of anatase TiO₂. The most common surfactant template used is a combination of ionic and non ionic surfactant, namely triblock copolymer from the Fluoronic family, such as poly (ethylene oxide) (PEO) and poly (propylene oxide) (PPO). PEO group normally composed of hydrophilic ligand. While the PPO contains hydrophobic ligand. By mixing the two surfactant, surfactant micelles with variable morphology and the hydrophilic part at the outside of the micelles, depending on the mixture ratio of the two component, can be obtained. The morphology and porosity properties of polymer template can be further modified by combining ternary or quaternary polymer system, producing unique polymer micelles templates. The TiO₂ layer can be then deposited onto the micelles via a number ways such as hydrothermal, alcoholysis and etc. By removing the surfactant template via annealing, porous TiO₂ nanostructure can be obtained. The faceting can be obtained by simply controlling the morphology of

the micelles by means of modification of mixture ratio between the two components of ionic and non ionic surfactant. For example, Yu et al. earlier reported that by using the surfactant template from mixture of ionic and non ionic surfactant and followed with the removal of the surfactant via calcination at 500 °C has effectively solidified the framework and pore-wall crystallization. The result was the porous structure and it produced surface area as high as 100 m²/g, which is equivalent to porosity as high as 40% providing three-dimensional communicated pore system. The porous anatase TiO₂ was highly transparent and exhibit outstanding photocatalytic properties in acetone reduction [139]. Ortel et al. used different polymer template, i.e a combination of polymer micelles and PMMA sphere, in the formation of highly porous TiO₂ system in the presence of a suitable titanium dioxide precursor, i.e. titanium(IV) bis(ammonium lactato) dihydroxide, and the presence of other reagent, such as colloidal Pd nanoparticles (Fig. 20), may form
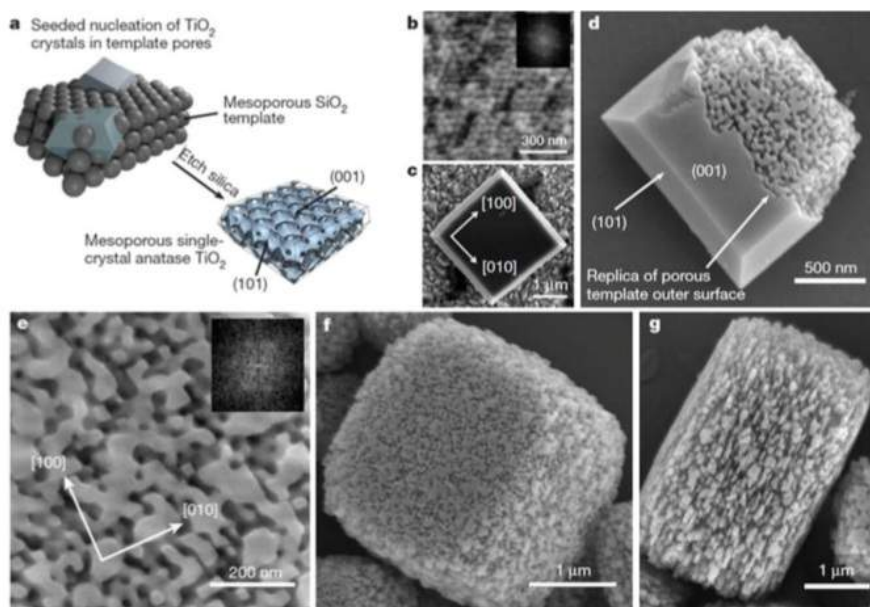
Fig. 16. (a) Mechanism of mesoporous single crystal (MSC) synthesis of TiO_2. (b), Typical pristine silica template used in the approach made up of quasi-close-packed silica beads (fast Fourier transform (FFT) with sixfold symmetry with 49 ± 3 nm spacing (inset). c–d), FESEM image of non-porous TiO_2 crystal prepared in a 20-mM TiF_4 solution at 210 μC. (e), Expanded image of the mesoscale pore structure within the templated region (reaction conditions 170 μC, 40 mM TiF_4). (f and g), Typical morphology of fully mesoporous TiO_2 crystals. (Reprinted from Ref. [19], Copyright 2013 Nature Publishing Group).

porous Pd-doped TiO_2 nanostructures. In this method, it was demonstrated that the porosity properties could be finely controlled by the concentration of the precursor and the pH of the reaction. The highly porous Pd-TiO_2 nanostructure system exhibited excellent photocatalytic properties in hydrogenation of 1,3 butadiene [140]. Unique to the polymer template system, the pore size and density as well as the morphology, such as two-

dimensional or three-dimensional pore structure, of the TiO_2 nanostructures can be straightforwardly controlled by changing the dimension of the ionic and non-ionic surfactant or using a mixture of ternary or quaternary polymer surfactants used during the growth process. The method for the preparation of three-dimensional pore structure in TiO_2 nanostructure has been well-summarized in Ref. [141].
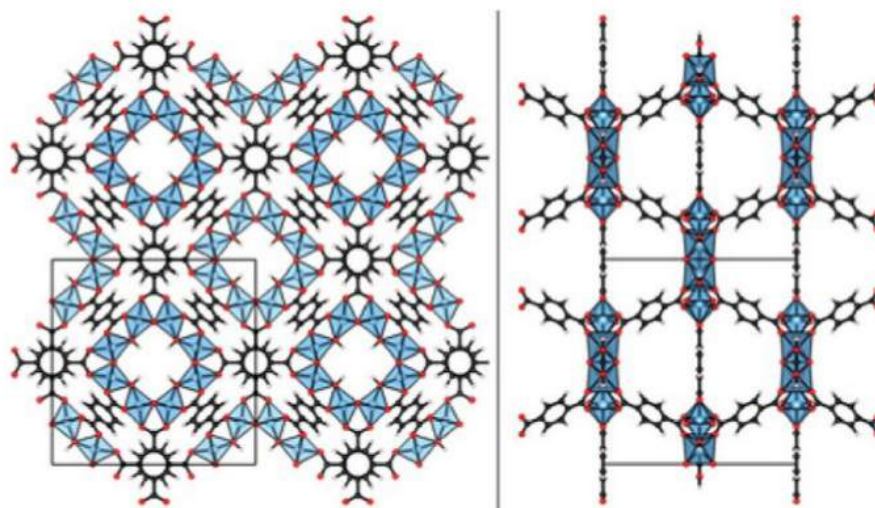
Fig. 17. (left) Schematic visualization of MIL-125 template visualized from [001] and (right) [010] orientations. Ti, O, C, and H are depicted in blue, red, black, and beige, respectively. Porous TiO_2 nanostructures can be realized by simply applying a thermal decomposition of the template. (Reprinted from Ref. [128], Copyright 2013 American Chemical Society). (For interpretation of the references to colour in this figure legend, the reader is referred to the web version of this article.)
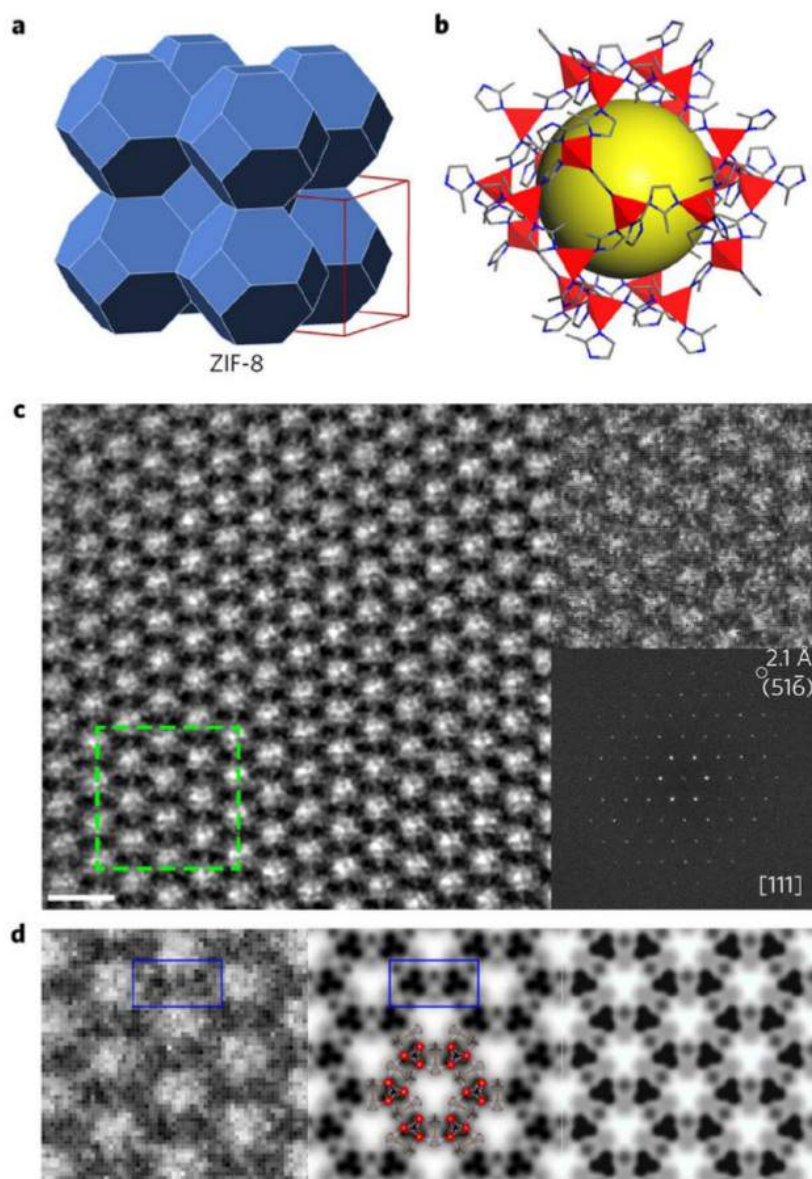
Fig. 18. (a), Structural model of ZIF-8 and (b), ZIF-8 sodalite cage. The yellow ball represents void space with red, grey and blue structure are the ZnN_4 tetrahedra, C and N atoms, respectively. (c), HRTEM image of ZIF-8 along the [111] axis (scale bar, 2 nm) with unfiltered (upper inset) and FFT (lower inset), respectively. (d), (Left), CTF-corrected (using a Wiener filter) image within the green square in c. (middle and right panel) are symmetry-imposed and simulated projected potential map of the structure in where individual atomic columns of Zn and imidazole rings can be identified. (Reprinted from Ref. [134], Copyright 2017 Nature Publishing Group). (For interpretation of the references to colour in this figure legend, the reader is referred to the web version of this article.)

Graphene-template method has also been reported to be potential for the preparation of highly porous anatase TiO_2 nanostructure. Li et al. [142] has successfully made a sandwich structure of mesoporous TiO_2-graphene-mesoporous TiO_2 by using GO nanosheet as a substrate for anatase TiO_2 nucleation in an ammonia-assisted hydrolysis of titania precursor and followed by a thermal annealing treatment in Ar. Under this process, the amorphous TiO_2 shell could be crystalized and GO reduced to graphene. In typical procedure, a very thin nanosheet of graphene-anatase TiO_2 composite with thickness was less than 50 nm and BET

surface area of 252 cm^2g^{-1} were obtained (see Fig. 21). Anatase TiO_2 with such properties and in the presence of graphene nanosheet may find potential used in photocatalysis and battery. The use of graphene oxide or reduced-graphene oxide templates have also been demonstrated for the preparation of two-dimensional porous TiO_2 nanostructures [143,144].

3.1.2.2. Etching method. Etching method has been present as an alternative, versatile approach for the preparation of hollow and porous anatase TiO_2 nanostructure. It normally uses an ammonia or
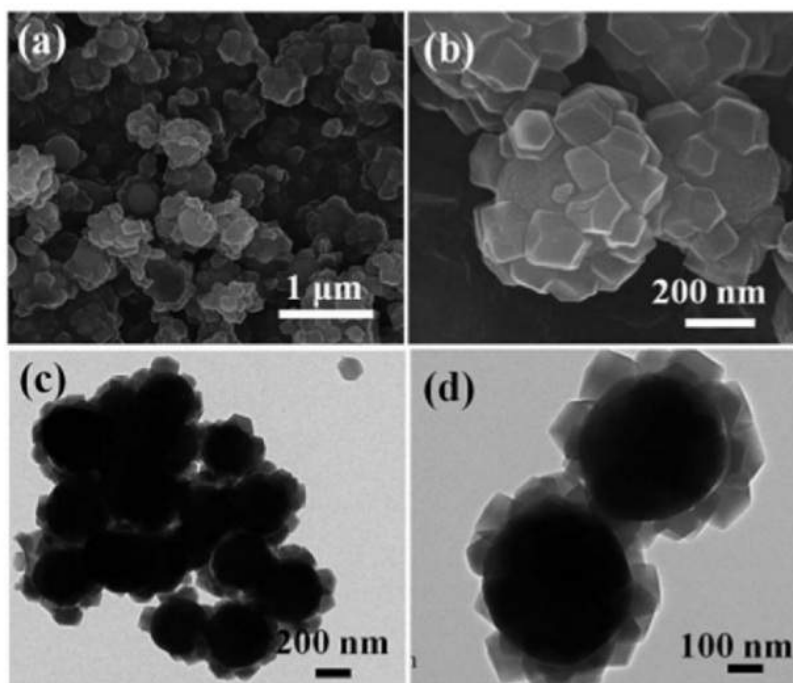
Fig. 19. Typical microscopic image of TiO₂/ZIF-8 hybrid beads showing the morphology of the nanostructure. (a) and (b) are FE-SEM images, and (c) and (d) are TEM images. (Reprinted from Ref. [136], Copyright 2017 The Royal Society of Chemistry).

a strong base [145–147] and acid [148] as the etchant agent. Li et al. [149,150], for example, following a single step process, namely preparation of amorphous silica protected TiO₂ in the presence of ammonia etchant could produce hollow anatase TiO₂ sphere. By subjecting the sample to a thermal annealing, porous, hollow spherical anatase TiO₂ nanostructure were obtained (see Fig. 22). The shell structure of the sphere is characterized with a rich (001) facet. The thickness of the TiO₂ shell can also be further modified by

following additional etching and thermal annealing on the porous and hollow nanostructures. Wang et al. in separate study reported that by applying an acetic acid on anatase TiO₂ thin film, highly porous two-dimensional anatase TiO₂ could be realized. They reported that the effectiveness of porous structure formation were determined by the concentration of acetic acid used and the pH of the reaction [151]. Although its straightforward procedure, due to the nature of etching process is chemically massive process, the
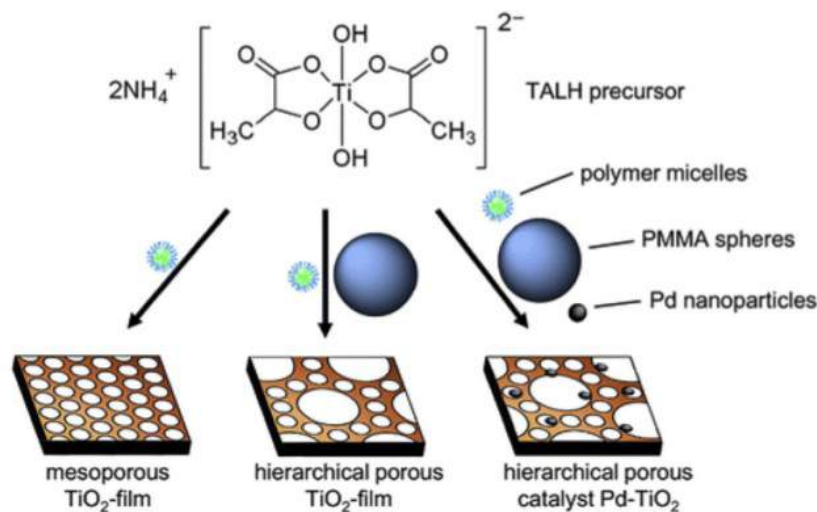
Fig. 20. Schematic mechanism for the formation of hierarchical porous TiO₂ nanostructure prepared using polymer pore templates. (Reprinted from Ref. [140], Copyright 2012 The American Chemical Society).
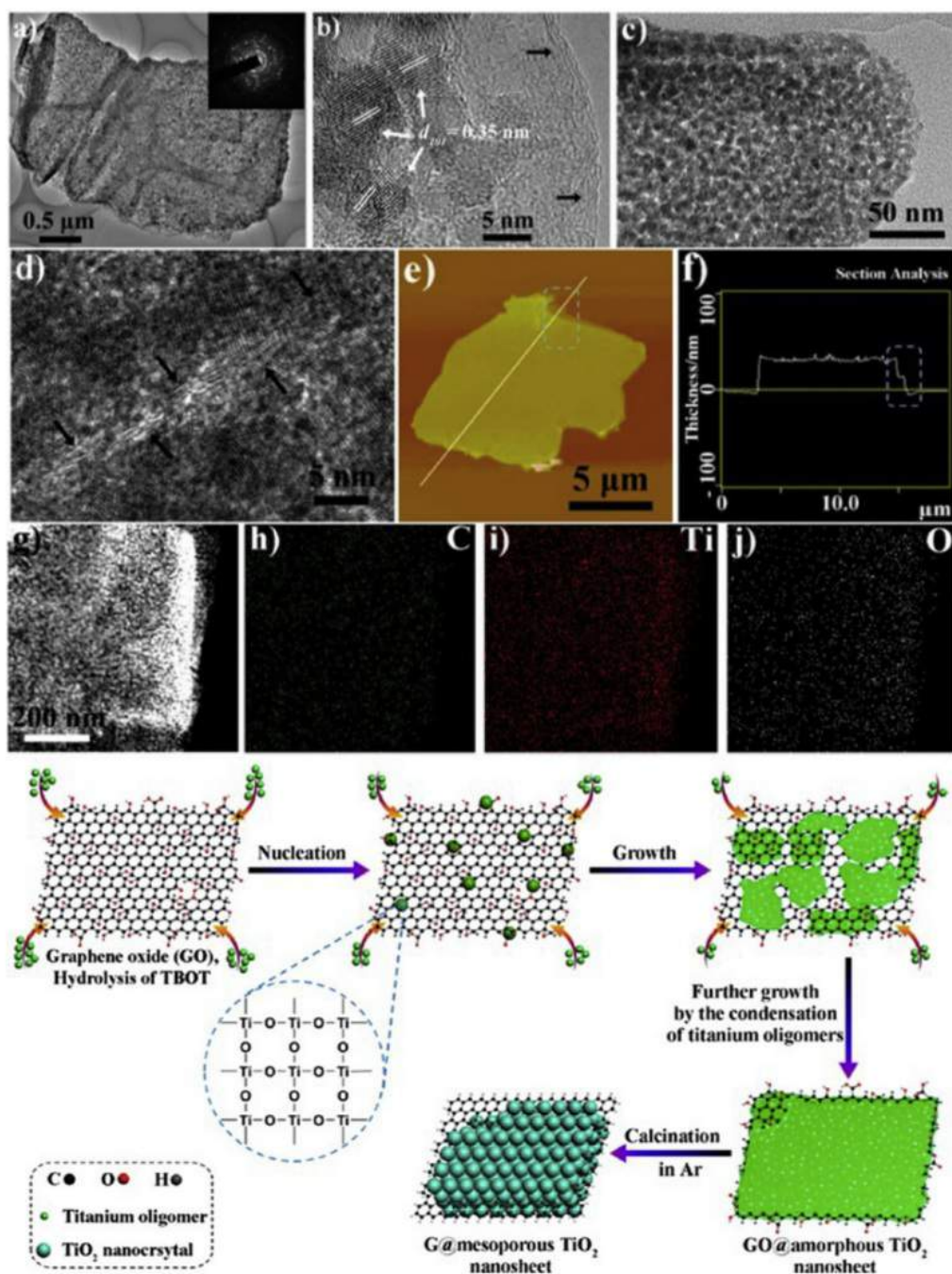
Fig. 21. Top panel: (a–d) Typical TEM images of TiO₂ nanosheets prepared using graphene-template. Graphene sheet remains in the structure after the growth process. (e–f) AFM topography images of the sample on a mica substrate and its corresponding height-profile. (g–o) STEM image and EDX elemental maps of C, Ti, and O of the samples, respectively. Lower panel: Schematic formation process of the mesoporous TiO₂ nanosheets. (Reprinted from Ref. [142], Copyright 2015 The American Chemical Society).

reaction is hardly controlled so that the faceted, porous TiO_2 nanostructure is limitedly produced. Nevertheless, if suitable reaction parameters are discover, porous and morphology-controlled TiO_2 nanostructure can be obtained.

3.1.2.3. Alcoholysis method. In most approached, aqueous phase reaction is used to prepare TiO_2 nanostructure both in solution and on the substrate surface. In this regards, the presence of H_2O solvent has facilitated the hydrolysis of the TiO_2 precursors. However, the reaction will produce titanium hydroxide complexes, which
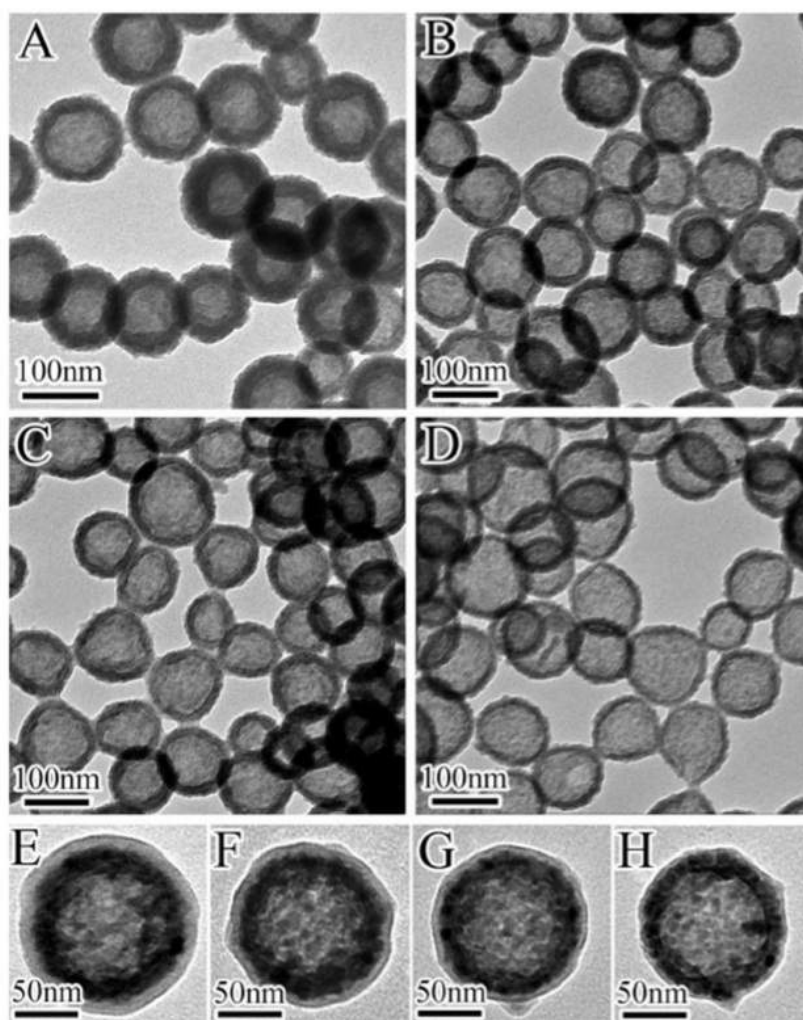
Fig. 22. (A–D) Typical TEM of the porous TiO₂ nanostructure prepared using etching method at different temperature (A: ambient temperature; B: 40 °C, C: 60 °C and D: 80 °C). (E–H) Their corresponding high-magnification TEM images. (Reprinted from. [150], Copyright 2016 The American Chemical Society).

mainly resides on the surface and via thermal decomposition low surface crystallinity of anatase TiO₂ is obtained. The existence of titanium complexes along with the TiO₂ phase more or less deteriorate the surface structure of the materials, especially during the thermal decomposition of the complexes. Hence, their surface chemistry properties. In order to obtaining a well-crystallinity of anatase TiO₂, non-aqueous phase process, typically alcohol phase, is normally used. Jin et al. [152], for example, developed a solvothermal alcoholysis of TiO₂ precursors, to obtain a well-crystallinity of porous anatase TiO₂. They found that a porous and high-energy facet anatase TiO₂ can be simply realized using the solvothermal alcoholysis mixture solution of 3 mL of titanium tetrachloride (TiCl₄) with 84 mL of isopropanol and then the solution was magnetically stirred for 30 min prior to further reaction process. Finally, the reaction was transferred into a Teflon-line autoclave for a solvothermal reaction at 200 °C for 24 h. The product was then collected and washed via centrifugation. In a typical procedure, a hierarchical structure that composed of straight nanorods and nanochannel with high-percentage of (001)

facet was obtained. The formation of anatase TiO₂ with such unique structure and morphology is predicted via the releasing of water molecules from an esterification process of alcohol that promoted hydrolyzing of titanium precursors. Hydrogen ion that is required in this process was produced from the solvothermal alcoholysis process. Due to and Oswald ripening process during the reaction has led to the formation of anatase TiO₂. In a medium of alcohol and acetone mixture, hollow nanosphere were formed. In the effort for minimizing the high surface energy of TiO₂ nucleates, they attached each other, in many case, via oriented-attachment mechanism. Such process is selective and only occur on a similar crystalline plane. Thus, single crystal of hierarchical structure is possible to obtain via this process. In this process, it was assumed that the Cl ion may also play a central role in directing the formation of nanorods component in the hierarchical structure by attaching onto the (001) faces. Thus, the nanostructure product is reach of high-energy (001) facet.

Up to date, several modification in the reaction composition, such as using a different Ti precursors, and reaction condition in
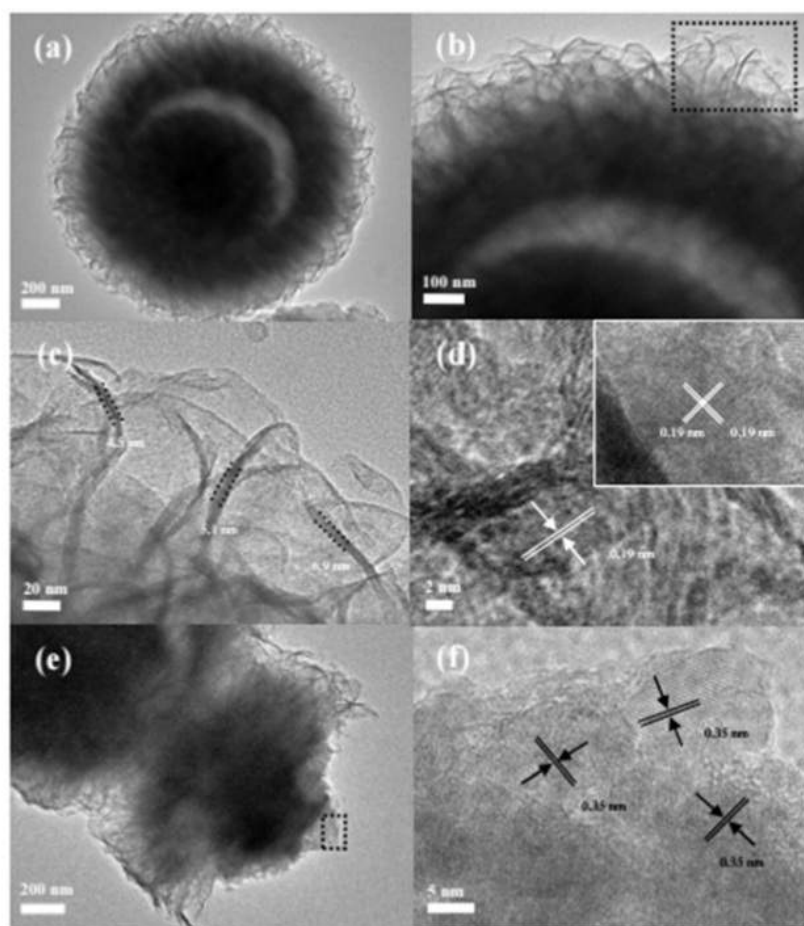
Fig. 23. Structure and morphology of TiO₂YSHSs prepared using water-based hydrolysis hydrothermal method prepared at 200 °C for 24 h. (Reprinted from Ref. [154], Copyright 2012 The Royal Society of Chemistry).

alcoholysis approach, porous and high-energy faceted TiO₂ nanostructure with large range of morphology, particularly hierarchical structure, yolk-shell [153], etc., have been impressively achieved.

3.1.2.4. Hydrothermal method. While alcoholysis method utilises alcohol ligand in dissociating the TiO₂ precursor in the presence of thermal heating, water base reaction or hydrolysis is also capable to realize the formation of anatase TiO₂ nanostructure from the TiO₂ precursors. Due to its simplicity and greener process, it has been widely used for the preparation of TiO₂ nanostructure with wide-range morphologies. Fang et al., for example, reported the synthesis of porous (001) faceted TiO₂ nanostructure via surfactant-assisted-hydrothermal method [154]. Two-different nanostructure of anatase TiO₂ with rich of (001) facets exposure were obtained, namely yolk-shell and nanosheet product, which were achieved via two different reactions condition. For the case of yolk-shell morphology synthesis, diethylenetriamine surfactant was introduced into the reaction that contains titanium oxide precursor (i.e. titanium isopropoxide). Meanwhile for the nanosheet of anatase TiO₂, the surfactant was replaced with hidrofluoro acid (HF). The reaction was carried out using a hydrothermal method in an autoclave at a temperature of 200 °C for 24 h. Regarding the nanosheet TiO₂, more or less similar steps was also used. However,

the hydrothermal reaction temperature was lower than the yolk-shell structure of TiO₂, i.e. 180 °C for 24 h. With time growth, the precipitate of anatase TiO₂ is obtained in the solution and via centrifugation, powder of a highly crystalline anatase TiO₂ were obtained.

FESEM analysis on the result indicated the formation of yolk-shell structure if using amine surfactant, meanwhile nanosheet product were obtained when the amine surfactant were replaced by the HF in the reaction. An interesting point to be underlined here that both structure were characterized by rich of (001) high energy facet of anatase phase TiO₂, as judged by the X-ray diffraction results. As can be seen from Fig. 23, the yolk-shell structure possess a dimension in the range of 1–1.5 μm wide of diameter. When the structure brought into HRTEM analysis, it was surprisingly established that the rounded structure of yolk-shell morphology is indeed a hierarchical structure that composed by large-number of small-flakes that randomly assembled into a microsphere. The shell thickness was in the range of approximately 200 nm thick, meanwhile the inner sphere structure possess diameter as large as 650 nm.

As can be seen from the figure, the nanosheet structure that composed the yolk-shell structure contain lattice fringe spacing as high as 0.19 nm, which is corresponding to (001) facets (Fig. 23d).
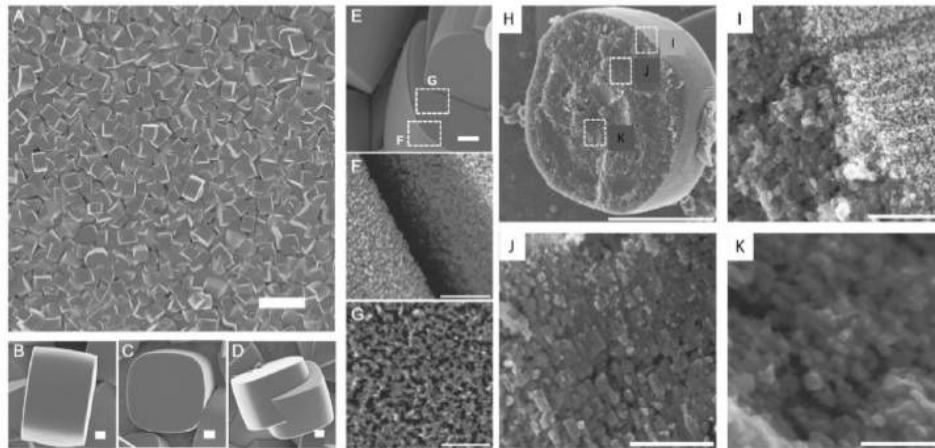
Fig. 24. The typical morphology of porifeorus TiO$_2$ microtablet prepared using surfactant-directed hydrothermal method (A–G). The reaction contains 0.5 M of ammonium hexafluorotitanate and 1 M of boric acid. The growth time is 15 h. (H–K) The FESEM image of the inner structure of the microtablet showing the brick-like assembly of the nanocuboid of TiO$_2$. The scale bars are 20 μm in (A), 1 μm in (B)–(D), 200 nm in (F), 100 nm in (G), 5 μm in (H) and 250 nm in (I) to (K). (Reprinted from Ref. [94], Copyright 2013 Elsevier B.V.).
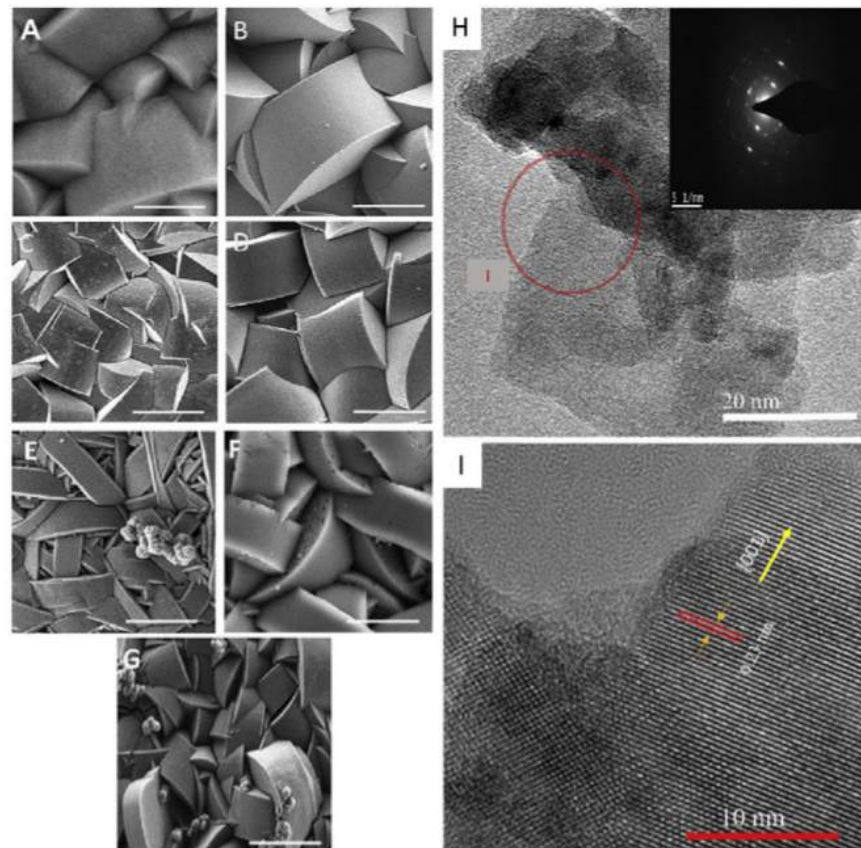
Fig. 25. The modification of the microtablet morphology to diatom-like structure upon being doped with Ga of different concentration, i. e. 0.005 (A), 0.010 (B), 0.015 (C), 0.020 (D), 0.025 (E), 0.030 (F) and 0.035 mM (G). (H) TEM image shows the nanostructures is constructed by TiO$_2$ nanoplatelet. Inset in H is typical SAED pattern of the structure showing with normal plane is (001). The scales bars are 2 μm in A to G. (Reprinted from Ref. [93], Copyright 2016 Elsevier B.V.).

The nanosheet is single-crystalline in nature. The portion of exposed (001) facets on the nanosheet is approximately 87%, which is extremely wide in term of nanospherical morphology structure. A different facet, namely (101), was also discovered in the nanostructure, particularly the aged sample, which was predicted due to the Oswald annealing effect on the nanostructure. Interestingly, the BET surface area of the nanostructure is distinguish high, i.e. 245.1 $m^2 g^{-1}$, which is almost doubled of the surface of the nanosheet anatase TiO_2 itself (88.9 $m^2 g^{-1}$). These feature may facilitate excellent molecular adsorption and efficient interfacial charge transport.

Wang et al. in a different study also obtained that by modifying the precursor of the reaction, including the introduction of impurity, porous and high-portion of energy facet of (001) can be obtained. It was found that the presence of impurity during the growth process has driven the faceting process in the anatase TiO_2

system. In addition, owing to the existence of impurity, namely Bi ions, Bi doped porous and high-energy facet anatase TiO_2 system can be obtained [155]. Large range of anatase TiO_2 morphology were then obtained via the hydrothermal method, that ranges from cube to boxes, hierarchical structure, etc., potential for high-performance catalyst or photoanode systems.

3.1.2.5. Surfactant-directed hydrothermal method. As has been previously discussed, the hydrothermal method, even though with the absence of any directing agent, has demonstrated an excellent capability for producing high-energy facet anatase TiO_2 nanostructure. Nevertheless, this process is vulnerable to limited success and solely depend on the uniqueness of the chemical precursors to produce faceted anatase TiO_2 nanostructure. Therefore, a generalized procedure is highly demanded in order to attaining a better control over the formation of TiO_2 nanostructure with high energy
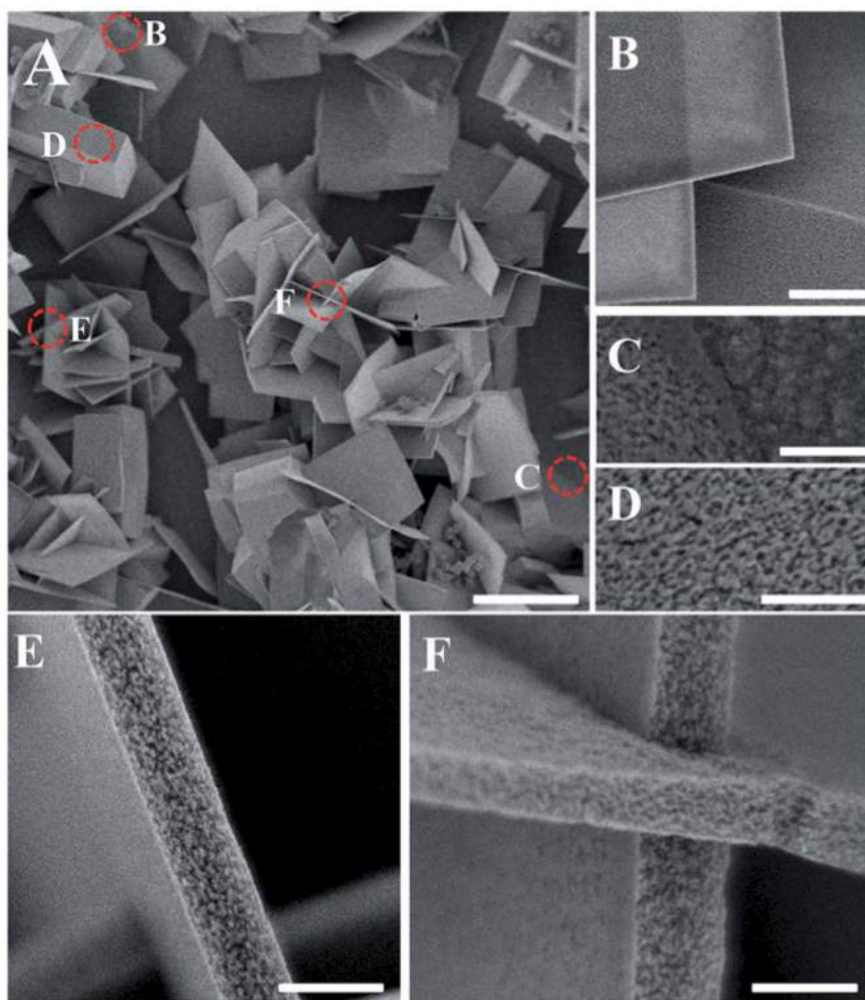
Fig. 26. Morphology of TiO_2 nanocrystals prepared using surfactant directed-hydrothermal method with Zn doping prepared using an equimolar mixture (0.5 M) of $(NH_4)_2TiF_6$, $Zn(NO_3)_2 \cdot xH_2O$ and HMT. Growth temperature and growth time are 90 °C and 5 h, respectively. Scale bars are 1 mm for (A), 500 nm for (B) and 100 nm for (C) to (F). (Reprinted from [95], Copyright 2013 Elsevier B.V.).
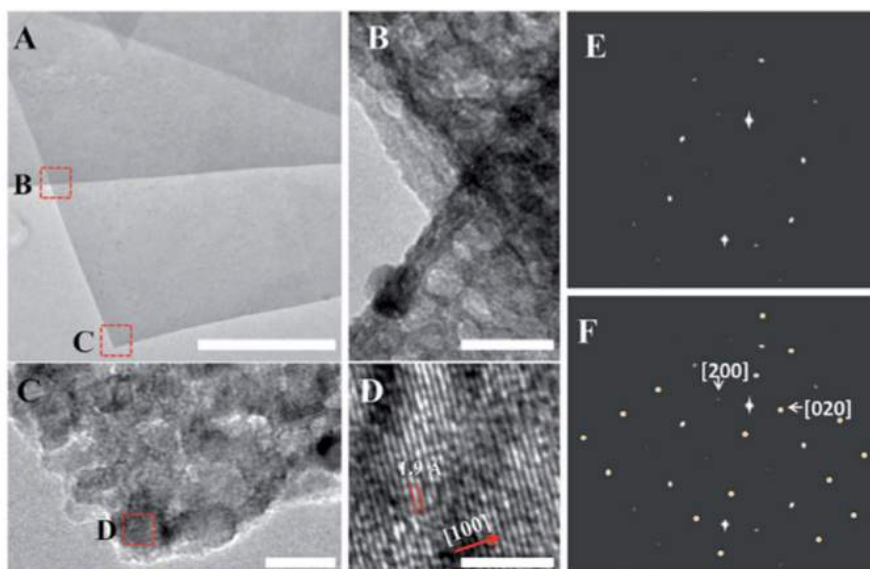
Fig. 27. TEM and SAED analysis result for Zn-TiO$_2$ nanowall confirming the (001)-faceted nature. Scale bars are 1 mm, 20 nm, 5 nm, 2.5 nm for (A), (B), (C) and (D), respectively. (Reprinted from Ref. [95], Copyright 2014 The Royal Society of Chemistry).

faceted. One well-known method is to introduce a directing agent in the hydrothermal method. Our group has also been working in the realization of anatase TiO$_2$ growth containing high-energy facet of (001) with surface area via a liquid phase deposition (LPD) method with several modification [93,94,156] in the presence of surfactant directing agent. LPD method is a wet-chemical process that was normally used to grow metal oxide complex thin film on a solid surface. By following a thermal annealing in air, corresponding metaloxide film can be obtained. The thin film of metaloxide is formed via a ligand-exchange process of metalfluoro complex involving a scavenging of F$^-$ anion by the fluor anion scavenger of boric acid. For the case of TiO$_2$, typical product is a continuous thin films with visible crack due to high surface tension of the material. The crack structure becomes persistent with the increasing of the reaction time and thermal annealing temperature.

In our typical approach, a different TiO$_2$ nanostructure instead of continuous thin film can be realized by controlling the amount of ligand-exchange generated F$^-$ anion in the reaction. By increasing the concentration of F$^-$ anion during the growth process, TiO$_2$ nanostructure with cubic and nanoplates morphologies, which are rich of (001) facet, can be obtained. The concept is more or less similar with the addition of fluoric acid in to the reaction for achieving high concentration of F$^-$ anion. We used two different approaches for this purpose: (i) by increasing the metal-fluoro complex concentration in the reaction, exceeding the concentration of scavenger [94]. When all the scavenger have been consumed the F$^-$ anion freely available in the bulk solution and attached onto the growing plane of the TiO$_2$ nanocrystal. The preferred plane for F$^-$ anion attachment is (001) so that the product of the nanocrystal growth is characterized with large-percentage of (001) facet (Fig. 24). Unique to the structure prepared using this approach, the
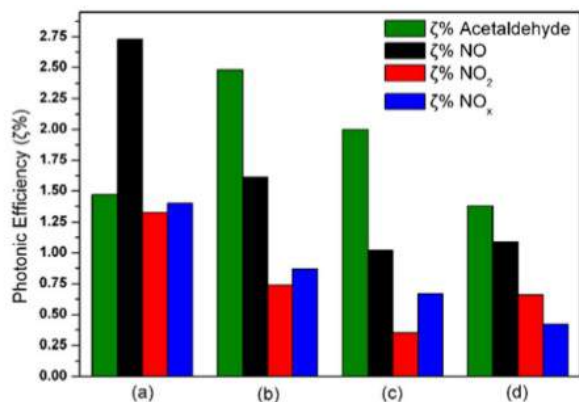
Fig. 28. Comparison of photocatalytic properties of TiO$_2$ anatase calcined nanoplates (a), washed nanoplates (b) and P25 (c), for NO oxidation and acetaldehyde decomposition. (Reprinted from Ref. [158], Copyright 2013 Elsevier B.V.).
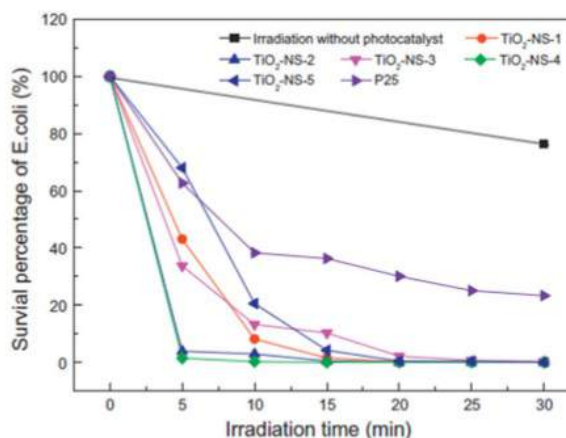
Fig. 29. Performance of photocatalytic disinfection of *E. coli* by TiO$_2$ nanosheet with rich (001) facet under visible light irradiation. (Reprinted from Ref. [165], Copyright 2013 Elsevier B.V.).

nanostructure are actually hierarchical system with small (001) faceted nanocuboid as the key element that constructs the structure, which are arranged resembling a brick-like construction via an oriented-attachment process (See Fig. 24H–K). As the result, the nanostructure contains high-density nanovoids or so called microporous (see Fig. 24J–K).

The morphology of the nanostructure was modified when metal dopant is introduced into the growth reaction. For example, when Ga dopant introduced in the growth reaction [93], the product change from microtablet to diatom-like morphology (see Fig. 25). Despite change in the overall morphology, the structure also composed (001) faceted small nanocuboid that are hierarchically assembled forming microstructures. HRTEM analysis result as shown in Fig. 25H–I indicates that the structure is composed of (001) faceted nanocuboids.

Much different morphology were obtained when the Zn [95] or Cu [109] were doped into the anatase TiO_2. Instead of microtablets or nanodiatoms, the anatase TiO_2 morphology when being doped with Zn and Cu cations change to "thin" nanoplates morphology. Unique to our present approach, the nanoplates grew vertically on the substrate forming nanowall-like morphology (Fig. 26). However, similar to our earlier results, the nanowalls were also hierarchical structure that were composed by nanocuboids structure with (001) faceted surface (Fig. 27).

3.2. Photocatalytic properties

3.2.1. Non-porous system

When the TiO_2 or other semiconducting materials interacts with photo irradiation with energy larger than the optical energy gap of the material, electron in the valence band of the material will excite to conduction band, leaving hole (a quasi-particle with positive charge) in the valence band. The photogenerated electron and hole can then react with any chemical species adsorbed or in the vicinity of the material surface, triggering a redox reaction or a charge transfer reaction. Uniquely, the photogenerated electron and hole position in the anatase TiO_2 are also facet dependent, where hole prefers to reside on the (001) facet, meanwhile the electrons are on the (101) facet, enabling a selective photogenerated surface or charge transfer reaction. In addition to the (001) facet, it provides facile adsorption and reaction of adsorbed species during the photocatalytic process due to its higher conduction band minimum in which it produces more strongly reductive electron, accelerating

the reaction on the surface [157]. Thus, the existence of surface orientation-photoactivity dependence has highlighted a site selective reduction and oxidation on the surface of anatase TiO_2, enabling a different photocatalytic properties towards difference redox species, and further allows the design of special catalyst for specific application, placing the anatase TiO_2 at the forefront of most photoprocess applications [89].

Sofianou et al. [158] discovered such phenomena when using anatase TiO_2 containing large-portion of (001) facet in the nanocrystals in the oxidation of NO and acetaldehyde gases. In typical process, the (001) faceted anatase nanoparticles powder, which were prepared using a hydrothermal process, were pressed in a sample holder with a surface area of 20 cm^2. The sample was then soaked in a UV-A lamp with intensity of 10 W/m^2 for three days. This is to remove any organic residue and pollutant on the surface. The sample were then placed into a reactor that allows gas flow through the powder. The reactor possesses a quartz window for sample irradiation using UV-A. The photocatalytic reduction of NO and acetaldehyde gases on several condition of anatase TiO_2 are shown in Fig. 28. As can be seen from the figure, a clear difference in the photoactivity of anatase TiO_2's facet is demonstrated. Where, the anatase TiO_2 containing (001) facet, namely platelet morphology, exhibit superior activity compared to anatase TiO_2 with other dominant facets. As has been earlier mentioned, the existence of the photoexcited electron and hole segregation in anatase TiO_2 to (101) and (001) facets, respectively, enables such unique selectivity properties. On the (101) facet, photogenerated electron initiate an oxidation reaction via the generation of superoxide (O^{2-}) radical, which is required for degradation of reducing gas such as NO. Meanwhile the photogenerated hole on (001) triggers the reduction reaction via the production of hydroxyl (OH^-), superoxide ($\cdot O_2^-$) and peroxide (H_2O_2) radical [159], which is crucial for degradation of oxidizing gas such as acetaldehyde. All these process are indicated from the results as shown in Fig. 28, where on the (001) facet, the NO experienced a sluggish degradation process. Contrary, the acetaldehyde underwent rapid degradation, exceeding the efficiency of degradation by the (101) plane.

Crystalline facet-photoactivity relationship is further verified in the photocatalytic dissociation of CO_2 molecules. For example, Mino et al. envisaged that the CO_2 is favoured to be adsorbed on the (101) facet, meanwhile the formation of variety of surface carbonates is preferred on the (001) facet [160]. In an independent study, Huygh et al. explored how the nature of CO_2 molecules adsorbed on
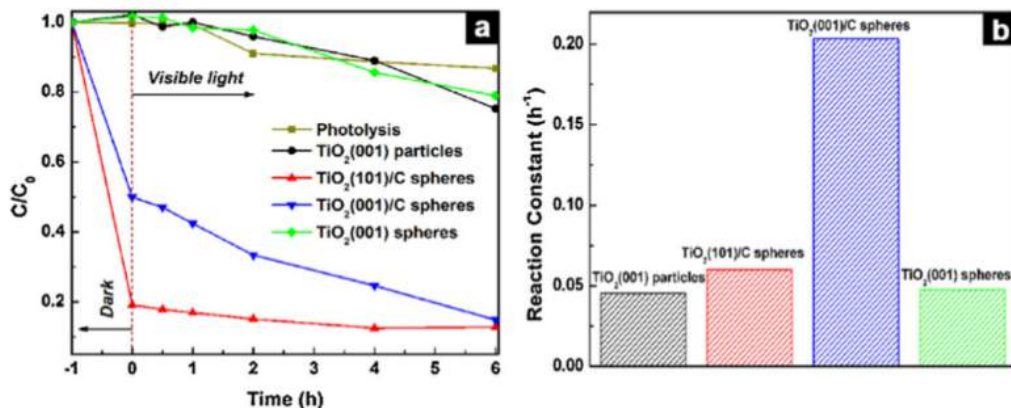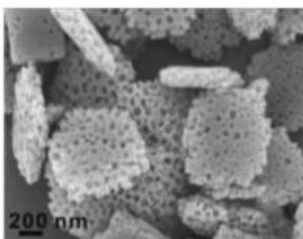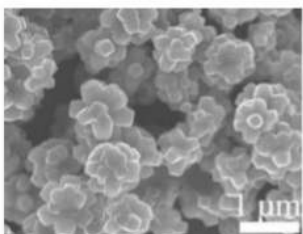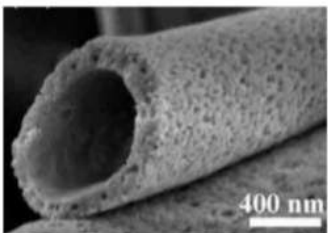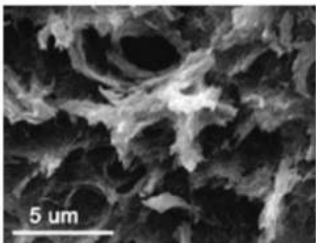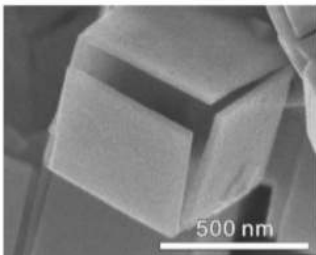

Fig. 30. Comparison of photocatalytic performance of anatase TiO_2 with (001) over other structure in the degradation of MB under visible light. (Reprinted from Ref. [170], Copyright 2014 Elsevier B.V.).

Table 4
Photocatalytic performance of porous and (001) faceted anatase TiO$_2$ nanostructures.

No	Sample	Picture	Performance	Reference
1.	Mesoporous TiO$_2$ single crystals		Oxidative photocatalytic activity with performance up to 90% for R-MSC-0.3 and 97% for A-MSC-0.3 after the irradiation for 180 min for MO degradation under white light.	[117]
2.	Flower-like TiO$_2$ nanostructures with exposed (001) facets		The photocatalytic degradation rate constant can be up to 1.23×10^{-2} min^{-1}, which is almost double of that for the P25 TiO$_2$ powders under visible light.	[172]
3.	TiO$_2$ hollow fibers		Higher efficient photocatalytic activities and stabilities toward the hydrogen evolution with a rate of ~499.1 μmol g^{-1} h^{-1} and ~99.5% degradation Rhodamine B (RhB) in 60 min under white light	[173]
4.	Mesoporous TiO$_2$ nanocrystals grown in situ on graphene aerogels		The sample can degrade methyl orange (MO, 10 mg/l) up to 90% on within 5 h of reaction under Solar light irradiation. This is far higher than the performance demonstrated by the P25-based GA catalysts (67 wt %). The photocatalytic stability is high where the performance maintain at 83% after 5 cycles of uses. While the P25/GAs decreased rates of MO degradation (9.4%) for the same measurement cycles.	[174]
5.	Hollow TiO$_2$ boxes		The porous TiO$_2$ nanoboxes exhibites excellent performance in H$_2$ evolution with rate as high as 7.55 mmol g^{-1} h^{-1} under white light	[175]

Table 4 (*continued*)
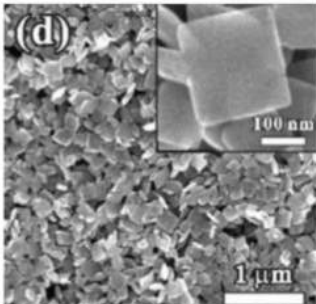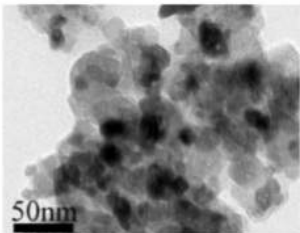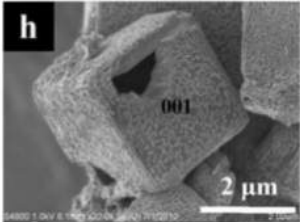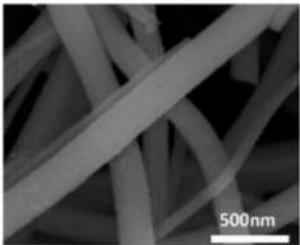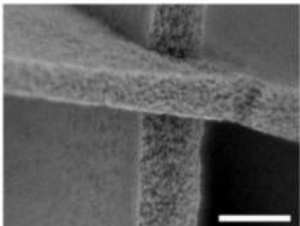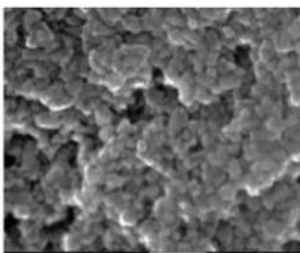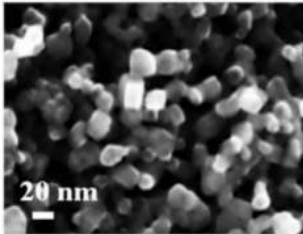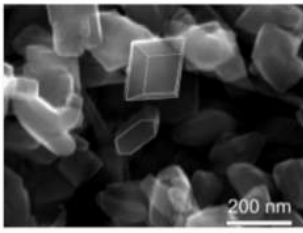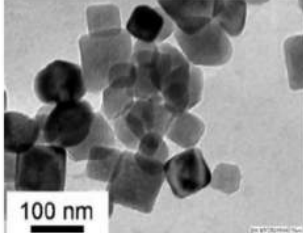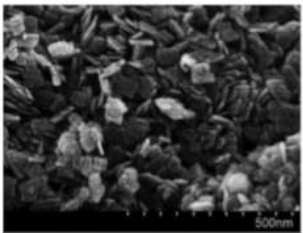
No	Sample	Picture	Performance	Reference
6.	Carbonate ions-assisted syntheses of anatase TiO_2 nanoparticles		The sample with high-percentage of (001) facet can degrade up to 95% of MB under irradiation of white light, which is double from the sample with (101) facet (46%) during 20 min of reaction under white light.	[176]
7.	Mesoporous TiO_2 nanoparticles terminated with carbonate-like groups		Photocatalytic activity as high as 90.2% for 60 min was obtained for the degradation of RhB compared to SA sample (64.1% for 180 min) under visible light.	[177]
8.	TiO_2 cubical morphology		The efficiency of hydrogen evolution can be up to 7054.5 mmol h^{-1} g^{-1} on the samples under white light.	[178]
9.	TiO_2 and heterogeneous carbon core–shell nanofibers		The sample shows excellent performance in the degradation of Rhodamine B with degradation up to 51.6% for 30 min of reaction under white light	[179]
10.	Anatase TiO_2 nanowalls		The sample can degrade MB up to 31.6% during 120 min of the reaction with kinetic rate as high as 0.0029 min^{-1} under UV light.	[95]
11.	Nanocuboid TiO_2 based organic-inorganic hybrids		Catalytic performance in the degradation of Rhodamine B is 5 times (96%) higher than P25 during 10 min reaction under white light. Scale bar is 100 nm.	[180]

Table 4 (*continued*)

No	Sample	Picture	Performance	Reference
12.	TiO_2 nanocrystals with internal pores		The sample can degrade the concentration of crystal violet (CV) under the UV irradiation up to 97% compare to 70% on P25 within 80 min of reaction.	[181]
13.	Single-crystal TiO_2 nanoparticle film with exposed (001) facets		The sample demonstrate excellent performance in the degradation of 4-chlorophenol and MO with rate constant 5.15×10^{-3} min^{-1} and 1.24×10^{-2} min^{-1}, respectively, under UV light irradiation	[182]
14.	Platonic TiO_2 crystal facets with (001) facet.		The sample effectively degrade the MO with rate constant as high as 0.031min^{-1}, 7.7 times higher than conventional TiO_2 nanoparticles.	[183]
15.	TiO_2 nanosheets with (001) facet.		The sample exhibits excellent performance in the degradation of oxalic acid up to 86% during a reaction time of 240 min under ozonation process.	[184]

the (001) facet, especially during the dissociation of CO_2 molecules [161]. They highlighted that the monodentated carbonate-like structure is the most stable form of CO_2 adsorption on the (001) facet of anatase TiO_2. However, the dissociation of CO_2 is unworkable on the stoichiometric surface. It was also indicated that the presence of oxygen deficiency on the surface of anatase TiO_2 may produce additional high stability CO_2 adsorption configuration that is played by a stronger C—O bond. Thus, efficient CO_2 conversion on the (001) facet was achieved.

As has been discussed earlier, such unique photocatalytic properties of different facet in the anatase TiO_2 system is merely due to the difference activity of the electronic system in O 2p orbital [162] and it can be further modified and enhanced by introducing a defect, impurity or oxygen vacancy in the anatase lattice. These processes in turn intensively perturbed the occupied d_{xy} and empty d_{yz} orbitals as well as the enhancement of the electronic degeneracy [43] in the material. All these effects may then actively transfer negatively charged particles to the adsorbate molecules for

enhanced surface reaction [163]. Such process are certainly concentration dependent [164].

Wang et al. [165] investigated the photoactivity of (001) faceted anatase TiO_2 when being co-doped with B$^-$ and F$^-$ anions in the degradation of methylene blue dye and inactivation of e-coli bacteria. The performance was compared to the commercially available P25 anatase TiO_2. They prepared the nanosheet of anatase TiO_2 and co-doped with B$^-$ and F$^-$ anions using one-pot hydrothermal approach in the presence of hydrofluoric acid and obtained the (001) faceted anatase TiO_2 with several morphology, such as rounded and square nanosheet. It was realized that the square-shape nanosheet exhibited higher photocatalytic performance compared to others morphologies, thanks to its unique shape containing large-density high-energy site, such as vertexes. The existence of co-dopant of B$^-$ and F$^-$ anions might also take an additional role in the improvement of the performance in the photodegradation. In the typical procedure, it was able to degrade the methylene blue dye up to 95% within only 5 h. This
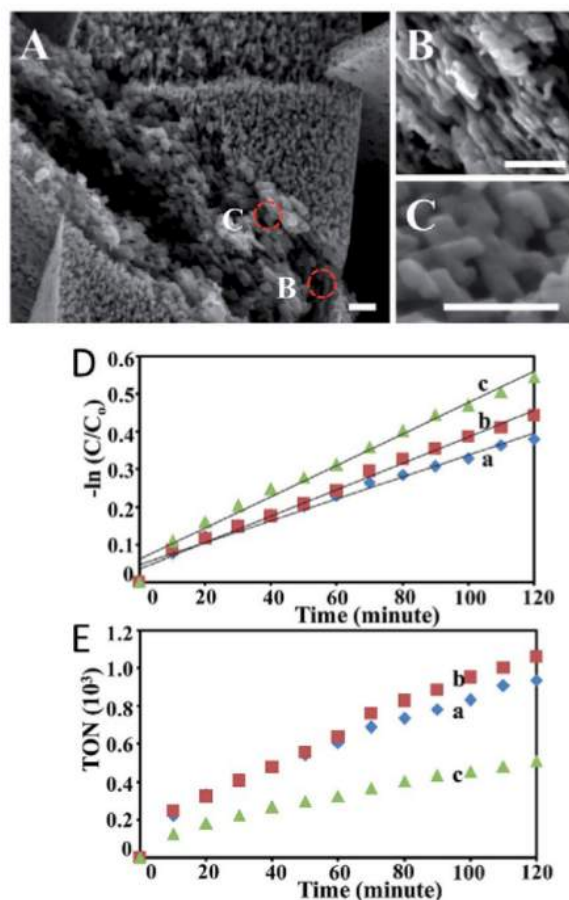
Fig. 31. FESEM image and their corresponding photocatalytic performance of porous anatase TiO₂ nanowall with rich (001) facet and comparison with the performance after being doped with Zn and the performance of anatase TiO₂ microtablet. (a) TNW, (b) ZTNW and (c) microtablet. (Scale bars are 100 nm in (A). (Reprinted from Ref. [95], Copyright 2014 The Royal Society of Chemistry).

photocatalytic properties was then further shown in the inactivation of e-coli bacteria under visible irradiation (Fig. 29) in which it is indicated that the bacteria was fully inactivated within only a very short time, i.e. 15 min. This process is associated with is due to a combinative effect of highly active (001) facet of anatase TiO₂ and the existence of co-doping. While the high-energy facet of (001) promote intense surface adsorption and reaction, remarkable active surface reaction and charge transfer are further augmented by the co-doping effect via band gap narrowing due to the mixing of B 2p-orbital with O 2p [166] and partial reduction of Ti⁴⁺ to Ti³⁺, which acts as a photo-induced electron trap and charge separation [167].

Amano et al. in a different study discovered that the doping of anatase TiO₂ with non-metal, such as hydrogen, which was achieved via hydrogen thermal treatment, has efficiently improved its electrical conductivity, photoactivity and photoelectrochemical properties via the increasing of electron trapping at the Ti lattice site (Ti³⁺) [168,169]. In a recent investigation by Li et al., it was understood that the introduction of carbonaceous materials in the lattice or in the vicinity of (001) faceted anatase TiO₂ has also effectively expanded its photoactivity and shifted its photosensitivity to visible region (see Fig. 30) [170].

3.2.2. Porous system

Porous TiO₂ nanostructure system has come as promising alternative for high performance in photocatalysis, dye sensitize solar cell, and other surface photo physico-chemical process. Beside enhancing the mass transport, porosity also modifies the nature of redox species adsorption onto the surface of the catalyst, modifying the nature of the catalyst-redox species interaction and determining the efficiency and the selectivity [171]. There are wide range of study that have been carried out on determining the relationship between the porosity and the catalytic performance of the porous anatase TiO₂. In Table 4, we list down several recent study on this issue with application ranging from pollutant degradation, hydrogenation or dehydrogenation and hydrogen evolution reactions. For example, in our recent study, it was found that the photocatalytic performance of (001) faceted anatase TiO₂ can be further enhanced up to multiple order by preparing them in the form of porous structure, i.e. nanowall that is composed of hierarchical assembly of high-energy facet contained nanocuboids [95]. In typical process, it was understood that the porous nanowall exhibited much higher photocatalytic performance in the degradation of methylene blue dye with TOF reaches the value of 9.84 min⁻¹ (see Fig. 31) compared to the performance shown by the non-porous system. Different investigation using porous anatase system also indicated that the availability of large-area of high-energy facet anatase TiO₂ has effectively augmented the mass of adsorbates adsorption and accelerated the reaction. Besides this phenomena, the accumulation of optical field inside the porous structure has further multiplied the photoactivation of the high-energy facet anatase TiO₂, enhancing the performance.

Yang et al. [185] has investigated such porosity effect on the photocatalytic performance of hierarchical spherical-shape anatase TiO₂ nanostructure in the degradation of several organic dye, such as phenolphthalein and methyl orange. They found that the porous hierarchical structure of anatase TiO₂ demonstrated an exceptional high performance if compared to the solid spherical structure or spherical P25 due to its much higher pore density (0.27 cm³g⁻¹) and surface area (223 m²/g) compared to solid spherical structure (pore density and surface area of 0.05 cm³g⁻¹ and 26 m²/g, respectively). For example in the case of methylene blue degradation, it was required as short as 50 min to completely remove a 100 mL of 30 mgL⁻¹ methylene blue. Meanwhile, it was around 70 min if using solid spherical nanoparticle of TiO₂ and even it was longer if using P25 nanoparticles. Similar trend was also observed in the case of other dye, such as methyl orange, phenolphthalein and procion red (Fig. 32).

Further, such phenomenon was also observed by Zheng et al. [117] By preparing porous anatase TiO₂ nanostructure with dominant (001) crystalline plane, which is constructed by (001) faceted small structure, outstanding photocatalytic performance has been obtained in the degradation of methylene orange dye. The performance of porous anatase nanocrystal was compared with the non-porous anatase single crystal, rutile single crystal and mesoporous rutile single crystal (see Fig. 33). As can be seen from the figure, the mesoporous anatase single crystal (A-MSC) TiO₂ sample shows exceptionally high catalytic performance compared to the non-porous single crystal or even compared to the rutile mesoporous nanocrystal in the degradation of MO. As has been predicted, it is due to the efficient adsorbates diffusion and attachment onto the surface of catalyst, facilitating facile surface reaction and charge transfer process. It was also understood that the porous structure provides a facile charge transport from the bulk to the nanocrystal surface, enabling the suppression of photogenerated electron and hole recombination. Thus, activating massive photocatalytic process. Similar phenomena have also been observed by several researchers [186,187] earlier, where the enhancement in the
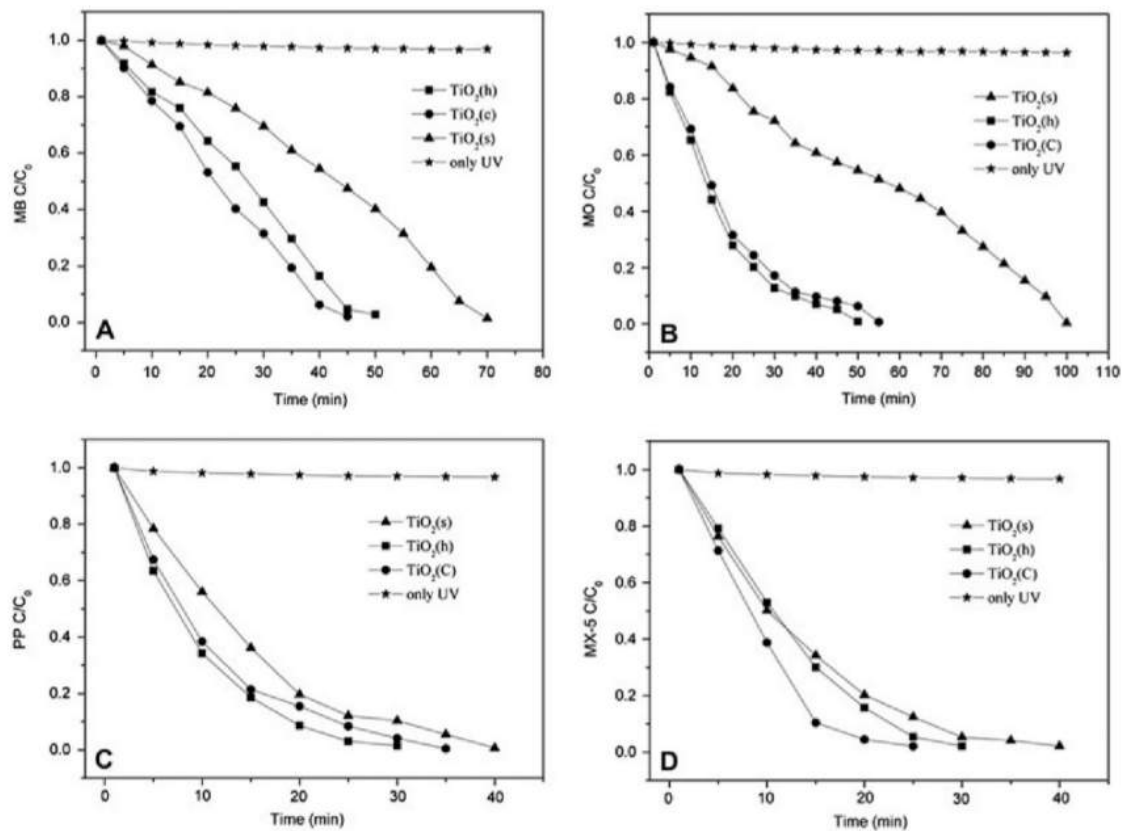
Fig. 32. Photocatalytic performance of porous TiO₂ in the degradation of (A) MB, (B) MO, (C) PP, and (D) MX-5, under UV irradiation. (Reprinted from Ref. [185], Copyright 2012 Elsevier Inc.).
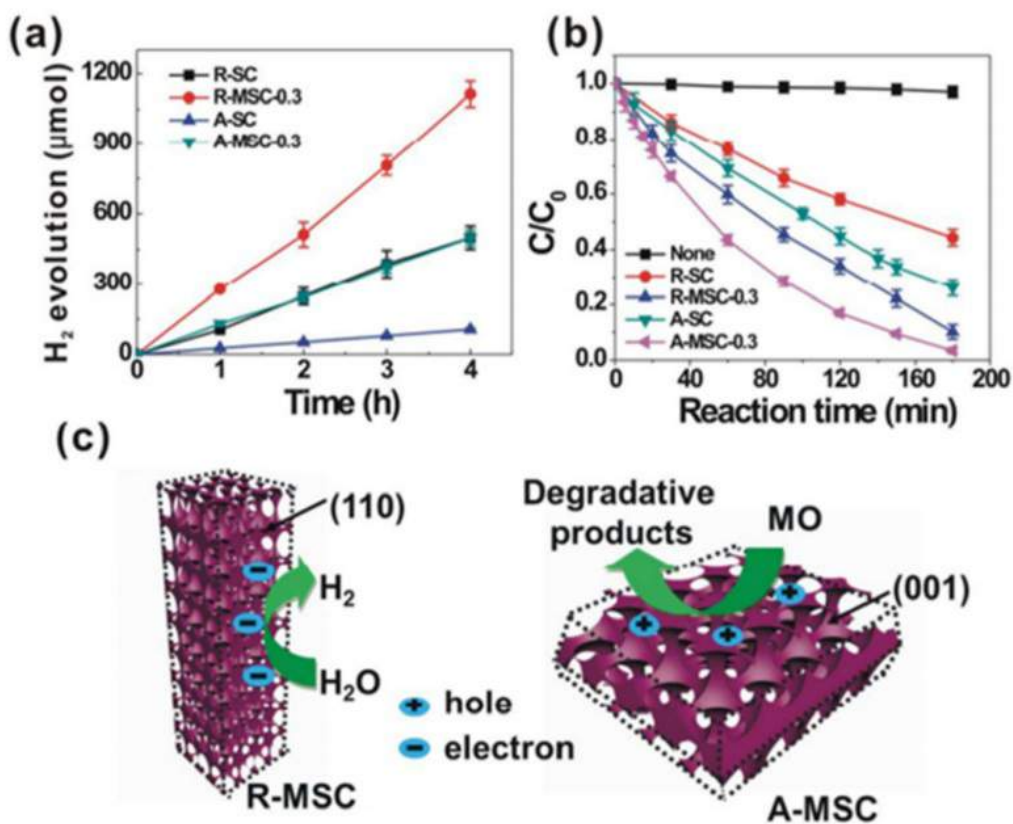
photocatalytic performance of anatase TiO2 can be realized when the nanostructure were prepared in the form of porous properties and containing (001) crystalline facet.

Nevertheless, while the porosity effectively gives rise to the catalytic performance via an enhanced adsorbates adsorption and surface reaction as well as augmented photoactivation effects, the performance can be further upgraded by introducing dopant into the porous anatase TiO2 lattice. We have recently observed this process by comparing the photocatalytic properties of doped (Zn) and undoped porous high-energy facet anatase TiO2, i.e. TiO2 nanowalls and TiO2 microtablets, respectively. As has been expected, despite in the typical process the BET surface area of the TiO2 nanowall much lower than the TiO2 microtablet, its photo-catalytic performance is higher than the undoped TiO2 micro-tablets. As has been already discussed earlier, this is certainly due to the modification of electronic properties of the surface upon being doped, enhancing the surface reaction and charge transfer on the surface. Such unique performance was also demonstrated in the solar cell applications [156]. Nevertheless, the introduction of dopant into the porous anatase lattice may affect the nanocrystal growth morphology, but the (001) facet nature is maintained [93].

Cheng et al. [188] also demonstrated how the doping process modified the photocatalytic performance of the porous anatase TiO2 system. By carrying out a straightforward hydrothermal approach, porous anatase TiO2 doped with several transition metal of 2⁺ oxidation state, i.e. Co, Zn and Ni were prepared (Fig. 34). The

porous doped samples were high in surface area with BET surface area of approximately as high as 208 m²/g. It was also found that the doping process has dramatically enhanced the photocatalytic performance of the porous samples via a modification of their electrical and optical properties (Fig. 34e). The process was understood to be a type of metal dopant dependent.

Enhancement in the photocatalytic hydrogen evolution has also been demonstrated from porous and hollow N-doped anatase TiO2 [150]. Hollow sphere with variable thickness were prepared and was realized that the thinner the sphere shell the higher the pho-tocatalytic hydrogen evolution was (see Fig. 35). The improvement of the photocatalytic performance in the thinner shell sample was assumed due to the increasing of the specific surface area and reactive active sites for redox reactions. The existence of facile carrier transfer and separation during the photoexcitation in the shell was also considered to contribute to the enhancement of the photocatalytic performance. It was also found that the nano-structure with lowest shell's thickness enabled rapid diffusion due to short pathway to the reactive site. Such unique structure and porosity as well as crystalline facet availability properties have also enabled high-photocatalytic performance in conversion CO2 into renewable fuels [189], water splitting [190], decomposition of dye molecules [146,191,192], anti-bacterial [193], Doping or composi-tion of hollow sphere anatase TiO2 with metal, such as Au [194,195], Ag [196], Pt [197], C [198], etc., have also further enhanced its performance in existing application.

Fig. 33. Photocatalytic performance of mesoporous faceted anatase TiO_2 with different porosity properties in hydrogen evolution (a) and methyl orange degradation (b) compared to their rutile counterpart. (c) The mechanism of photoreduction for hydrogen evolution on R-MSCs and photo-oxidation MO degradation on AMSCs, respectively. (Reprinted from Ref. [117], Copyright 2013 The American Chemical Society).

4. Conclusions and outlook

This review is to provide a selected strategy to realize high-energy facet of anatase TiO_2 nanostructure with porous structure and to introduce a metal or non-metal dopants into their lattice as the effort to modify their electrical, optical and photocatalytic properties. There have been a couple of methods available nowadays that may realize the formation of such nanocrystals. They can be clustered into several group, including template, etching and surfactant directed methods. The template approach may present as a versatile strategy to prepare highly porous high-energy facet TiO_2 nanostructure by simply using a pre-existing mould during the growth process, which could be from hard or soft templates, and removing them via etching or thermal annealing. The etching method presents as different potential alternative strategy for the preparation of high-energy facet and porous anatase TiO_2 nanostructures. The selection of facet selective etching agent may further enable the formation of controlled-facet and porosity properties of anatase TiO_2 nanostructures. Meanwhile, the surfactant directed method so far is the most versatile strategy to realize porous and high-energy faceted anatase TiO_2 nanostructures, which ranging from fluorination process to using a more complexes surfactant system for surface passivation of porosity formations. The anatase TiO_2 nanostructures with such these properties have demonstrated exceptionally high performance compared to anatase TiO_2 with different morphology. It was highlighted that the existence of facet selected photogenerated carrier segregation is considered as a driving factor for the boosting of their performance in photocatalysis application and others photoprocess. For example, the (001) facets is favoured to be occupied by the photogenerated hole, enhancing a reduction reaction on this surface. Meanwhile, the photogenerated electrons are favoured to be segregated into the (101) facet, promoting active oxidation reaction on this surface.

Owing to the important role of facets on any photoprocess as the presence of facile photogenerated carrier segregation, to continue the effort to develop a new strategy in order to realize anatase TiO_2 containing special facet, such as (110), (111), etc., is highly demanded in short future, providing the avenue for exceptionally high-performance in photocatalysis applications. We estimate that the proper approach to achieve this goal is to use surfactant directed approach to control the growth of the anatase TiO_2 nanocrystal, beside the fluorination effect. Potential surfactant could be polyvinylpyrrolidone, cetyltrimethylammonium bromide, hexamethyletetramine, etc., which are well-known agent for platonic nanocrystal growth in metals and metaloxides nanostructures. By using combinative effect of different surfactants as well as fluorination effect, controlled growth of high energy facet anatase TiO_2 nanocrystals could be realized.

It is also well understood that the particular physico-chemical process is facet depended process involving unique interaction
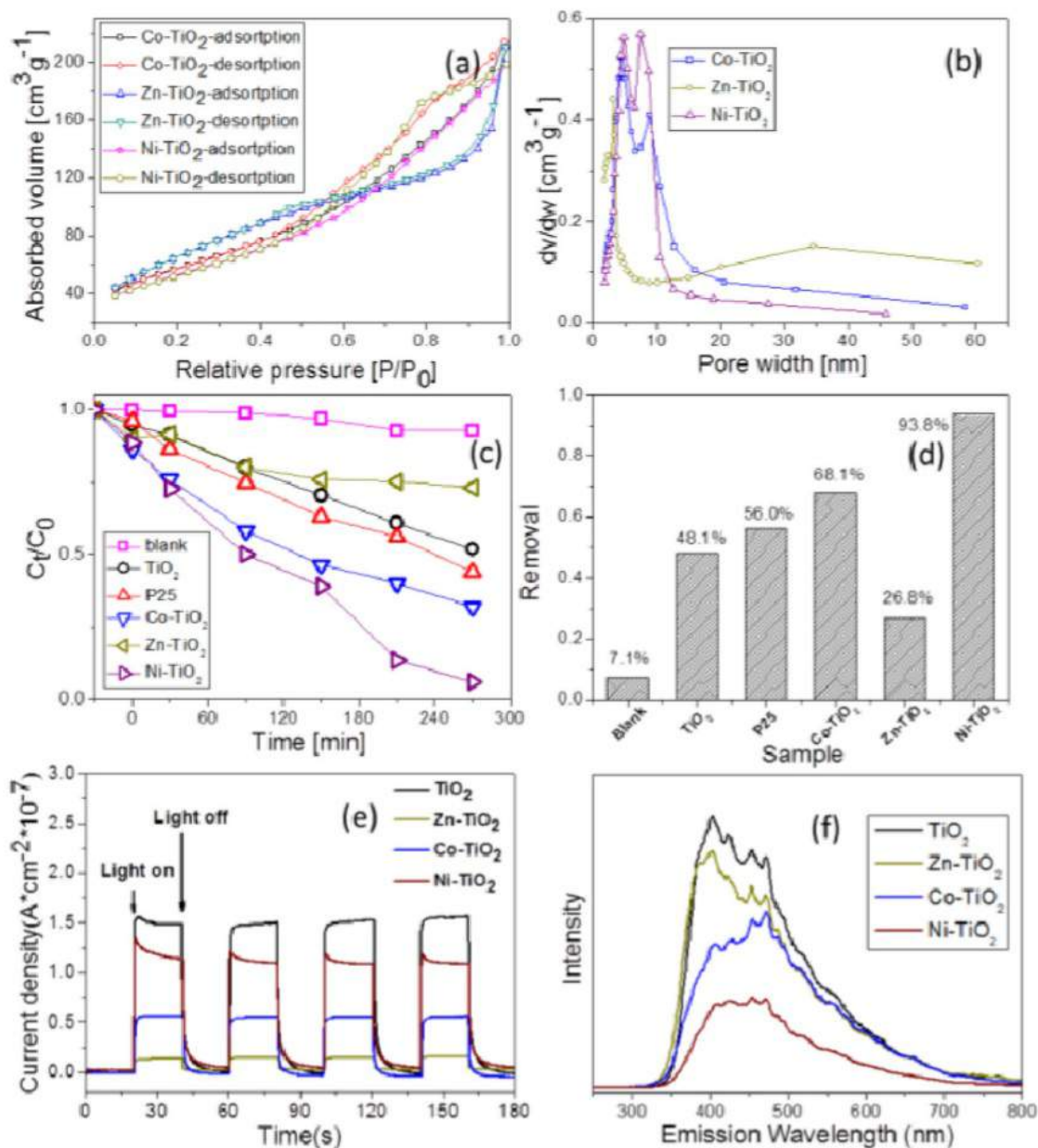
Fig. 34. Performance of N-doped porous anatase TiO$_2$ in the degradation of rhodamine B. (a) Nitrogen adsorption–desorption isotherms and (b) pore size distribution of doped TiO$_2$ products; (c) change of rhodamine B concentration (Ct/C0) during photocatalysis process under a 500 W Xe lamp with a 420 nm cutoff filter; (d) Degradation rate of rhodamine B removal; (e) Photocurrents response of doped TiO$_2$ sample under a 500 W Xe lamp light irradiation at a constant potential; (f) PL spectra of the sample at room-temperature with the excitation wavelength of 200 nm. (Reprinted from Ref. [188], Copyright 2015 The Royal Society of Chemistry).
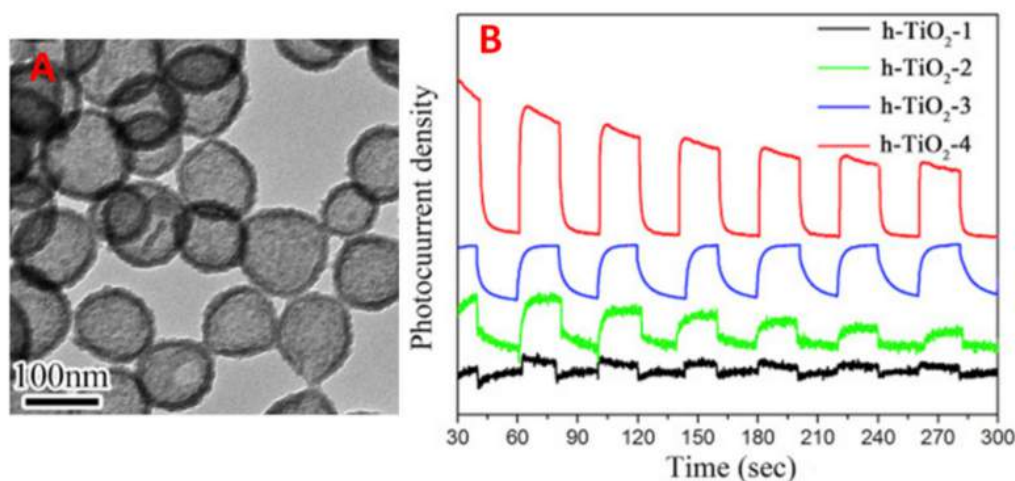
Fig. 35. Photoactivity of porous and hollow sphere anatase. (A) TEM image and (B) Photocurrent vs. time (I–t) curves of the porous TiO_2 hollow spheres with different shell thicknesses under UV light irradiation ($\lambda < 400$ nm). Bias potential is 0.8 V vs. Ag/AgCl. (Reprinted from Ref. [150], Copyright 2016 Elsevier B.V.).

between the surface atom and the reactant, such as photolysis of water preferred to occur on (101) surface meanwhile hydrogen adsorption favour (001) facets. To design porous anatase TiO_2 containing controlled the right facet ratio is highly desired to facilitate expanded-photolysis of water and hydrogen capturing. Potential performance in existing application could also be produced if porous (001) faceted TiO_2 nanostructure containing mixed phase of anatase and rutile is prepared.

As the quantum effect always generates unusual phenomena in the materials system, especially the two-dimensional (2D) system, atomically thin nanoplates (i.e. few nanometers thick) anatase TiO_2 will offer outstanding performance in applications, thanks to unique one-dimensional confinement of photogenerated electron and holes. Introduction of porosity in the atomically thin sheet will further augment the surface active sites, thus their photocatalytic properties. Therefore, the future research direction should be focused on the attempt to realize atoms thick porous anatase TiO_2 nanosheet. The method should also have capability to produce different crystalline facet and surface properties so that outstanding photocatalytic properties in strategic field, such as energy and environment issue, could be achieved.

Acknowledgements

References

[1] A.J. Nozik, Photoelectrolysis of water using semiconducting TiO_2 crystals, Nature 257 (1975) 383–386.

[2] M. Fujihira, Y. Satoh, T. Osa, Heterogeneous photocatalytic oxidation of aromatic compounds on TiO2, Nature 293 (1981) 206–208.

[3] A. Fujishima, K. Honda, Electrochemical photolysis of water at a semiconductor electrode, Nature 238 (1972) 37–38.

[4] B. O'Regan, M. Gratzel, A low-cost, high-efficiency solar cell based on dye-sensitized colloidal TiO2 films, Nature 353 (1991) 737–740.

[5] J. Bai, B. Zhou, Titanium dioxide nanomaterials for sensor applications, Chem. Rev. 114 (2014) 10131–10176.

[6] Y. Wang, J. Liu, M. Wang, C. Pei, B. Liu, Y. Yuan, S. Liu, H. Yang, Enhancing the sensing properties of TiO2 nanosheets with exposed {001} facets by a hydrogenation and sensing mechanism, Inorg. Chem. 56 (2017) 1504–1510.

[7] S.U.M. Khan, M. Al-Shahry, W.B. Ingler, Efficient photochemical water splitting by a chemically modified n-TiO_2, Science 297 (2002) 2243–2245.

[8] A. Tanaka, K. Teramura, S. Hosokawa, H. Kominami, T. Tanaka, Visible light-induced water splitting in an aqueous suspension of a plasmonic Au/TiO2 photocatalyst with metal co-catalysts, Chem. Sci. 8 (2017) 2574–2580.

[9] I.S. Cho, J. Choi, K. Zhang, S.J. Kim, M.J. Jeong, L. Cai, T. Park, X. Zheng, J.H. Park, Highly efficient solar water splitting from transferred TiO2 nanotube arrays, Nano Lett. 15 (2015) 5709–5715.

[10] T.M. Breault, J.J. Brancho, P. Guo, B.M. Bartlett, Visible light water oxidation using a Co-Catalyst loaded anatase-structured Ti1−(5x/4)NbxO2−y−δNy compound, I.norg. Chem. 52 (2013) 9363–9368.

[11] K. Drew, G. Girishkumar, K. Vinodgopal, P.V. Kamat, Boosting fuel cell performance with a semiconductor Photocatalyst: TiO2/Pt−Ru hybrid catalyst for methanol oxidation, J. Phys. Chem. B 109 (2005) 11851–11857.

[12] B. Seger, P.V. Kamat, Fuel cell geared in reverse: photoelectric hydrogen production using a TiO2/Nafion/Pt membrane assembly with No applied bias, J. Phys. Chem. C 113 (2009) 18946–18952.

[13] M. Antoniadou, D.I. Kondarides, D.D. Dionysiou, P. Lianos, Quantum dot sensitized titania applicable as photoanode in photoactivated fuel cells, J. Phys. Chem. C 116 (2012) 16901–16909.

[14] P. Dhanasekaran, S.V. Selvaganesh, S.D. Bhat, A nitrogen and cobalt co-doped titanium dioxide framework as a stable catalyst support for polymer electrolyte fuel cells, RSC Adv. 6 (2016) 88736–88750.

[15] J. Kim, D. Monllor-Satoca, W. Choi, Simultaneous production of hydrogen with the degradation of organic pollutants using TiO2 photocatalyst modified with dual surface components, Energy & Environ. Sci. 5 (2012) 7647–7656.

[16] C.M. Schmidt, A.M. Buchbinder, E. Weitz, F.M. Geiger, Photochemistry of the indoor air pollutant acetone on degussa P25 TiO2 studied by chemical ionization mass spectrometry, J. Phys. Chem. A 111 (2007) 13023–13031.

[17] H. Chen, C.E. Nanayakkara, V.H. Grassian, Titanium dioxide photocatalysis in atmospheric chemistry, Chem. Rev. 112 (2012) 5919–5948.

[18] V.P. Gupta, N.M. Ravindra, Optoelectronic properties of rutile (TiO2), J. Phys. Chem. Solids 41 (1980) 591–594.

[19] E.J.W. Crossland, N. Noel, V. Sivaram, T. Leijtens, J.A. Alexander-Webber, H.J. Snaith, Mesoporous TiO2 single crystals delivering enhanced mobility and optoelectronic device performance, Nature 495 (2013) 215–219.

[20] Y. Li, J.K. Cooper, W. Liu, C.M. Sutter-Fella, M. Amani, J.W. Beeman, A. Javey, J.W. Ager, Y. Liu, F.M. Toma, I.D. Sharp, Defective TiO2 with High Photoconductive Gain for Efficient and Stable Planar Heterojunction Perovskite Solar Cells, vol. 7, 2016, p. 12446.

[21] C.T. Dominguez, Y. Lacroute, D. Chaumont, M. Sacilotti, C.B. de Araújo, A.S.L. Gomes, Microchip random laser based on a disordered TiO2-nanomembranes arrangement, Opt. Express 20 (2012) 17380–17385.

[22] R. Asahi, Y. Taga, W. Mannstadt, A.J. Freeman, Electronic and optical properties of anatase TiO2, Phys. Rev. B 61 (2000) 7459–7465.

[23] U. Bach, D. Lupo, P. Comte, J.E. Moser, F. Weissortel, J. Salbeck, H. Spreitzer, M. Gratzel, Solid-state dye-sensitized mesoporous TiO2 solar cells with high photon-to-electron conversion efficiencies, Nature 395 (1998) 583–585.

[24] N.P. Chadwick, A. Kafizas, R. Quesada-Cabrera, C. Sotelo-Vazquez, S.M. Bawaked, M. Mokhtar, S.A. Al Thabaiti, A.Y. Obaid, S.N. Basahel, J.R. Durrant, C.J. Carmalt, I.P. Parkin, Ultraviolet radiation induced dopant loss in a TiO2 photocatalyst, ACS Catal. 7 (2017) 1485–1490.

[25] K.C. Christoforidis, M. Fernandez-Garcia, Photoactivity and charge trapping sites in copper and vanadium doped anatase TiO2 nano-materials, Catal. Sci. Technol. 6 (2016) 1094–1105.

[26] T. Luttrell, S. Halpegamage, J. Tao, A. Kramer, E. Sutter, M. Batzill, Why is anatase a better photocatalyst than rutile? - Model studies on epitaxial TiO2 films, Sci. Rep. 4 (2014) 4043.

[27] U. Diebold, The surface science of titanium dioxide, Surf. Sci. Rep. 48 (2003) 53–229.

[28] N. Roy, Y. Park, Y. Sohn, K.T. Leung, D. Pradhan, Green synthesis of anatase TiO2 nanocrystals with diverse shapes and their exposed facets-dependent photoredox activity, ACS Appl. Mater. Interfaces 6 (2014) 16498–16507.

[29] B. Sambandam, A. Surenjan, L. Philip, T. Pradeep, Rapid synthesis of C-TiO2: tuning the shape from spherical to rice grain morphology for visible light photocatalytic application, ACS Sustain. Chem. Eng. 3 (2015) 1321–1329.

[30] M. Enachi, I. Tiginyanu, V. Sprincean, V. Ursaki, Self-organized nucleation layer for the formation of ordered arrays of double-walled TiO2 nanotubes with temperature controlled inner diameter, Phys. Status Solidi (RRL) – Rapid Res. Lett. 4 (2010) 100–102.

[31] Z. Lian, W. Wang, G. Li, F. Tian, K.S. Schanze, H. Li, Pt-enhanced mesoporous Ti3+/TiO2 with rapid bulk to surface electron transfer for photocatalytic hydrogen evolution, ACS Appl. Mater. Interfaces 9 (2016) 16959–16966.

[32] S.-Y. Luo, B.-X. Yan, J. Shen, Intense photocurrent from Mo-Doped TiO2 film with depletion layer array, ACS Appl. Mater. Interfaces 6 (2014) 8942–8946.

[33] Q. Meng, T. Wang, E. Liu, X. Ma, Q. Ge, J. Gong, Understanding electronic and optical properties of anatase TiO2 photocatalysts co-doped with nitrogen and transition metals, Phys. Chem. Chem. Phys. 15 (2013) 9549–9561.

[34] G. Liu, H.G. Yang, J. Pan, Y.Q. Yang, G.Q. Lu, H.-M. Cheng, Titanium dioxide crystals with tailored facets, Chem. Rev. 114 (2014) 9559–9612.

[35] F. De Angelis, C. Di Valentin, S. Fantacci, A. Vittadini, A. Selloni, Theoretical studies on anatase and less common TiO2 phases: bulk, surfaces, and nanomaterials, Chem. Rev. 114 (2014) 9708–9753.

[36] K. Bourikas, C. Kordulis, A. Lycourghiotis, Titanium dioxide (anatase and rutile): surface chemistry, liquid–solid interface chemistry, and scientific synthesis of supported catalysts, Chem. Rev. 114 (2014) 9754–9823.

[37] R. Asahi, T. Morikawa, H. Irie, T. Ohwaki, Nitrogen-doped titanium dioxide as visible-light-sensitive photocatalyst: designs, developments, and prospects, Chem. Rev. 114 (2014) 9824–9852.

[38] L. Forro, O. Chauvet, D. Emin, L. Zuppiroli, H. Berger, F. Lévy, High mobility n-type charge carriers in large single crystals of anatase (TiO2), J. Appl. Phys. 75 (1994) 633–635.

[39] H. Tang, K. Prasad, R. Sanjinès, P.E. Schmid, F. Lévy, Electrical and optical properties of TiO2 anatase thin films, J. Appl. Phys. 75 (1994) 2042–2047.

[40] Q. Hou, C. Zhao, L. Qu, Effects of V heavy doping on the magnetic and optical properties in anatase TiO2, Int. J. Mod. Phys. B 31 (2017) 1650240.

[41] X.D. Liu, E.Y. Jiang, Z.Q. Li, Q.G. Song, Electronic structure and optical properties of Nb-doped anatase TiO2, Appl. Phys. Lett. 92 (2008) 252104.

[42] Z. Zongyan, L. Qingju, Effects of lanthanide doping on electronic structures and optical properties of anatase TiO2 from density functional theory calculations, J. Phys. D Appl. Phys. 41 (2008) 085417.

[43] B. Shao, Y.-f. He, M. Feng, Y. Lu, X. Zuo, Unexpected magnetic anisotropy induced by oxygen vacancy in anatase TiO2: a first-principles study, J. Appl. Phys. 115 (2014) 17A915.

[44] B. Bharti, S. Kumar, H.-N. Lee, R. Kumar, Formation of oxygen vacancies and Ti3+ state in TiO2 thin film and enhanced optical properties by air plasma treatment, Sci. Rep. 6 (2016) 32355.

[45] S. Ohta, T. Sekiya, S. Kurita, Pressure dependence of optical properties of anatase TiO2 single crystal, Phys. Status Solidi (b) 223 (2001) 265–269.

[46] C.C. Mercado, F.J. Knorr, J.L. McHale, S.M. Usmani, A.S. Ichimura, L.V. Saraf, Location of hole and electron traps on nanocrystalline anatase TiO2, J. Phys. Chem. C 116 (2012) 10796–10804.

[47] R.E. Rex, Y. Yang, F.J. Knorr, J.Z. Zhang, Y. Li, J.L. McHale, Spectroelectrochemical photoluminescence of trap states in H-Treated rutile TiO2 nanowires: implications for photooxidation of water, J. Phys. Chem. C 120 (2016) 3530–3541.

[48] C. Mercado, Z. Seeley, A. Bandyopadhyay, S. Bose, J.L. McHale, Photoluminescence of dense nanocrystalline titanium dioxide thin films: effect of doping and thickness and relation to gas sensing, ACS Appl. Mater. Interfaces 3 (2011) 2281–2288.

[49] H. Tang, H. Berger, P.E. Schmid, F. Lévy, Optical properties of anatase (TiO2), Solid State Commun. 92 (1994) 267–271.

[50] B.T. Chiad, M.A. Hameed, K.H. Latif, F.J. AL-Maliki, Transition from Amplified Spontaneous Emission to Laser Action in Disordered Media of R6G Dye and TiO2 Nanoparticles Doped with PMMA Polymer, J. Eur. Opt. Soc. 6 (2011) 11049.

[51] H. Tang, H. Berger, P.E. Schmid, F. Lévy, G. Burri, Photoluminescence in TiO2 anatase single crystals, Solid State Commun. 87 (1993) 847–850.

[52] A. Amtout, R. Leonelli, Time-resolved photoluminescence from excitons in TiO2, Solid State Commun. 84 (1992) 349–352.

[53] D.K. Pallotti, L. Passoni, F. Gesuele, P. Maddalena, F. Di Fonzo, S. Lettieri, Giant O2-Induced photoluminescence modulation in hierarchical titanium dioxide nanostructures, ACS Sensors 2 (2017) 61–68.

[54] B. Roose, S. Pathak, U. Steiner, Doping of TiO2 for sensitized solar cells, Chem. Soc. Rev. 44 (2015) 8326–8349.

[55] A.K. Rumaiz, J.C. Woicik, E. Cockayne, H.Y. Lin, G.H. Jaffari, S.I. Shah, Oxygen vacancies in N doped anatase TiO2: experiment and first-principles

[56] E. Finazzi, C. Di Valentin, A. Selloni, G. Pacchioni, First principles study of nitrogen doping at the anatase TiO2(101) surface, J. Phys. Chem. C 111 (2007) 9275–9282.

[57] C.L. Muhich, J.Y. Westcott, T. Fuerst, A.W. Weimer, C.B. Musgrave, Increasing the photocatalytic activity of anatase TiO2 through B, C, and N doping, J. Phys. Chem. C 118 (2014) 27415–27427.

[58] C. Sotelo-Vazquez, N. Noor, A. Kafizas, R. Quesada-Cabrera, D.O. Scanlon, A. Taylor, J.R. Durrant, I.P. Parkin, Multifunctional P-Doped TiO2 films: a new approach to self-cleaning, transparent conducting oxide materials, Chem. Mater. 27 (2015) 3234–3242.

[59] K. Yang, Y. Dai, B. Huang, Understanding photocatalytic activity of S- and P-Doped TiO2 under visible light from first-principles, J. Phys. Chem. C 111 (2007) 18985–18994.

[60] S.A. Bakar, C. Ribeiro, Prospective aspects of preferential {001} facets of N,S-co-doped TiO2 photocatalysts for visible-light-responsive photocatalytic activity, RSC Adv. 6 (2016) 89274–89287.

[61] J. Chung, J.W. Chung, S.-Y. Kwak, Adsorption-assisted photocatalytic activity of nitrogen and sulfur codoped TiO2 under visible light irradiation, Phys. Chem. Chem. Phys. 17 (2015) 17279–17287.

[62] N. Liu, C. Schneider, D. Freitag, U. Venkatesan, V.R.R. Marthala, M. Hartmann, B. Winter, E. Spiecker, A. Osvet, E.M. Zolnhofer, K. Meyer, T. Nakajima, X. Zhou, P. Schmuki, Hydrogenated anatase: strong photocatalytic dihydrogen evolution without the use of a Co-Catalyst, Angew. Chem. Int. Ed. 53 (2014) 14201–14205.

[63] N. Liu, C. Schneider, D. Freitag, U. Venkatesan, V.R.R. Marthala, M. Hartmann, B. Winter, E. Spiecker, A. Osvet, E.M. Zolnhofer, K. Meyer, T. Nakajima, X. Zhou, P. Schmuki, Hydrogenated anatase: strong photocatalytic dihydrogen evolution without the use of a Co-Catalyst, Angew. Chem. 126 (2014) 14425–14430.

[64] E.M. Samsudin, S.B.A. Hamid, J.C. Juan, W.J. Basirun, G. Centi, Enhancement of the intrinsic photocatalytic activity of TiO2 in the degradation of 1,3,5-triazine herbicides by doping with N, F, Chem. Eng. J. 280 (2015) 330–343.

[65] S.A. Bakar, C. Ribeiro, Nitrogen-doped titanium dioxide: an overview of material design and dimensionality effect over modern applications, J. Photochem. Photobiol. C Photochem. Rev. 27 (2016) 1–29.

[66] M.-Y. Xing, W.-K. Li, Y.-M. Wu, J.-L. Zhang, X.-Q. Gong, formation of new structures and their synergistic effects in boron and nitrogen codoped TiO2 for enhancement of photocatalytic performance, J. Phys. Chem. C 115 (2011) 7858–7865.

[67] R. Long, N.J. English, First-Principles calculation of synergistic (N, P)-Codoping effects on the visible-light photocatalytic activity of anatase TiO2, J. Phys. Chem. C 114 (2010) 11984–11990.

[68] C. Di Valentin, E. Finazzi, G. Pacchioni, A. Selloni, S. Livraghi, A.M. Czoska, M.C. Paganini, E. Giamello, Density functional theory and electron paramagnetic resonance study on the effect of N–F codoping of TiO2, Chem. Mater. 20 (2008) 3706–3714.

[69] J.Z. Bloh, A. Folli, D.E. Macphee, Adjusting nitrogen doping level in titanium dioxide by codoping with tungsten: properties and band structure of the resulting materials, J. Phys. Chem. C 118 (2014) 21281–21292.

[70] C. Fàbrega, D. Monllor-Satoca, S. Ampudia, A. Parra, T. Andreu, J.R. Morante, Tuning the Fermi level and the kinetics of surface states of TiO2 nanorods by means of ammonia treatments, J. Phys. Chem. C 117 (2013) 20517–20524.

[71] E.M. Neville, M.J. Mattle, D. Loughrey, B. Rajesh, M. Rahman, J.M.D. MacElroy, J.A. Sullivan, K.R. Thampi, Carbon-doped TiO2 and carbon, tungsten-codoped TiO2 through sol–gel processes in the presence of melamine borate: reflections through photocatalysis, J. Phys. Chem. C 116 (2012) 16511–16521.

[72] Z. Zhao, Z. Li, Z. Zou, Water adsorption and decomposition on N/V-Doped anatase TiO2 (101) surfaces, J. Phys. Chem. C 117 (2013) 6172–6184.

[73] L. Sun, X. Zhao, X. Cheng, H. Sun, Y. Li, P. Li, W. Fan, Synergistic effects in La/N codoped TiO2 anatase (101) surface correlated with enhanced visible-light photocatalytic activity, Langmuir 28 (2012) 5882–5891.

[74] X. Zhang, F. Liu, Q.-L. Huang, G. Zhou, Z.-S. Wang, Dye-sensitized W-Doped TiO2 solar cells with a tunable conduction band and suppressed charge recombination, J. Phys. Chem. C 115 (2011) 12665–12671.

[75] V. Jovic, K.E. Smith, H. Idriss, G.I.N. Waterhouse, Heterojunction synergies in titania-supported gold photocatalysts: implications for solar hydrogen production, ChemSusChem 8 (2015) 2551–2559.

[76] M.J. Muñoz-Batista, A. Kubacka, M. Fernández-García, Effective enhancement of TiO2 photocatalysis by synergistic interaction of surface species: from promoters to Co-catalysts, ACS Catal. 4 (2014) 4277–4288.

[77] M. Eltermann, K. Utt, S. Lange, R. Jaaniso, Sm3+ doped TiO2 as optical oxygen sensor material, Opt. Mater. 51 (2016) 24–30.

[78] L.R. Sheppard, S. Hager, J. Holik, R. Liu, S. Macartney, R. Wuhrer, Tantalum segregation in Ta-Doped TiO2 and the related impact on charge separation during illumination, J. Phys. Chem. C 119 (2015) 392–400.

[79] Y. Wang, R. Zhang, J. Li, L. Li, S. Lin, First-principles study on transition metal-doped anatase TiO2, Nanoscale Res. Lett. 9 (2014) 46.

[80] Y. Xia, K. Zhu, T.C. Kaspar, Y. Du, B. Birmingham, K.T. Park, Z. Zhang, Atomic structure of the anatase TiO2(001) surface, J. Phys. Chem. Lett. 4 (2013) 2958–2963.

[81] H. Tang, Z. Cheng, S. Dong, X. Cui, H. Feng, X. Ma, B. Luo, A. Zhao, J. Zhao, B. Wang, Understanding the intrinsic chemical activity of anatase TiO2(001)-(1 × 4) surface, J. Phys. Chem. C 121 (2017) 1272–1282.

[82] N. Liu, K. Li, X. Li, Y. Chang, Y. Feng, X. Sun, Y. Cheng, Z. Wu, H. Zhang,

Crystallographic facet-induced toxicological responses by faceted titanium dioxide nanocrystals, ACS Nano 10 (2016) 6062—6073.

[83] N. Liu, Y. Chang, Y. Feng, Y. Cheng, X. Sun, H. Jian, Y. Feng, X. Li, H. Zhang, {101}—{001} surface heterojunction-enhanced antibacterial activity of titanium dioxide nanocrystals under sunlight irradiation, ACS Appl. Mater. Interfaces 9 (2017) 5907—5915.

[84] J.-G. Ma, C.-R. Zhang, J.-J. Gong, B. Yang, H.-M. Zhang, W. Wang, Y.-Z. Wu, Y.-H. Chen, H.-S. Chen, The adsorption of α-cyanoacrylic acid on anatase TiO2(101) and (001) surfaces: a density functional theory study, J. Chem. Phys. 141 (2014) 234705.

[85] S. Liu, J. Yu, M. Jaroniec, Anatase TiO2 with dominant high-energy {001} facets: synthesis, properties, and applications, Chem. Mater. 23 (2011) 4085—4093.

[86] S.-J. Liu, X.-X. Wu, B. Hu, J.-Y. Gong, S.-H. Yu, Novel anatase TiO2 boxes and tree-like structures assembled by hollow tubes: d,l-malic acid-assisted hydrothermal synthesis, growth mechanism, and photocatalytic properties, Cryst. Growth & Des. 9 (2009) 1511—1518.

[87] X. Zhao, W. Jin, J. Cai, J. Ye, Z. Li, Y. Ma, J. Xie, L. Qi, Shape- and size-controlled synthesis of uniform anatase TiO2 nanocuboids enclosed by active {100} and {001} facets, Adv. Funct. Mater. 21 (2011) 3554—3563.

[88] H.G. Yang, C.H. Sun, S.Z. Qiao, J. Zou, G. Liu, S.C. Smith, H.M. Cheng, G.Q. Lu, Anatase TiO2 single crystals with a large percentage of reactive facets, Nature 453 (2008) 638—641.

[89] J. Pan, G. Liu, G.Q. Lu, H.-M. Cheng, On the true photoreactivity order of {001}, {010}, and {101} facets of anatase TiO2 crystals, Angew. Chem. Int. Ed. 50 (2011) 2133—2137.

[90] G. Liu, H.G. Yang, X. Wang, L. Cheng, H. Lu, L. Wang, G.Q. Lu, H.-M. Cheng, Enhanced photoactivity of oxygen-deficient anatase TiO2 sheets with dominant {001} facets, J. Phys. Chem. C 113 (2009) 21784—21788.

[91] X. Han, Q. Kuang, M. Jin, Z. Xie, L. Zheng, Synthesis of titania nanosheets with a high percentage of exposed (001) facets and related photocatalytic properties, J. Am. Chem. Soc. 131 (2009) 3152—3153.

[92] B. Wu, C. Guo, N. Zheng, Z. Xie, G.D. Stucky, Nonaqueous production of nanostructured anatase with high-energy facets, J. Am. Chem. Soc. 130 (2008) 17563—17567.

[93] A.Y. Ahmed Al-She'irey, S.K. Md Saad, A.A. Umar, M.Y.A. Rahman, M.M. Salleh, (001) faceted-Ga-TiO2 microtablet synthesis and its organic perovskite sensitized solar cells characterization, J. Alloys Compd. 674 (2016) 470—476.

[94] A.A. Umar, S. Nafisah, S.K.M. Saad, S. Tee Tan, A. Balouch, M. Mat Salleh, M. Oyama, Poriferous microtablet of anatase TiO2 growth on an ITO surface for high-efficiency dye-sensitized solar cells, Sol. Energy Mater. Sol. Cells 122 (2014) 174—182.

[95] S.K.M. Saad, A. Ali Umar, H. Quan Nguyen, C. Fu Dee, M. Mat Salleh, M. Oyama, Porous (001)-faceted Zn-doped anatase TiO2 nanowalls and their heterogeneous photocatalytic characterization, RSC Adv. 4 (2014) 57054—57063.

[96] A.A. Shah, A.A. Umar, M.M. Salleh, Porous (001)-faceted anatase TiO2 nanorice thin film for efficient dye-sensitized solar cell, EPJ Photovolt. 7 (2016) 70501.

[97] X.-L. Cheng, M. Hu, R. Huang, J.-S. Jiang, HF-free synthesis of anatase TiO2 nanosheets with largely exposed and clean {001} facets and their enhanced rate performance as anodes of lithium-ion battery, ACS Appl. Mater. Interfaces 6 (2014) 19176—19183.

[98] C. Chen, L. Xu, G.A. Sewvandi, T. Kusunose, Y. Tanaka, S. Nakanishi, Q. Feng, Microwave-assisted topochemical conversion of layered titanate nanosheets to {010}-Faceted anatase nanocrystals for high performance photocatalysts and dye-sensitized solar cells, Cryst. Growth & Des. 14 (2014) 5801—5811.

[99] W. Yang, J. Li, Y. Wang, F. Zhu, W. Shi, F. Wan, D. Xu, A facile synthesis of anatase TiO2 nanosheets-based hierarchical spheres with over 90%{001} facets for dye-sensitized solar cells, Chem. Commun. 47 (2011) 1809—1811.

[100] W. Sun, T. Peng, Y. Liu, W. Yu, K. Zhang, H.F. Mehnane, C. Bu, S. Guo, X.-Z. Zhao, Layer-by-layer self-assembly of TiO2 hierarchical nanosheets with exposed {001} facets as an effective bifunctional layer for dye-sensitized solar cells, ACS Appl. Mater. Interfaces 6 (2014) 9144—9149.

[101] Z. He, L. Wen, D. Wang, Y. Xue, Q. Lu, C. Wu, J. Chen, S. Song, Photocatalytic reduction of CO2 in aqueous solution on surface-fluorinated anatase TiO2 nanosheets with exposed {001} facets, Energy & Fuels 28 (2014) 3982—3993.

[102] R. Yoshida, Y. Suzuki, S. Yoshikawa, Syntheses of TiO2(B) nanowires and TiO2 anatase nanowires by hydrothermal and post-heat treatments, J. Solid State Chem. 178 (2005) 2179—2185.

[103] H. Xu, X. Tao, D.-T. Wang, Y.-Z. Zheng, J.-F. Chen, Enhanced efficiency in dye-sensitized solar cells based on TiO2 nanocrystal/nanotube double-layered films, Electrochimica Acta 55 (2010) 2280—2285.

[104] W. Fumin, S. Zhansheng, G. Feng, J. Jinting, M. Adachi, Morphology control of anatase TiO2 by surfactant-assisted hydrothermal method** supported by the natural science foundation of tianjin (No. 06YFJMJC05000), Chin. J. Chem. Eng. 15 (2007) 754—759.

[105] E. Ghadiri, N. Taghavinia, S.M. Zakeeruddin, M. Grätzel, J.-E. Moser, Enhanced electron collection efficiency in dye-sensitized solar cells based on nanostructured TiO2 hollow fibers, Nano Lett. 10 (2010) 1632—1638.

[106] M. Safaei, R. Sarraf-Mamoory, M. Rashidzadeh, The interactive effect of agitation condition and titania particle size in hydrothermal synthesis of titanate nanostructures, J. Nanopart Res. 12 (2010) 2723—2728.

[107] O. Game, T. Kumari, U. Singh, V. Aravindan, S. Madhavi, S.B. Ogale, (001)

[108] faceted mesoporous anatase TiO2 microcubes as superior insertion anode in practical Li-ion configuration with LiMn2O4, Energy Storage Mater. 3 (2016) 106—112.

[108] Z. Xiu, M.H. Alfaruqi, J. Gim, J. Song, S. Kim, T.V. Thi, P.T. Duong, J.P. Baboo, V. Mathew, J. Kim, Hierarchical porous anatase TiO2 derived from a titanium metal—organic framework as a superior anode material for lithium ion batteries, Chem. Commun. 51 (2015) 12274—12277.

[109] D. Dahlan, S.K.M. Saad, A.U. Berli, A. Bajili, A.A. Umar, Synthesis of two-dimensional nanowall of Cu-Doped TiO2 and its application as photo-anode in DSSCs, Phys. E Low-dimensional Syst. Nanostructures 91 (2017) 185—189.

[110] A. Umar, M. Rahman, S. Saad, M. Salleh, M. Oyama, Preparation of grass-like TiO2 nanostructure thin films: effect of growth temperature, Appl. Surf. Sci. 270 (2013) 109—114.

[111] S. Illa, R. Boppella, S.V. Manorama, P. Basak, Mesoporous assembly of cuboid anatase nanocrystals into hollow spheres: realizing enhanced photoactivity of high energy {001} facets, J. Phys. Chem. C 120 (2016) 18028—18038.

[112] Z. Zhao, Z. Sun, H. Zhao, M. Zheng, P. Du, J. Zhao, H. Fan, Phase control of hierarchically structured mesoporous anatase TiO2 microspheres covered with {001} facets, J. Mater. Chem. 22 (2012) 21965—21971.

[113] B. Jin, S.-Z. Huang, J. Shu, H.-E. Wang, Y. Li, Y. Yu, L.-H. Chen, B.-J. Wang, B.-L. Su, Highly porous TiO2 hollow microspheres constructed by radially oriented nanorods chains for high capacity, high rate and long cycle capability lithium battery, Nano Energy 16 (2015) 339—349.

[114] B. Liu, K. Nakata, M. Sakai, H. Saito, T. Ochiai, T. Murakami, K. Takagi, A. Fujishima, Mesoporous TiO2 core—shell spheres composed of nanocrystals with exposed high-energy facets: facile synthesis and formation mechanism, Langmuir 27 (2011) 8500—8508.

[115] S. Liu, H. Jia, L. Han, J. Wang, P. Gao, D. Xu, J. Yang, S. Che, Nanosheet-constructed porous TiO2—B for advanced lithium ion batteries, Adv. Mater. 24 (2012) 3201—3204.

[116] P. Zhai, T.Y. Hsieh, C.Y. Yeh, K.S.K. Reddy, C.C. Hu, J.H. Su, T.C. Wei, S.P. Feng, Trifunctional TiO2 nanoparticles with exposed {001} facets as additives in cobalt-based porphyrin-sensitized solar cells, Adv. Funct. Mater. 25 (2015) 6093—6100.

[117] X. Zheng, Q. Kuang, K. Yan, Y. Qiu, J. Qiu, S. Yang, Mesoporous TiO2 single crystals: facile shape-, size-, and phase-controlled growth and efficient photocatalytic performance, ACS Appl. Mater. Interfaces 5 (2013) 11249—11257.

[118] C. Song, L. Wang, F. Gao, Q. Lu, Two-dimensional hollow TiO2 nanoplates with enhanced photocatalytic activity, Chem. — A Eur. J. 22 (2016) 6368—6373.

[119] Z. Yao, C. Wang, Y. Li, N.-Y. Kim, AAO-assisted synthesis of highly ordered, large-scale TiO(2) nanowire arrays via sputtering and atomic layer deposition, Nanoscale Res. Lett. 10 (2015) 166.

[120] J. Xue, F. Song, X.-W. Yin, Z.-L. Zhang, Y. Liu, X.-L Wang, Y.-Z. Wang, Cellulose nanocrystal-templated synthesis of mesoporous TiO2 with dominantly exposed (001) facets for efficient catalysis, ACS Sustain. Chem. Eng. 5 (2017) 3721—3725.

[121] M. Marszewski, J. Marszewska, S. Pylypenko, M. Jaroniec, Synthesis of porous crystalline doped titania photocatalysts using modified precursor strategy, Chem. Mater. 28 (2016) 7878—7888.

[122] W. Sun, W. Zhou, B. You, L. Wu, Facile fabrication and high photoelectric properties of hierarchically ordered porous TiO2, Chem. Mater. 24 (2012) 3800—3810.

[123] N. Vogel, M. Retsch, C.-A. Fustin, A. del Campo, U. Jonas, Advances in colloidal assembly: the design of structure and hierarchy in two and three dimensions, Chem. Rev. 115 (2015) 6265—6311.

[124] M.A. Boles, M. Engel, D.V. Talapin, Self-assembly of colloidal nanocrystals: from intricate structures to functional materials, Chem. Rev. 116 (2016) 11220—11289.

[125] Z. Xiu, M.H. Alfaruqi, J. Gim, J. Song, S. Kim, T.V. Thi, P.T. Duong, J.P. Baboo, V. Mathew, J. Kim, Hierarchical porous anatase TiO2 derived from a titanium metal-organic framework as a superior anode material for lithium ion batteries, Chem. Commun. 51 (2015) 12274—12277.

[126] J. Dou, Y. Li, F. Xie, X. Ding, M. Wei, Metal—organic framework derived hierarchical porous anatase TiO2 as a photoanode for dye-sensitized solar cell, Cryst. Growth & Des. 16 (2016) 121—125.

[127] Y.V. Kaneti, J. Tang, R.R. Salunkhe, X. Jiang, A. Yu, K.C.W. Wu, Y. Yamauchi, Nanoarchitectured design of porous materials and nanocomposites from metal-organic frameworks, Adv. Mater. 29 (2017) 1604898.

[128] C.H. Hendon, D. Tiana, M. Fontecave, C. Sanchez, L. D'arras, C. Sassoye, L. Rozes, C. Mellot-Draznieks, A. Walsh, Engineering the optical response of the titanium-MIL-125 metal—organic framework through ligand functionalization, J. Am. Chem. Soc. 135 (2013) 10942—10945.

[129] Z. Xiu, M.H. Alfaruqi, J. Gim, J. Song, S. Kim, P.T. Duong, J.P. Baboo, V. Mathew, J. Kim, MOF-derived mesoporous anatase TiO2 as anode material for lithium—ion batteries with high rate capability and long cycle stability, J. Alloys Compd. 674 (2016) 174—178.

[130] M. Zhao, T. Chen, C. Deng, Porous anatase TiO2 derived from a titanium metal-organic framework as a multifunctional phospho-oriented nanoreactor integrating accelerated digestion of proteins and in situ enrichment, RSC Adv. 6 (2016) 51670—51674.

[131] W.S. Chi, D.K. Roh, C.S. Lee, J.H. Kim, A shape- and morphology-controlled metal organic framework template for high-efficiency solid-state dye-

[132] J. Li, X. Xu, X. Liu, W. Qin, M. Wang, L. Pan, Metal-organic frameworks derived cake-like anatase/rutile mixed phase TiO2 for highly efficient photocatalysis, J. Alloys Compd. 690 (2017) 640–646.

[133] Y. Gu, K. Cheng, Y.-n. Wu, Y. Wang, C. Morlay, F. Li, Metal–organic framework-templated synthesis of bifunctional N-Doped TiO2–carbon nanotablets via solid-state thermolysis, ACS Sustain. Chem. Eng. 4 (2016) 6744–6753.

[134] Y. Zhu, J. Ciston, B. Zheng, X. Miao, C. Czarnik, Y. Pan, R. Sougrat, Z. Lai, C.-E. Hsiung, K. Yao, I. Pinnau, M. Pan, Y. Han, Unravelling surface and interfacial structures of a metal-organic framework by transmission electron microscopy, Nat. Mater. 16 (2017) 532–536.

[135] H. Yang, P.E. Kruger, S.G. Telfer, Metal–organic framework nanocrystals as sacrificial templates for hollow and exceptionally porous titania and composite materials, Lnorg. Chem. 54 (2015) 9483–9490.

[136] Q. Liu, B. Zhou, M. Xu, G. Mao, Integration of nanosized ZIF-8 particles onto mesoporous TiO 2 nanobeads for enhanced photocatalytic activity, RSC Adv. 7 (2017) 8004–8010.

[137] X.-N. Ren, L. Wu, J. Jin, J. Liu, Z.-Y. Hu, Y. Li, T. Hasan, X.-Y. Yang, G. Van Tendeloo, B.-L. Su, 3D interconnected hierarchically macro-mesoporous TiO2 networks optimized by biomolecular self-assembly for high performance lithium ion batteries, RSC Adv. 6 (2016) 26856–26862.

[138] Y. Cai, H-E. Wang, J. Jin, S.-Z. Huang, Y. Yu, Y. Li, S.-P. Feng, B.-L. Su, Hierarchically structured porous TiO2 spheres constructed by interconnected nanorods as high performance anodes for lithium ion batteries, Chem. Eng. J. 281 (2015) 844–851.

[139] J.C. Yu, X. Wang, X. Fu, Pore-wall chemistry and photocatalytic activity of mesoporous titania molecular sieve films, Chem. Mater. 16 (2004) 1523–1530.

[140] E. Ortel, S. Sokolov, C. Zielke, I. Lauermann, S. Selve, K. Weh, B. Paul, J. Polte, R. Kraehnert, Supported mesoporous and hierarchical porous Pd/TiO2 catalytic coatings with controlled particle size and pore structure, Chem. Mater. 24 (2012) 3828–3838.

[141] D. Fattakhova-Rohlfing, A. Zaleska, T. Bein, Three-dimensional titanium dioxide nanomaterials, Chem. Rev. 114 (2014) 9487–9558.

[142] W. Li, F.Wang, Y. Liu, J. Wang, J. Yang, L. Zhang, AA. Elzatahry, D. Al-Dahyan, Y. Xia, D. Zhao, General strategy to synthesize uniform mesoporous TiO2/graphene/mesoporous TiO2 sandwich-like nanosheets for highly reversible lithium storage, Nano Lett. 15 (2015) 2186–2193.

[143] Z. Hong, K. Zhou, J. Zhang, Z. Huang, M. Wei, Self-assembled synthesis of mesocrystalline TiO2@C-rGO hybrid nanostructures for highly reversible sodium storage, Cryst. Growth & Des. 16 (2016) 6605–6612.

[144] P. Wang, F. He, J. Wang, H. Yu, L. Zhao, Graphene oxide nanosheets as an effective template for the synthesis of porous TiO2 film in dye-sensitized solar cells, Appl. Surf. Sci. 358 (2015) 175–180.

[145] J.B. Joo, Q. Zhang, I. Lee, M. Dahl, F. Zaera, Y. Yin, Mesoporous anatase titania hollow nanostructures though silica-protected calcination, Adv. Funct. Mater. 22 (2012) 166–174.

[146] J.B. Joo, I. Lee, M. Dahl, G.D. Moon, F. Zaera, Y. Yin, Controllable synthesis of mesoporous TiO2 hollow shells: toward an efficient photocatalyst, Adv. Funct. Mater. 23 (2013) 4246–4254.

[147] X. Wang, J. Feng, Y. Bai, Q. Zhang, Y. Yin, Synthesis, properties, and applications of hollow micro-/nanostructures, Chem. Rev. 116 (2016) 10983–11060.

[148] Q. Yu, P. Wang, S. Hu, J. Hui, J. Zhuang, X. Wang, Hydrothermal synthesis of hollow silica spheres under acidic conditions, Langmuir 27 (2011) 7185–7191.

[149] L. Li, S. Zhou, E. Chen, R. Qiao, Y. Zhong, Y. Zhang, Z. Li, Simultaneous formation of silica-protected and N-doped TiO2 hollow spheres using organic-inorganic silica as self-removed templates, J. Mater. Chem. A 3 (2015) 2234–2241.

[150] L. Li, S. Bai, W. Yin, S. Li, Y. Zhang, Z. Li, A novel etching and reconstruction route to ultrathin porous TiO2 hollow spheres for enhanced photocatalytic hydrogen evolution, Int. J. Hydrogen Energy 41 (2016) 1627–1634.

[151] X. Wang, Z. Jia, F. Liu, H. Liang, X. You, K. Wang, X. Lou, W. Shuang, L. Xiao, B. Cai, L. Yang, The template-free synthesis of hierarchically porous anatase TiO2 via acid-etching for enhancing the cycling stability and reversible capacity of lithium ion batteries, RSC Adv. 6 (2016) 48985–48994.

[152] J. Jin, S.-Z. Huang, J. Shu, H.-E. Wang, Y. Li, Y. Yu, L.-H. Chen, B.-J. Wang, B.-L. Su, Highly porous TiO2 hollow microspheres constructed by radially oriented nanorods chains for high capacity, high rate and long cycle capability lithium battery, Nano Energy 16 (2015) 339–349.

[153] J. Jin, S.-Z. Huang, J. Li, H.-E. Wang, Y. Yu, L.-H. Chen, T. Hasan, B.-L. Su, Hierarchical nanosheet-constructed yolk-shell TiO2 porous microspheres for lithium batteries with high capacity, superior rate and long cycle capability, Nanoscale 7 (2015) 12979–12989.

[154] W.Q. Fang, X.H. Yang, H. Zhu, Z. Li, H. Zhao, X. Yao, H.G. Yang, Yolk@shell anatase TiO2 hierarchical microspheres with exposed {001} facets for high-performance dye sensitized solar cells, J. Mater. Chem. 22 (2012) 22082–22089.

[155] W. Wang, D. Zhu, Z. Shen, J. Peng, J. Luo, X. Liu, One-pot hydrothermal route to synthesize the Bi-doped anatase TiO2 hollow thin sheets with prior facet exposed for enhanced visible-light-driven photocatalytic activity, Industrial Eng. Chem. Res. 55 (2016) 6373–6383.

[156] S.K.M. Saad, A.A. Umar, M.Y.A. Rahman, M.M. Salleh, Porous Zn-doped TiO2 nanowall photoanode: effect of Zn2+ concentration on the dye-sensitized solar cell performance, Appl. Surf. Sci. 353 (2015) 835–842.

[157] S. Ma, W. Song, B. Liu, W. Zhong, J. Deng, H. Zheng, J. Liu, X.-Q. Gong, Z. Zhao, Facet-dependent photocatalytic performance of TiO2: a DFT study, Appl. Catal. B Environ. 198 (2016) 1–8.

[158] M.-V. Sofianou, V. Psycharis, N. Boukos, T. Vaimakis, J. Yu, R. Dillert, D. Bahnemann, C. Trapalis, Tuning the photocatalytic selectivity of TiO2 anatase nanoplates by altering the exposed crystal facets content, Appl. Catal. B Environ. 142–143 (2013) 761–768.

[159] H. Lee, T.-H. Park, D.-J. Jang, Preparation of anatase TiO2 nanotube arrays dominated by highly reactive facets via anodization for high photocatalytic performances, New J. Chem. 40 (2016) 8737–8744.

[160] L. Mino, G. Spoto, A.M. Ferrari, CO2 capture by TiO2 anatase surfaces: a combined DFT and FTIR study, J. Phys. Chem. C 118 (2014) 25016–25026.

[161] S. Huygh, A. Bogaerts, E.C. Neyts, How oxygen vacancies activate CO2 dissociation on TiO2 anatase (001), J. Phys. Chem. C 120 (2016) 21659–21669.

[162] R. Sanjinés, H. Tang, H. Berger, F. Gozzo, G. Margaritondo, F. Lévy, Electronic structure of anatase TiO2 oxide, J. Appl. Phys. 75 (1994) 2945–2951.

[163] M. Setvín, U. Aschauer, P. Scheiber, Y.-F. Li, W. Hou, M. Schmid, A. Selloni, U. Diebold, Reaction of O2 with subsurface oxygen vacancies on TiO2 anatase (101), Science 341 (2013) 988–991.

[164] S. Moser, L. Moreschini, J. Jaćimović, O.S. Barišić, H. Berger, A. Magrez, Y.J. Chang, K.S. Kim, A. Bostwick, E. Rotenberg, L. Forró, M. Grioni, Tunable polaronic conduction in anatase TiO2, Phys. Rev. Lett. 110 (2013) 196403.

[165] B. Wang, M.K.H. Leung, X.-Y. Lu, S.-Y. Chen, Synthesis and photocatalytic activity of boron and fluorine codoped TiO2 nanosheets with reactive facets, Appl. Energy 112 (2013) 1190–1197.

[166] W. Zhao, W. Ma, C. Chen, J. Zhao, Z. Shuai, Efficient degradation of toxic organic pollutants with Ni2O3/TiO2-xBx under visible irradiation, J. Am. Chem. Soc. 126 (2004) 4782–4783.

[167] I.E. Grey, C. Li, C.M. MacRae, L.A. Bursill, Boron incorporation into rutile. Phase equilibria and structure considerations, J. Solid State Chem. 127 (1996) 240–247.

[168] H. Liu, H.T. Ma, X.Z. Li, W.Z. Li, M. Wu, X.H. Bao, The enhancement of TiO2 photocatalytic activity by hydrogen thermal treatment, Chemosphere 50 (2003) 39–46.

[169] F. Amano, M. Nakata, A. Yamamoto, T. Tanaka, Effect of Ti3+ ions and conduction band electrons on photocatalytic and photoelectrochemical activity of rutile titania for water oxidation, J. Phys. Chem. C 120 (2016) 6467–6474.

[170] B. Li, Z. Zhao, F. Gao, X. Wang, J. Qiu, Mesoporous microspheres composed of carbon-coated TiO2 nanocrystals with exposed {0 0 1} facets for improved visible light photocatalytic activity, Appl. Catal. B Environ. 147 (2014) 958–964.

[171] J.A. Lapszewicz, H.J. Loeh, J.R. Chipperfield, The effect of catalyst porosity on methane selectivity in the Fischer-Tropsch reaction, J. Chem. Soc. Chem. Commun. (1993) 913–914.

[172] M. Liu, L. Piao, W. Lu, S. Ju, L. Zhao, C. Zhou, H. Li, W. Wang, Flower-like TiO 2 nanostructures with exposed {001} facets: facile synthesis and enhanced photocatalysis, Nanoscale 2 (2010) 1115–1117.

[173] H. Hou, M. Shang, L. Wang, W. Li, B. Tang, W. Yang, Efficient photocatalytic activities of TiO2 hollow fibers with mixed phases and mesoporous walls, Sci. Rep. 5 (2015).

[174] B. Qiu, M. Xing, J. Zhang, Mesoporous TiO2 nanocrystals grown in situ on graphene aerogels for high photocatalysis and lithium-ion batteries, J. Am. Chem. Soc. 136 (2014) 5852–5855.

[175] S. Xie, X. Han, Q. Kuang, J. Fu, L. Zhang, Z. Xie, L. Zheng, Solid state precursor strategy for synthesizing hollow TiO 2 boxes with a high percentage of reactive {001} facets exposed, Chem. Commun. 47 (2011) 6722–6724.

[176] X. Han, X. Wang, S. Xie, Q. Kuang, J. Ouyang, Z. Xie, L. Zheng, Carbonate ions-assisted syntheses of anatase TiO 2 nanoparticles exposed with high energy (001) facets, Rsc Adv. 2 (2012) 3251–3253.

[177] F. Liu, X. Yan, X. Chen, L. Tian, Q. Xia, X. Chen, Mesoporous TiO 2 nanoparticles terminated with carbonate-like groups: amorphous/crystalline structure and visible-light photocatalytic activity, Catal. Today 264 (2016) 243–249.

[178] C.Z. Wen, Q.H. Hu, Y.N. Guo, X.Q. Gong, S.Z. Qiao, H.G. Yang, From titanium oxydifluoride (TiOF 2) to titania (TiO 2): phase transition and non-metal doping with enhanced photocatalytic hydrogen (H 2) evolution properties, Chem. Commun. 47 (2011) 6138–6140.

[179] J. Cheng, Y. Wang, Y. Xing, M. Shahid, W. Pan, A stable and highly efficient visible-light photocatalyst of TiO 2 and heterogeneous carbon core–shell nanofibers, RSC Adv. 7 (2017) 15330–15336.

[180] X. Wei, J. Liu, Nanocuboid TiO2 based organic-inorganic hybrids for fast RhB trapping and photodegradation, Sol. Energy Mater. Sol. Cells 157 (2016) 139–145.

[181] L. Ren, Y. Li, J. Hou, X. Zhao, C. Pan, Preparation and enhanced photocatalytic activity of TiO2 nanocrystals with internal pores, ACS Appl. Mater. interfaces 6 (2014) 1608–1615.

[182] Y. Liao, H. Zhang, W. Que, P. Zhong, F. Bai, Z. Zhong, Q. Wen, W. Chen, Activating the single-crystal TiO2 nanoparticle film with exposed {001} facets, ACS Appl. Mater. interfaces 5 (2013) 6463–6466.

[183] N. Roy, Y. Sohn, D. Pradhan, Synergy of low-energy {101} and high-energy {001} TiO2 crystal facets for enhanced photocatalysis, Acs Nano 7 (2013) 2532–2540.

[184] Z. He, Q. Cai, F. Hong, Z. Jiang, J. Chen, S. Song, Effective enhancement of the degradation of oxalic acid by catalytic ozonation with TiO2 by exposure of {001} facets and surface fluorination, Industrial Eng. Chem. Res. 51 (2012) 5662—5668.

[185] X. Yang, H. Fu, A. Yu, X. Jiang, Large-surface mesoporous TiO2 nanoparticles: synthesis, growth and photocatalytic performance, J. Colloid Interface Sci. 387 (2012) 74—83.

[186] Z. Zhao, Z. Sun, H. Zhao, M. Zheng, P. Du, J. Zhao, H. Fan, Phase control of hierarchically structured mesoporous anatase TiO2 microspheres covered with {001} facets, J. Mater. Chem. 22 (2012) 21965—21971.

[187] B. Liu, K. Nakata, M. Sakai, H. Saito, T. Ochiai, T. Murakami, K. Takagi, A. Fujishima, Hierarchical TiO2 spherical nanostructures with tunable pore size, pore volume, and specific surface area: facile preparation and high-photocatalytic performance, Catal. Sci. Technol. 2 (2012) 1933—1939.

[188] G. Cheng, F. Xu, F.J. Stadler, R. Chen, A facile and general synthesis strategy to doped TiO2 nanoaggregates with a mesoporous structure and comparable property, RSC Adv. 5 (2015) 64293—64298.

[189] W. Tu, Y. Zhou, Q. Liu, Z. Tian, J. Gao, X. Chen, H. Zhang, J. Liu, Z. Zou, Robust hollow spheres consisting of alternating titania nanosheets and graphene nanosheets with high photocatalytic activity for CO2 conversion into renewable fuels, Adv. Funct. Mater. 22 (2012) 1215—1221.

[190] Y. Wang, J. Cai, M. Wu, H. Zhang, M. Meng, Y. Tian, T. Ding, J. Gong, Z. Jiang, X. Li, Hydrogenated cagelike titania hollow spherical photocatalysts for hydrogen evolution under simulated solar light irradiation, ACS Appl. Mater. Interfaces 8 (2016) 23006—23014.

[191] H. Zhang, G. Du, W. Lu, L. Cheng, X. Zhu, Z. Jiao, Porous TiO2 hollow nanospheres: synthesis, characterization and enhanced photocatalytic properties, CrystEngComm 14 (2012) 3793—3801.

[192] T. Leshuk, S. Linley, G. Baxter, F. Gu, Mesoporous hollow sphere titanium dioxide photocatalysts through hydrothermal silica etching, ACS Appl. Mater. Interfaces 4 (2012) 6062—6070.

[193] I.A. Kartsonakis, P. Liatsi, I. Danilidis, D. Bouzarelou, G. Kordas, Synthesis, characterization and antibacterial action of hollow titania spheres, J. Phys. Chem. Solids 69 (2008) 214—221.

[194] C.K. Ngaw, V.B. Wang, Z. Liu, Y. Zhou, S. Kjelleberg, Q. Zhang, T.T.Y. Tan, S.C.J. Loo, Enhancement in hydrogen evolution using Au-TiO2 hollow spheres with microbial devices modified with conjugated oligoelectrolytes, Npj Biofilms And Microbiomes 1 (2015) 15020.

[195] C.K. Ngaw, Q. Xu, T.T.Y. Tan, P. Hu, S. Cao, J.S.C. Loo, A strategy for in-situ synthesis of well-defined core—shell Au@TiO2 hollow spheres for enhanced photocatalytic hydrogen evolution, Chem. Eng. J. 257 (2014) 112—121.

[196] S. Feng, M. Wang, Y. Zhou, P. Li, W. Tu, Z. Zou, Double-shelled plasmonic Ag-TiO2 hollow spheres toward visible light-active photocatalytic conversion of CO2 into solar fuel, APL Mater. 3 (2015) 104416.

[197] H.R. Kim, J. Chattopadhyay, J.I. Son, D. Pak, Preparation of platinum-doped hollow spheres and their electrocatalytic activity in water electrolysis, Korean J. Chem. Eng. 25 (2008) 775—779.

[198] Y. Zhang, Z. Zhao, J. Chen, L. Cheng, J. Chang, W. Sheng, C. Hu, S. Cao, C-doped hollow TiO2 spheres: in situ synthesis, controlled shell thickness, and superior visible-light photocatalytic activity, Appl. Catal. B Environ. 165 (2015) 715—722.

Karya#33 Plagiasi

3% SIMILARITY INDEX

1% INTERNET SOURCES

4% PUBLICATIONS

% STUDENT PAPERS

1 Mirgender Kumar, Anuj Kumar, Aya Hekmet Makki, Kwang-Su Seong, Si-Hyun Park. "Quantum dot scaffold phosphors: Maximizing luminescence quantum yield via different stock environments", Materials Letters, 2020
Publication

1%

2 Gang Liu, Hua Gui Yang, Jian Pan, Yong Qiang Yang, Gao Qing (Max) Lu, Hui-Ming Cheng. "Titanium Dioxide Crystals with Tailored Facets", Chemical Reviews, 2014
Publication

1%

3 Kapilashrami, Mukes, Yanfeng Zhang, Yi-Sheng Liu, Anders Hagfeldt, and Jinghua Guo. "Probing the Optical Property and Electronic Structure of TiO2 Nanomaterials for Renewable Energy Applications", Chemical Reviews
Publication

1%

4 Zheng, Xiaoli, Qin Kuang, Keyou Yan, Yongcai Qiu, Jianhang Qiu, and Shihe Yang. "Mesoporous TiO2 Single Crystals: Facile Shape-, Size-, and Phase-Controlled Growth

1%

and Efficient Photocatalytic Performance", ACS
Applied Materials & Interfaces, 2013.

Exclude quotes	On	Exclude matches	< 1%
Exclude bibliography	On		